PHASE I TOPICAL REPORT

Development of Oxy-fuel Combustion Turbines with CO_2 Dilution for Supercritical Carbon Dioxide (sCO_2) Based Power Cycles

Rev. 1

October 8, 2019

SUBMITTED BY:

Southwest Research Institute

6220 Culebra Road

San Antonio, TX 76065

PRINCIPAL INVESTIGATOR

Jeff Moore, Ph.D.

210-522-5812

jeff.moore@swri.org

SUBMITTED TO:

U.S. Department of Energy (DOE)

National Energy Technology Laboratory (NETL)

U.S. DOE AWARD DE-FE0031620

SwRI® Project No. 18.23916

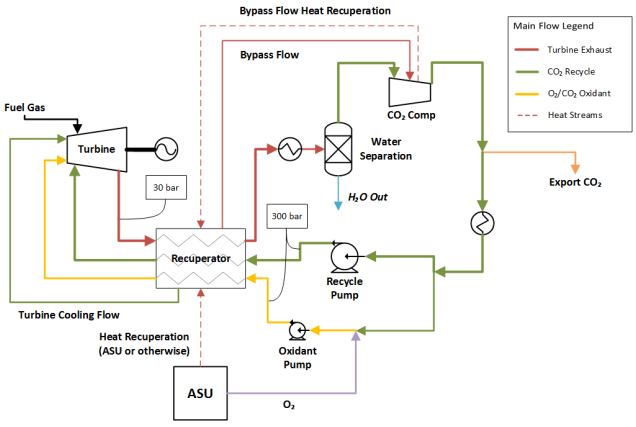

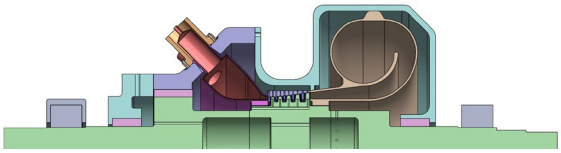

TABLE OF CONTENTS

TABLE OF FIGURES

A. EXECUTIVE SUMMARY

Supercritical Carbon Dioxide (sCO_2) power cycles are a transformational technology for the energy industry, providing a higher efficiency heat source energy conversion for conventional and alternative energy sources. The novel cycle significantly reduces capital costs because of smaller equipment footprints and design modularity and allows for rapid cyclic load and source following to balance solar and wind energy power swings. This topical report outlines progress made to develop an oxy-fuel combustion turbine to significantly improve the state-of-the-art for thermal efficiency and results in a high-pressure stream of CO_2 simplifying carbon capture making the power plant emission-free.

The team of Southwest Research Institute® (SwRI®), General Electric Global Research Center (GE-GRC), 8 Rivers, Air Liquide, Electric Power Research Institute, Inc. (EPRI), and Georgia Tech are working to develop a conceptual design for a sCO_2, coal syngas or natural gas-fired oxy-fuel turbine in the 150-300 MWe size range capable of 1,200°C turbine inlet temperature at 300 bar and exhaust temperatures in the 725-775°C range. This turbine will require cooled turbine nozzles and blades as well as advanced thermal management systems to accommodate these high temperatures. The team represents world leaders in the development of sCO_2 power technologies and has received numerous Department of Energy (DOE) and industry-funded projects to implement pilot scale sCO_2 power cycle component and system level equipment, as well as MW scale pilot plants.

Phase I work identified technology gaps and developed a detailed test plan to address these gaps through bench-scale testing. Phase I requirements as outlined in the funding opportunity announcement along with task assignments include:

- Develop a conceptual oxy-fuel sCO_2 combustion turbine design: SwRI and GE (Aero, mechanical, thermal management), Air Liquide (combustor), EPRI (materials), and Georgia Tech (combustion kinetics).
- Develop a thermodynamic cycle analysis (heat, mass, and energy balance) for a sCO_2 semi-closed recuperated Brayton cycle based on natural gas, as the fuel and the proposed sCO_2 turbine: 8 Rivers.
- Consistent with the conceptual design and cycle analysis, develop nominal engine component boundary conditions in terms of pressures, temperatures, mass flows, heat flux etc.: 8 Rivers, GE and SwRI.
- Consistent with the conceptual design and cycle analysis, develop and evaluate overall engine thermal management options and concepts including engine cooling fluids, airfoil thermal management, exhaust thermal management etc.: GE, SwRI, and Air Liquide.
- Develop a Technology Maturation Plan (TMP) leading to pre-commercial testing of the proposed oxy-fuel sCO_2 combustion turbine: Team with 8 Rivers lead.
- Develop a Test Plan with cost, schedule, and resources required to resolve identified technology gaps and that supports the advancement of a potential Phase II Preliminary Design: Team with SwRI lead.

The team, as assembled, is uniquely suited to accomplish the objectives of this project and each team member has demonstrated this through vast experience with the DOE, and commercially-funded power generation projects. All participants have valuable experience at both the system and component level of power generation and turbine design and realization. SwRI is one of the

oldest and largest independent non-profit applied research and development organizations in the United States. SwRI is a world leader in sCO_2 research, development, and implementation with millions of dollars of commercial and government research funding in this area. SwRI leveraged this experience along with their considerable experience with other power generation, turbomachinery design and testing, and new technology development to serve as prime for this effort by providing overall project management and contributing technically to the system design. General Electric is a company name synonymous with power generation for over 100 years. 8 Rivers is currently building a 25-MWe oxy-fuel combustor and is an early pioneer of this technology. Air Liquide brings air separation expertise and has unique oxy-combustion experience that was leveraged here. EPRI has been doing research related to power generation for many decades and possesses extensive materials expertise. Finally, the goal of Georgia Tech's task was to understand combustion chemical kinetics with CO_2 dilution at temperatures of 1,200°C and pressures of 300 bar.

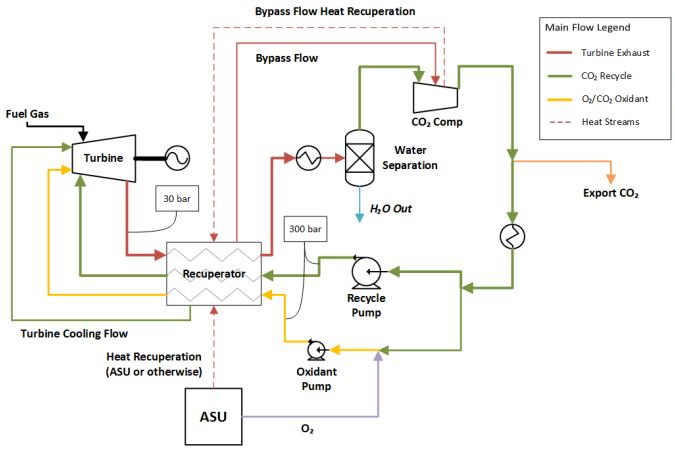

Figure 1. Sample Oxy-Combustion sCO_2 Brayton Cycle (NetPower.com)

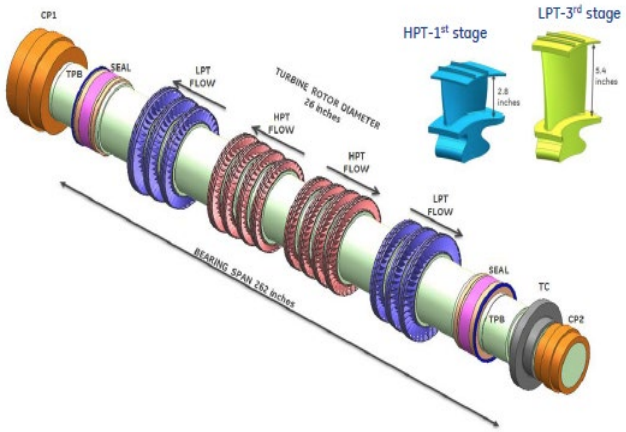

Figure 2. 450 MW sCO_2 Turbine Rotor Conceptual Design for Fossil Application

B. TASKS TO BE PERFORMED

Task 1.0: Project Management and Planning

The project was managed in accordance with a Project Management Plan to meet all technical, schedule and budget objectives, and requirements. Activities were coordinated in order to effectively accomplish the work. Project plans, results, and decisions were appropriately documented and project reporting and briefing requirements were satisfied.

The Project Management Plan was generated and refined as necessary throughout the project to accurately reflect the current status of the project. Management of project risks occurred in accordance with the risk management methodology delineated in the PMP in order to identify, assess, monitor and mitigate technical uncertainties as well as schedule, budgetary, and environmental risks associated with all aspects of the project. The results and status of the risk management process was presented during project reviews and in Progress Reports with emphasis placed on the medium- and high-risk items.

Task 2.0: Establish Cycle Model and Engine Boundary Conditions

SwRI worked with the project partners to define the overall commercial cycle application and configuration in which the turbine operates, including general cycle characteristics and requirements, target turbine output, fuel specifications and requirements, and other system-wide considerations.

Task 2.1: Develop Power Cycle Model

A thermodynamic analysis of the cycle was performed, including a static, full cycle heat and mass balance process model, to determine the overall system performance and define key cycle operating parameters. The project team developed a heat and mass balance for the full cycle utilizing computational modeling tools employing equations of state for predicting fluid thermophysical properties.

Task 2.2: Develop Nominal Engine Boundary Conditions

The Project Team developed nominal engine boundary conditions, in terms of pressures, temperatures, mass flows, heat flux, and other considerations. This was an iterative process between the conceptual turbine design effort and the cycle thermodynamic modeling effort to optimize operating conditions, flow rates, cooling approaches, and integration techniques between the turbine and the overall cycle.

Task 3.0: Conceptual Oxy-fuel sCO_2 Combustion Turbine Design

Under Task 3.0, the Project Team developed the conceptual design of the multi-stage, axial-flow turbine.

Task 3.1: Turbine Aerodynamic Design

The turbine aerodynamic flow path was designed using a one-dimensional (1-D) aero design tool, adapted for oxy-combustion products, to optimize a flow path geometry (corner points) and stage-count. This process was conducted iteratively until a suitable conceptual design was identified that meets the efficiency target and had the potential to meet mechanical and rotordynamic design constraints. Three-dimensional blade shapes were subsequently designed for the most critical stages by stacking three radial two-dimensional (2-D) cross-sections, where the airfoil shape at the hub, mid-span, and the shroud was defined and a three-dimensional (3-D) blade was generated through interpolation.

Task 3.2: Oxy-Fuel Combustor Conceptual Design

A conceptual design of the oxy-fuel combustor including fuel and oxygen delivery system and injector design was developed. The combustor design was based on the multiple co-axial fuel and oxidizer injectors. The updated kinetic models (developed under Task 5.0) was utilized for the combustion analysis.

Task 3.3: Turbine 2-D Layout

SwRI generated a 2-D layout of the machine incorporating the aerodynamics flow path and develop a rotor model incorporating inter-stage seals, shaft-end seals, bearings, and couplings. The rotor contains the cooling circuit required for blade cooling. SwRI performed casing stress calculations, determined bearing span limitations, developed 2-D inlet and exit plenum designs to meet flow velocity limits, performed containment checks, and determined torque and stress requirements in the rotor. These initial calculations established stage-count, rotor span, rotor hub and shroud diameters, and the overall size of the flow path and casing.

Task 3.4: Turbine Rotordynamic Analysis

A preliminary rotordynamic model was developed to show the validity of the concept. Compliance with American Petroleum Institute standards will be demonstrated as appropriate.

Task 3.5: Turbine Blade Heat Transfer Modeling

A 3-D heat transfer model of the first stage blade was developed to verify the internal blade cooling concept. Thermal Barrier Coatings (TBCs) was also evaluated. Thermal management of the combustor liner and exhaust collector was developed.

Task 3.6: Turbine End Seals Development

A conceptual design for turbine end seals will be developed. Baseline leakage rate and rotor axial length will be based on a conventional labyrinth seal design. Previously developed design tools will be utilized to generate a conceptual design for large diameter, high-temperature hydrodynamic face-end seals.

Task 4.0: Turbine High-Temperature Materials Evaluation

Expertise on materials in this high-temperature, high-pressure oxidizing environment was provided by EPRI. A literature search of oxy-fired environments and the interaction of materials with CO_2 environments for blading and casing was performed and alloys that provide acceptable behavior in this environment and stress state were recommended.

Task 5.0: Combustion Kinetics Evaluation

Fundamental combustion kinetics for natural gas and oxygen in this high-pressure, high-CO_2 concentration environment was reviewed. With the availability of more experimental data at high pressures, different kinetic mechanisms were revisited and evaluated based on newly produced ignition delay data at sCO_2 conditions in this task. A validated kinetic model was developed and used for the combustor design.

Task 6.0: Technology Maturation Plan Development

An overall TMP to advance the conceptual turbine design to commercial demonstration was generated. The plan identified the major technology gaps, define testing stages and scales required to move the turbine through pre-commercial demonstration, and describe a pathway to linking the turbine maturation with broader cycle development and demonstration activities already underway.

Task 7.0: Test Plan Development

A test plan was developed for rig testing to be conducted in a potential follow-on project. Test campaigns during future programs will consist of combustion testing and experimental testing to determine corrosion/erosion characteristics of turbine hot gas path materials and TBCs in the oxy-combustion environment.

C. MILESTONE LOG

Below is the status of the milestones for Phase I of the project. Each milestone shows the planned completion date assuming the project is kicked off on May 1, 2018, and has an 18-month duration.

Phase I:

- Optimize oxy-fuel combustion cycle to achieve equal to or greater than 58% thermal efficiency: 10/3/18 – 100% complete.

- Develop aerodynamic design for first stage nozzle and turbine blade with efficiency greater than 85%: 9/30/19 – 100% complete.
- Develop cooled nozzle and turbine blade design with metal temperature in high-stress areas less than 700°C: 9/30/19 – 100% complete.
- Develop a conceptual design for the oxy-fuel combustor to achieve a firing temperature of 1,200°C: 9/30/19 – 100% complete.
- Develop a conceptual layout for a turbine: 9/30/19 – 100% complete.
- Develop a conceptual design for shaft end and inter-stage seals: 9/30/19 – 100% complete.
- Develop thermal management concepts with pressure-containing metal temperature less than 700°C: 9/30/19 – 100% complete.
- Evaluate combustion kinetics by developing model: 9/30/19 – 100% complete.
- Select preferred materials for hot-section components that provide 100,000-hour creep life: 9/30/19 – 100% complete.
- Develop a TMP: 9/30/19 – 100% complete.
- Develop detail design and test plan: 9/30/19 – 100% complete.

D. FINAL UPDATE

Task 2.0: Establish Cycle Model and Engine Boundary Conditions

Task 2.1: Develop Power Cycle Model

A thermodynamic analysis of the cycle was performed, including a static, full cycle heat and mass balance process model, to determine overall system performance and define key cycle operating parameters. The goal is to develop a thermodynamic cycle analysis (heat, mass, and energy balance) and boundary conditions for a sCO_2 semi-closed recuperated Brayton cycle.

Utilizing a generic commercial-scale Aspen model previously developed, a first-pass heat and mass balance were calculated to provide a starting point for streams entering and exiting the turbine. This initial model is not optimized, as its purpose is to allow turbine design efforts to begin within roughly defined bounds. As turbine design advances, the model will be updated, and ultimately an optimized model will be developed.

In order to perform the calculations, several assumptions had to be made around the turbine. In addition to assumptions around performance, such as isentropic efficiency, there were model structural issues around dealing with the cooling flow and how to model the cooling flow impact on power production and performance of the turbine. Several possible structural options were discussed with the larger group and a choice was made.

The final assumptions used in the modeling are summarized as:

- Turbine modeled with a 90% isentropic efficiency.
- Turbine split into two to allow the introduction of cooling flow in between models.
- Two turbine models produce equal power.

- 10% of the main recycle flow is diverted to provide the cooling flow and is provided at 430°C
- Cooling flow is heated to 800°C internal to the turbine; this is modeled by using heat from the main flow before it enters the first turbine.
- Cooling flow is expanded to intermediate pressure during mixing with a main gas path between the two turbine models.
- Gibbs equilibrium reactor used for the combustor (i.e., reaction rates are not taken into account).
- The turbine inlet temperature is 1,200°C.
- Turbine inlet pressure is 305 bar, with an exhaust pressure of 30 bar.
- All streams entering the combustion turbine experience approximately a 3% pressure loss through the combustor.
- The equation-of-state used is Soave-Redlich-Kwong.

These assumptions led to an Aspen turbine hierarchy which was placed into a larger, previously-created Allam Cycle Aspen model. As the project has progressed, the model has been expanded to include balance piston and shaft seal loses. The updated turbine model specific to this project is shown in Figure 3.

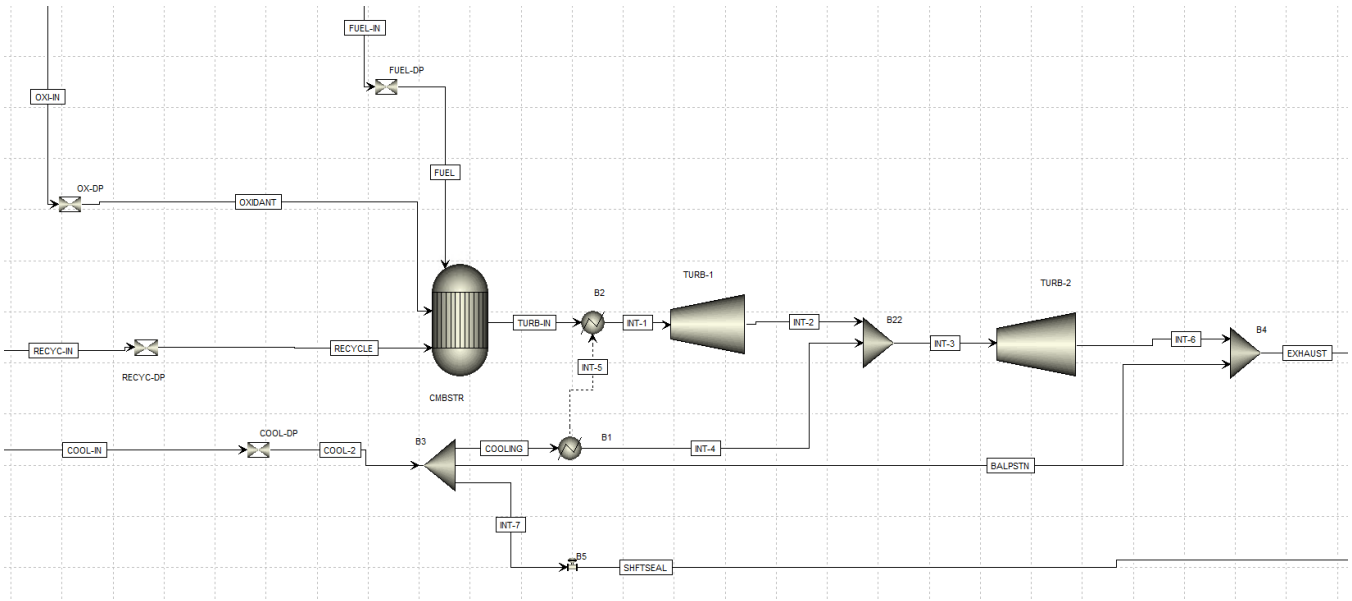

Figure 3. ASPEN Model Process Flow Diagram for Cycle Model

The stream data from the converged model was provided to the group to allow the different organizations to begin to examine and analyze as summarized in Table 1. It should be noted that the data in Table 1 is from the original Aspen model and does not include the recent changes which do not create substantive changes to the streams entering the turbine. Current cycle thermal efficiency is slightly above 58%, which includes the air separation unit and shaft seal leakage capture and recompression back into the cycle, all on a low heating value basis. As the design is further optimized, the team expects this number to increase.

Table 1. Summary of Oxy-Fuel Turbine Allam Cycle Results

	COOL-IN	COOLING	FUEL-IN	FUEL	OXI-IN	OXIDANT	RECYC-IN	RECYCLE	TURB-IN	EXHAUST
Substream: MIXED										
Mole Flow kmol/hr										
CH4	0	0	2436.61	2436.61	0	0	0	0	2.58E-22	2.58E-22
O2	40.7438	40.7438	0	0	5024.019	5024.019	366.6942	366.6942	517.4953	558.2391
AR	51.58562	51.58562	0	0	190.9455	190.9455	464.2706	464.2706	655.2161	706.8017
CO	0.010801	0.010801	0	0	0.034832	0.034832	0.097208	0.097208	0.137188	0.147989
H2	0.000336	0.000336	0	0	0.001084	0.001084	0.003025	0.003025	0.004269	0.004605
CO2	5106.204	5106.204	0	0	16467.09	16467.09	45955.83	45955.83	64859.53	69965.74
H2O	3.286727	3.286727	0	0	10.59943	10.59943	29.58054	29.58054	4913.4	4916.687
Mass Flow kg/hr										
CH4	0	0	39089.95	39089.95	0	0	0	0	4.14E-21	4.14E-21
O2	1303.753	1303.753	0	0	160763	160763	11733.77	11733.77	16559.23	17862.98
AR	2060.742	2060.742	0	0	7627.891	7627.891	18546.68	18546.68	26174.57	28235.32
CO	0.302536	0.302536	0	0	0.975654	0.975654	2.722823	2.722823	3.8427	4.145236
H2	0.000678	0.000678	0	0	0.002185	0.002185	0.006098	0.006098	0.008606	0.009284
CO2	224723	224723	0	0	724714	724714	2022510	2022510	2854460	3079180
H2O	59.21131	59.21131	0	0	190.9517	190.9517	532.9018	532.9018	88516.29	88575.5
Total Flow kmol/hr	5201.831	5201.831	2436.61	2436.61	21692.69	21692.69	46816.48	46816.48	70945.79	76147.62
Total Flow kg/hr	228147	228147	39089.95	39089.95	893296	893296	2053320	2053320	2985710	3213860
Total Flow cum/hr	1043.836	1073.55	226.2845	231.2627	6348.024	6538.998	13745.19	14156.04	30544.29	223808
Temperature C	430	429.5408	72.06623	71.4434	739	739.2248	739	739.1531	1200.009	778.3606
Pressure bar	316.5	306.5	315	305	315	305	315	305	305	30

The cycle model was used to optimize the arrangement of the turbine by comparing the overall cycle performance considering both a single and double flow turbine arrangement. The double flow provides symmetry of the case and balances out the axial thrust. Low pressure steam turbines are typically double flow. However, the double flow design requires more than double the total number of stages, thereby increasing the cooling flow requirements. This hurts the cycle efficiency. The single flow design, which is more typical of most gas turbines, requires a balance piston to balance out the thrust and has higher internal seal leakage than the double flow, but much lower cooling flow. Therefore, the cycle model was used to determine the optimum configuration.

The previous Aspen model was structurally modified to take into account balance piston losses as predicted by the turbine designers. This balance piston loss takes a portion of the cooling flow and bypass all of the turbine stages and empties into the turbine exhaust. This is a net loss on the efficiency of the plant as it directly quenches the turbine exhaust and also increases the parasitic load on the cycle.

In addition to the structural model changes, a trade study was performed to examine the impact of cooling flow and turbine efficiency on the overall cycle efficiency. An increase in cooling flow has the tendency to decrease the overall cycle efficiency. Likewise, an increase in turbine efficiency has the tendency to increase the overall cycle efficiency. This analysis was performed to assist the turbine designer in choosing a single flow versus a double flow turbine, and in determining the optimum number of stages for the engine. During this analysis, no attempt at optimization was performed. Instead, all other model variables were held constant so that the impact of the changes were determined without being masked by other changes, which would occur during optimization. Table 2 summarizes these calculations for five different single flow stage-counts and one stage for the double flow.

Table 2. Optimization of Turbine Arrangement and Stage-Count

FLAVOR	STAGES	COOLING	SEAL LEAKAGE	TOTAL	AERO	RELATIVE EFFICIENCY CHANGE
	#	% of Recycle Flow			%	%
SINGLE	4	4.16	3.40	7.56	88.3	1.19
SINGLE	5	5.55	3.40	8.95	90.0	1.92
SINGLE	6	7.47	3.40	10.87	91.1	1.69
SINGLE	8	11.20	3.40	14.60	92.0	0.00
SINGLE	10	15.86	3.40	19.26	92.1	-3.13
DOUBLE	8	8.00	7.50	14.30	89.8	-1.99

The double flow stage-count was already optimized by GE using their aero design tools. The cooling flow rates were provided by GE using their preliminary 1D blade cooling design tool. The seal leakages were obtained by SwRI using geometry from the layout and running the XLLaby program from Texas A&M University (TAMU). Table 2 shows that the single flow design is better than the double flow, assuming the same stage-count. Further optimizing revealed that the 5-stage design is optimum when considering both blade efficiency and cooling flow requirements. The single flow design has a larger hub diameter and shorter bearing span, which is better from a rotordynamic point of view. Therefore, based on this work, the 5-stage single flow design was selected for the layout. The rotordynamics and pressure containment feasibility was verified as well. Now that the arrangement and stage-count is selected, the remaining work on the combustor and transition duct along with 3-D design of the first stage nozzle/buckets is proceeding.

In addition, investigations into balance piston and shaft seal leakage rates have been investigated to guide selection and possible investigation of new seal types. See discussion in Task 3.6 for more information.

Task 2.2: Develop Nominal Engine Boundary Conditions

Initial boundary conditions including temperatures, pressures, and flow rates were obtained from the cycle model for the turbine to permit the aerodynamic design of the turbine bladed components.

Task 3.0: Conceptual Oxy-fuel sCO_2 Combustion Turbine Design

Task 3.1: Turbine Aerodynamic Design

Various preliminary sizing studies were conducted to explore flow-path layout options (stage-count, flow-path hub and case diameters) for target 3,600 rpm turbine design inlet flow conditions and turbine pressure ratio. Initial scope-out was done using simple mass-energy balance calculations to estimate blade heights, hub diameter by loading airfoils in different ways on Smith's chart. This process includes picking various locations on Smith's chart for the first stage (Figure 4), then compute stage height and hub-diameter for any given stage-count. The intent is to keep first stage height to ~1 inch to minimize end-wall losses. As seen in Figure 5, the initial estimate for an 8-stage layout with average work and flow coefficient of 1.5 and 0.575 would result in first stage height of ~1 inch, with flow path hub diameter around 40 inches.

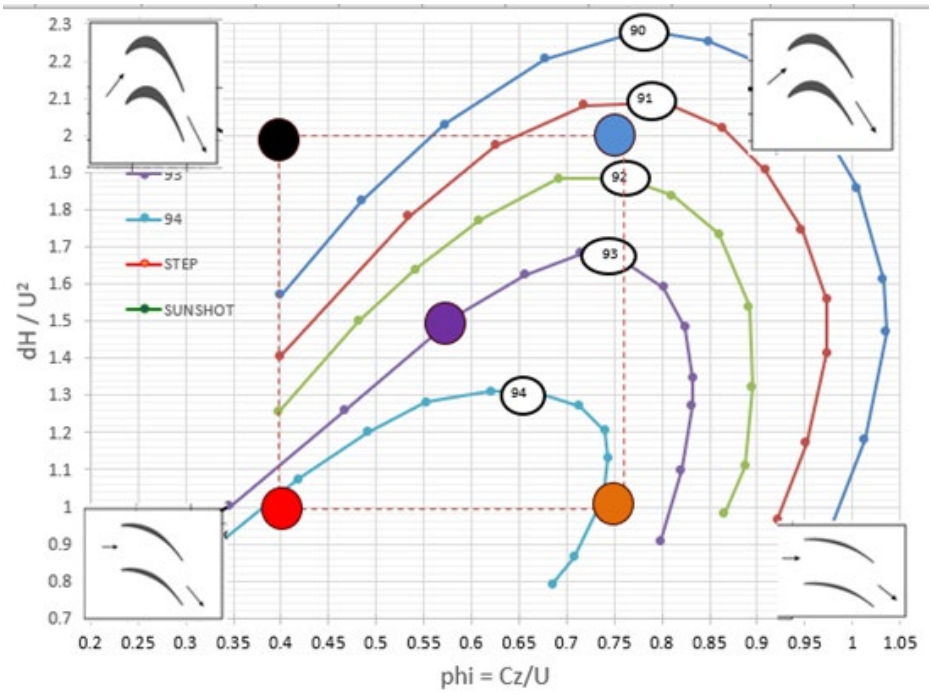

Figure 4. Smith's Chart with Five Locations Marked (Picked to Estimate Stage Height and Required Hub Diameter for given Stage-Count) with Solid Circles

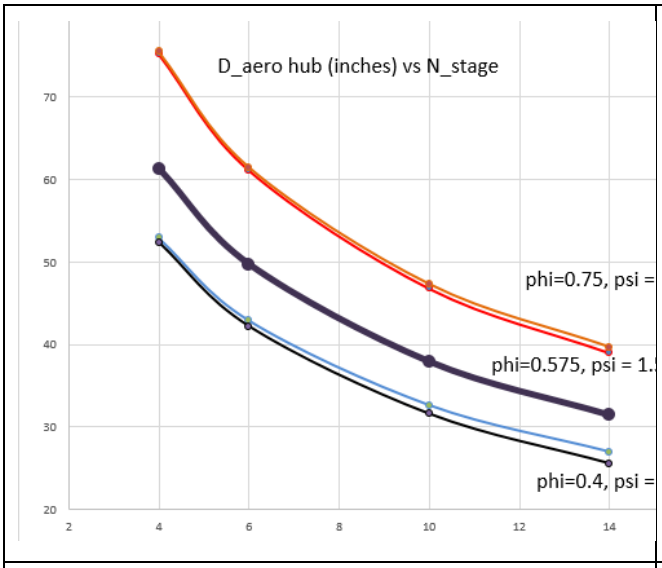

(a) Aero Hub Diameter vs. Stage-count

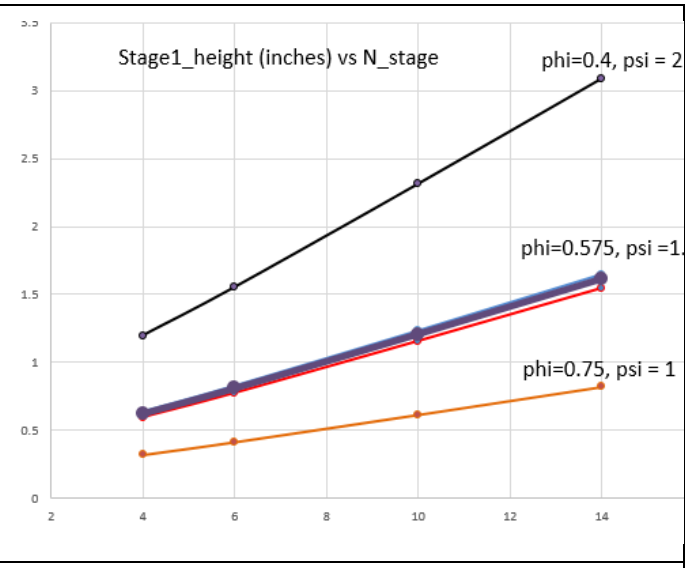

(b) First Stage Height vs. Stage-count

Figure 5. Tradeoff Trends with a Number of Stages for Various Work and Flow Coefficients. "PSI" is Work Coefficient and "phi" is Flow Coefficient on Smith's Chart

Following the initial screening, a detailed 2-D layout evaluation was conducted that provides the airfoil corner points. Table 3 shows hub-diameter and turbine length for various stage-count choices for a single flow turbine design. An additional design evaluation was made for a double/split flow turbine, listed in the same table. Figure 6 shows the location of individual stages for each of the stage-count configuration for a single flow layout. Various tradeoffs during this process include hub diameter, stage height, temperature drop across the stage, blade count and overall aero-flow path efficiency. As expected, larger stage-count results in lower hub diameter

but also slower temperature drop along the turbine. Figure 7 shows temperature and flow-path efficiency variations as stage-count is increased. An 8-stage configuration appears to be a potential choice for a single-flow design in terms of overall turbine size, efficiency, and temperature drop considerations.

Following single flow layout evaluations, a double flow configuration was explored. The team initially preferred the double flow arrangement since it provides thrust balance and eliminated the losses and the need to cool a balance piston. The layout and rotordynamics analysis of the double flow design, however, demonstrated the single flow is preferred from a performance and rotordynamics point of view as discussed above.

Table 3. Summary of the Hub-diameter and Turbine Length for Various Stage-Count Selections

	Single Flow Turbine						**Double/Split Flow Turbine**
Stage-Count	4-Stage	5-Stage	6-Stage	8-Stage	10-Stage	12-Stage	12-Stage
Aero Hub Diameter (Inches)	58	52	47	40.25	37	34	34.5
Shaft Total-Total Efficiency	88.3	90	91.1	92	92.1	92.3	92.1
Blade-count/Stage	142	142	142	142	96	96	140
Turbine Length (Inches)	21	22	24	35	40	43	40

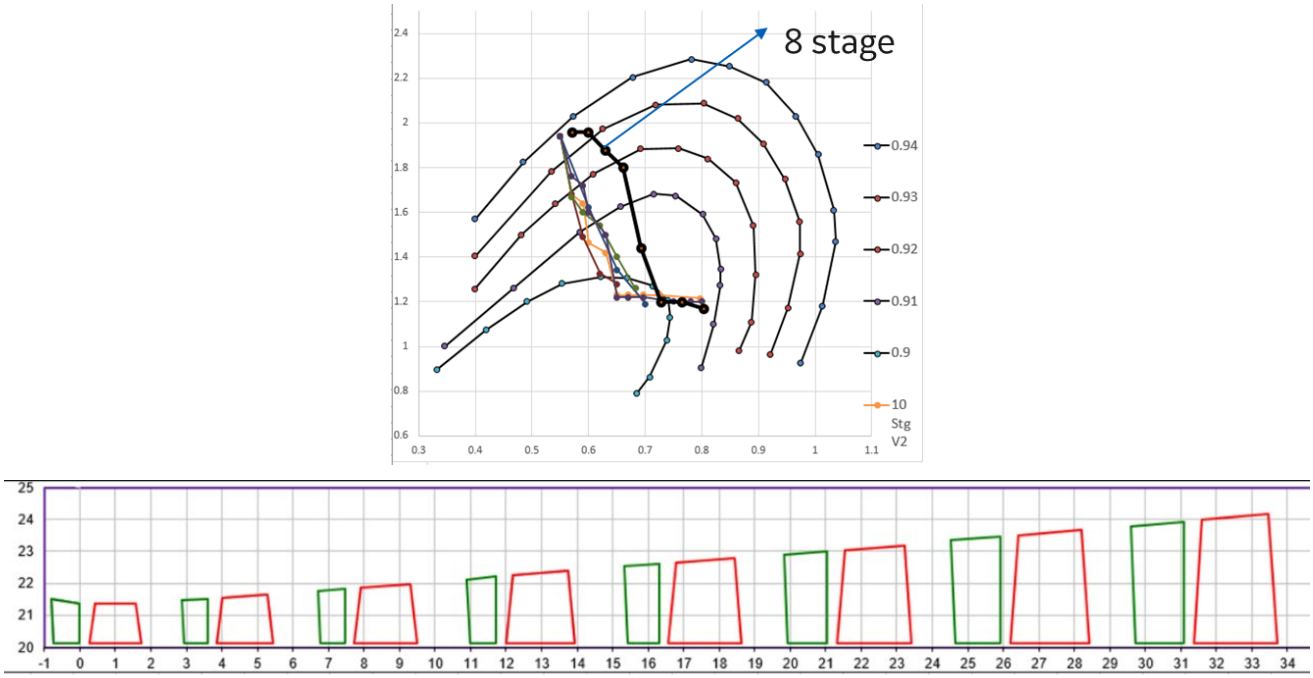

Figure 6. Placement of Stages on Smith's Chart for Various Stage-count Choices in Table 3. 8-stage Layout is Highlighted along with Blade-corner Points (Inter-stage Gaps are left to Extend Nozzles as needed for Mechanical Stress Requirements)

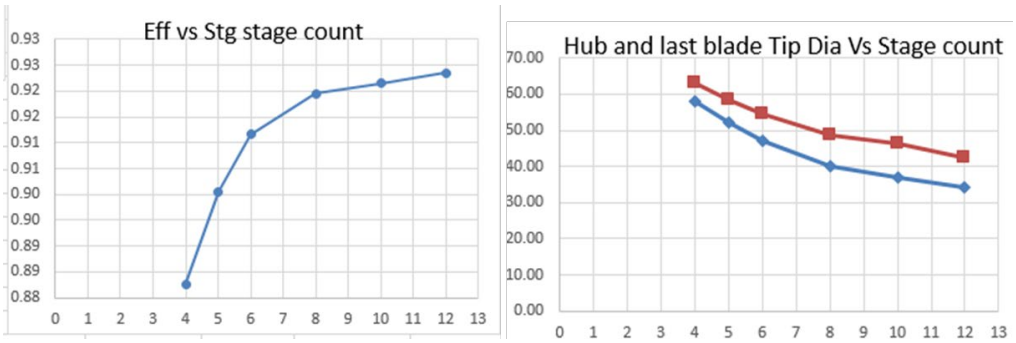

(a)

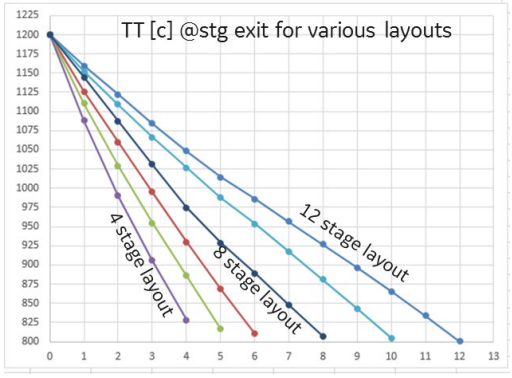

(b)

Figure 7. Single Flow Layout Option Evaluations: (a) Flow-path Efficiency, Aero-hub Diameter and Last-stage Tip Diameter Variations with Stage-count Selection; (b) Temperature Drop Along Turbine

Task 3.2: Oxy-Fuel Combustor Conceptual Design

Yasunori Iwai et al., (Toshiba Corporation) has published the design and test results of the combustor for the sCO_2 turbine (GT2015-43160, Proceedings of ASME Turbo Expo 2015: Turbine Technical Conference and Exposition). The combustor is developed for 50 MWt pilot demonstration plant at the operating pressure of 30 MPa. The test combustor was scaled down 1 to 5 to reduce the flow requirements. Figure 8 shows the cross-sectional view of test combustor. The inner diameter of the combustor is 83 mm; the length of the combustor is 409 mm.

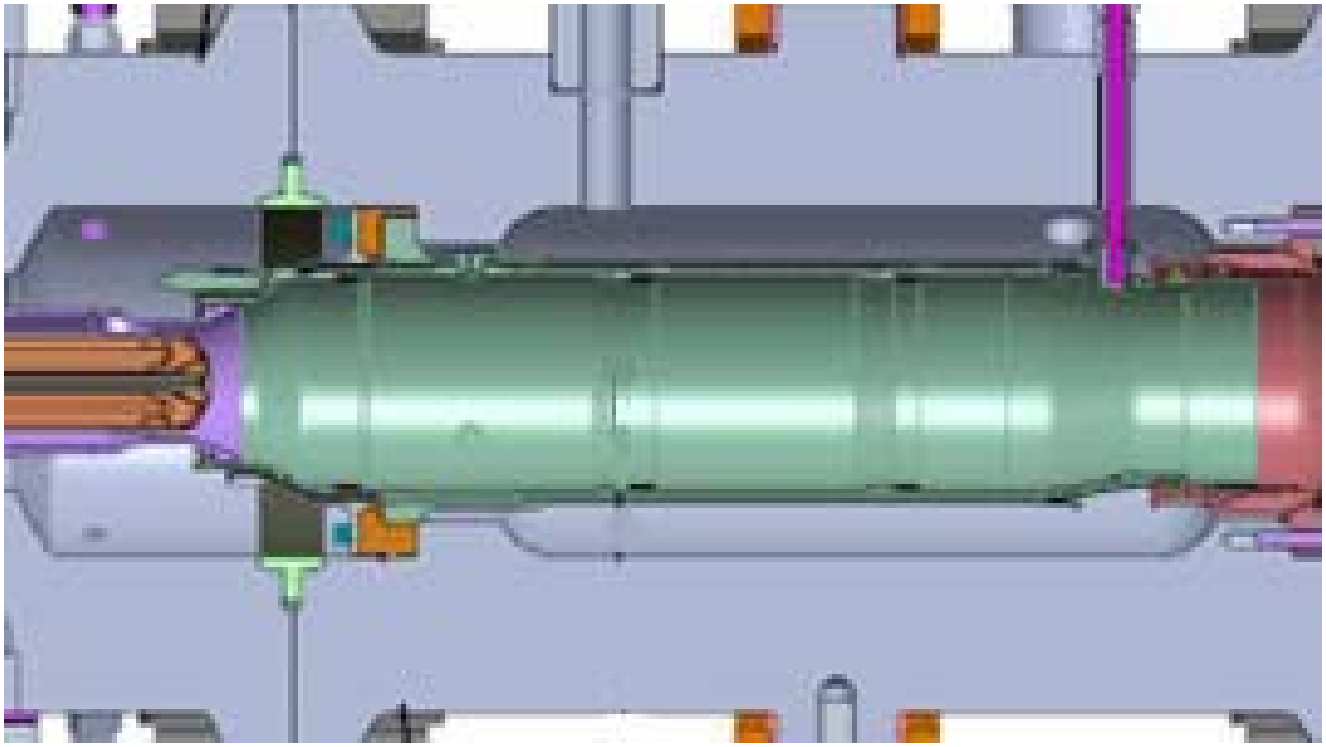

Figure 8. Cross Section of Test Combustor [GT2015-43160]

A simple single swirler device was applied to the combustor. The swirl vane angle and total velocity were determined using results from a computational fluid dynamics (CFD) study. Authors utilized NUIG C3_4_1 mechanism and GRI_Mech_3.0 for combustion simulations.

A similar design methodology will be applied to the present task. Basic design parameters such as reactant injection velocities, swirl strength, and combustor exit conditions will be studied using 2-D axisymmetric CFD. Detailed design and 3-D CFD will follow based on the findings from 2-D CFD results.

The average velocity would be a primary design parameter to conceptualize the size of the system. The combustor shown in Figure 8 is scaled to 10 MWt. Although the velocity or detail geometry was not published, the average flow velocity was estimated using the flow condition provided by 8 Rivers in the present project. The average flow velocity at the combustor exit is estimated at about 29 m/s. The typical flow velocity is 25 ft/s (7.6 m/s) in a reverse-flow combustor and is between 80 ft/s (24.4 m/s) and 135 ft/s (41.1 m/s) in a straight-through flow turbojet combustor (Gas turbine Engineering Handbook, 4th Edition, Meherwan P. Boyce). For the first try, the average velocity of 25 m/s was studied with 8 identical combustors.

Table 4 summarizes the single combustor and injector parameters for the first 2-D CFD case. Other configurations were simulated based on the result of case 1. The tangential velocity at 25 m/s will be applied to OXY-IN stream for case 1. Figure 9 shows the sketch of overall geometry for CFD study. The thickness of injectors is calculated using ASME B31.3 seamless pipe thickness equation with Inconel 740H maximum allowable stress of 345 bar at 800°C. The 2-D study is only for determining the design parameters and the results will be the basis of a detailed combustor design.

Table 4. Combustor 2-D CFD Case

	Case 1	FUEL-IN	OXI-IN	RECYC-IN	TURB-IN
	Temperature C	72.06623	739	739	1,200.009
	Pressure Bar	315	315	315	305
8	Combustor [MWt]	67.8645			
1	Injectors per Combustor [MWt]	67.8645			
1	Injector Flow Rate [kg/hr]	4,886.244	111,662	256,665	373,213.8
1	Injector Flow Rate [m^3/hr]	28.28556	793.503	1,718.149	3,818.036
	Injector Inner Diameter [m]	0.02	0.11	0.24	0.24
	Injector Thickness [m]	0.006	0.035	0.08	0.08
	Injector Outer Diameter [m]	0.032	0.18	0.4	0.4
	Area [m2]	0.000314	0.008699	0.019792	0.045239
	Average Velocity [m/s]	25.00993	25.33805	24.11392	23.44365

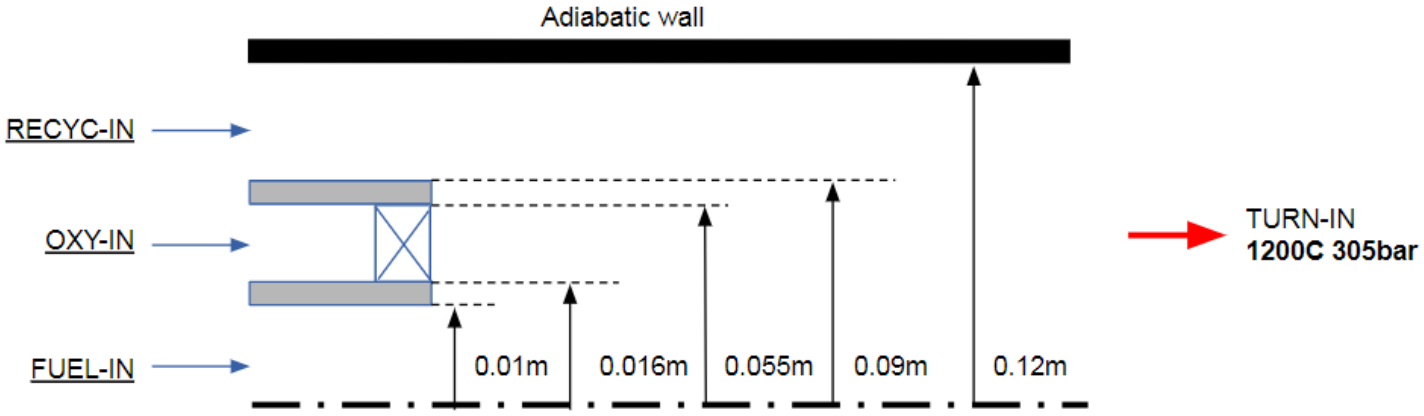

Figure 9. Geometry Sketch for 2-D CFD Parametric Study (not in Scale)

Combustion kinetics is one of the important factors for the reacting flow CFD study. According to the recent progress by the project partner (Georgia Tech), the Aramco mechanism performs the best at high-pressure conditions. The Aramco mechanism involves multiple species and reactions. As Methane is the primary fuel, the kinetic mechanism can be reduced to improve the computational efficiency. Combustion kinetic models were systematically reduced by using the Path Flux Analysis method (Combustion and Flame, Vol. 157(7), 2010, pp. 1,298-1,307). The performance of reduced models (19, 28, 31, and 35 species) is compared against the original mechanism. Figure 10, Figure 11, and Figure 12 show the ignition delay times and flame speed comparison. Although the flame speed is not measurable at high pressures above 20 bar due to

the flame instability, those have been used to compare the performance of reduced models. Simulations were done by using Cantera 2.4 (https://cantera.org/).

The performance of 19 and 28 species models deviated from the original mechanism significantly, by up to 400% in ignition delay and 23% in flame speed. Species 31 and 35 had good agreement with an original mechanism having lower than 5% of error for ignition delay time and flame speed, except for the fuel rich conditions (equivalence ratio higher than 1.3). The flame speed kept increasing as equivalent ratio increase for the case of 300 bar. It would be worth to study this phenomenon. However, it is not the primary objective and the nominal equivalent ratio at the combustor inlet is about 0.97 based on the cycle stream summary. Based on the performance of reduced models, 31 species model was chosen for the initial 2-D CFD simulation as an optimal reduction keeping efficient computation and fidelity of the kinetic mechanism.

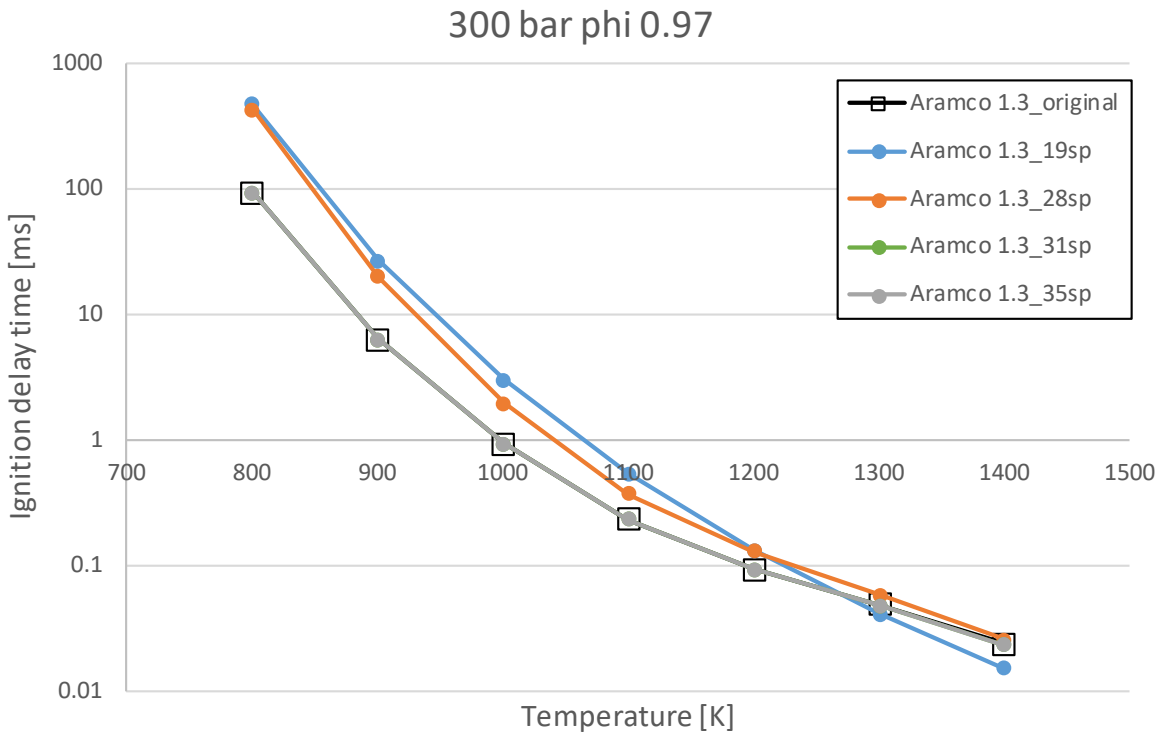

Figure 10. Ignition Delay Time Comparison at 300 Bar

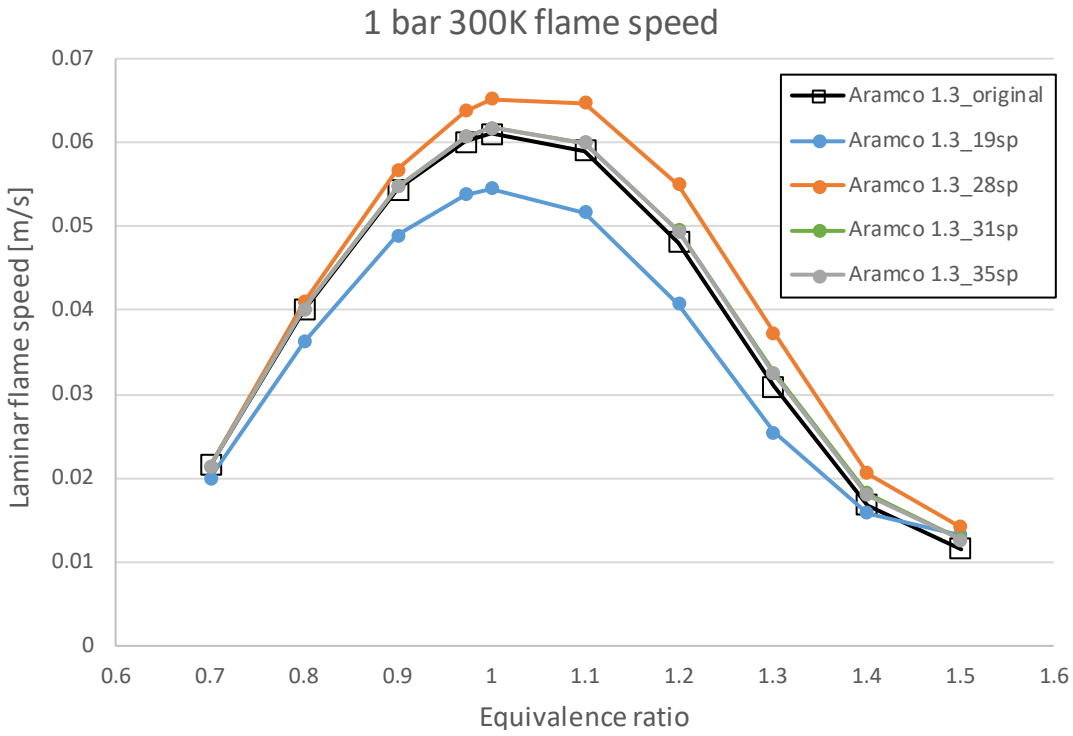

Figure 11. Laminar Flame Speed Comparison at 1 Bar

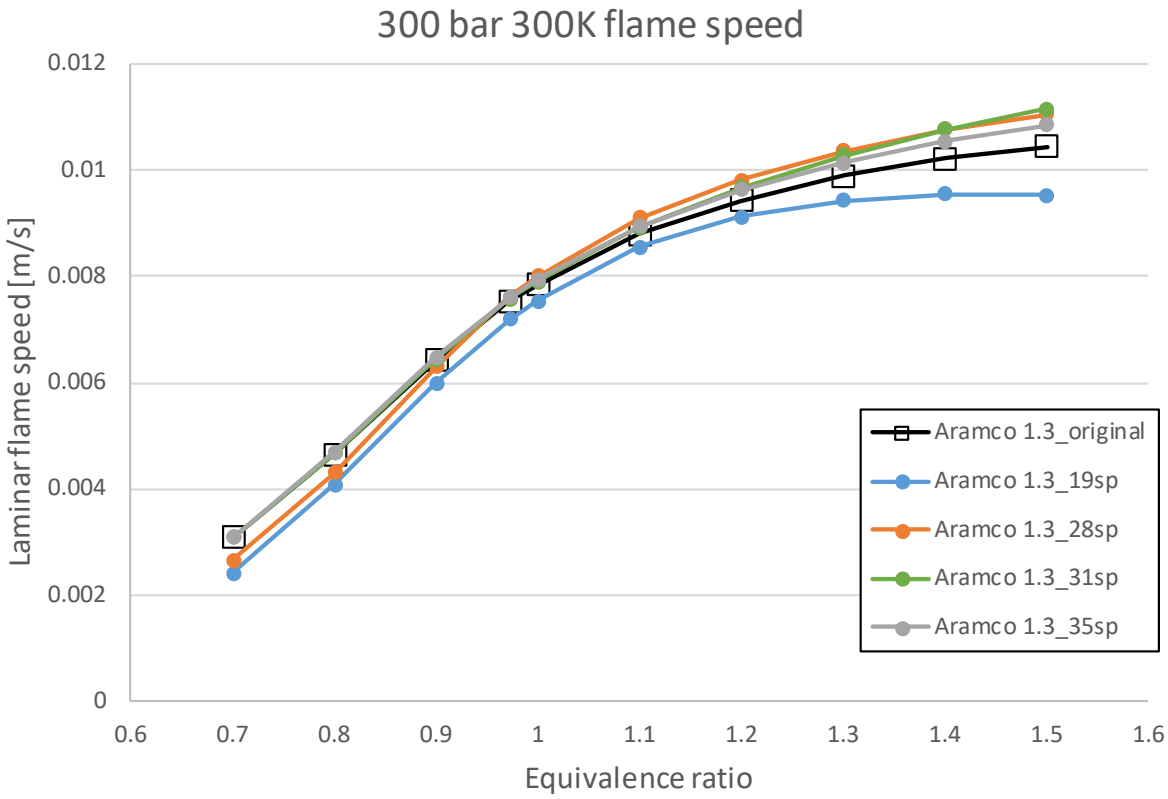

Figure 12. Laminar Flame Speed Comparison at 300 Bar

Combustor 2-D axisymmetric CFD studies were conducted using reduced Aramco 31 species chemistry model in order to understand the combustor design parameters. The injection

velocities of fuel, oxidizer, and recycled streams were varied as well as the swirl strength of oxidizer stream. The recycled flow was distributed along the combustor liner to provide the proper film cooling effect. Table 5 summarizes the simulation parameters. For each case, the temperature distribution and CO mole fraction at the combustion exit, combustor inner wall temperature, and pressure drop were evaluated.

Table 5. Summary of Combustor 2-D CFD

Case #	Combustor			Average Injection Velocity [m/s]			Oxidizer Swirl Angle [deg]	Note
	Qty.	Inner Diameter [m]	Length [m]	Fuel	Oxidizer	Recycle		
1-0	8	0.24	2	25.0	25.3	24.1	45	Fuel injector no recess
1-1								Fuel injector 0.5D recess
1-2								Fuel injector 1.0D recess
2-0	12	0.2	2	11.6	36.7	23.1	45	
3-0	12	0.24	2	10.3	21.8	8.0	48	Radial angle on Oxidizer flow
3-1							58	
3-2							64	
4-0	12	0.24	2	10.3	14.8	8.0	59	Removed radial angle on Oxidizer
4-1							67	
4-2							72	
5-0	12	0.24	2	10.7	42.8	5.1	45	Oxidizer staging
5-1							45	No oxidizer stating
6-0	12	0.48	2	10.7	23.5	7.4	45	Reduced combustor exit area
6-1							45	Matching area of combustor exit to the turbine inlet
7-0	6	0.48	2	21.3	46.9	8.2	45	
7-1	8	0.48	2	16.0	35.2	6.1	45	
7-2							60	
7-3							75	
8-0	4	0.4	1.25	25.5	57.4	7.2	45-60	80% recycled flow
8-1					46.4		45-60	
8-2					96.8		45-60	

Figure 13 shows the temperature profile and velocity streamline results of case 8-2. Oxidizer swirl created a strong inner recirculation and the recycled flow kept the inner wall temperature of combustion liner below 2,100°F (1,150°C). The average exit temperature is about 1,300°C because only 80% of recycled flow was introduced in the combustor for this case. The remaining 20% of recycled flow will be utilized for the film cooling on the plenum structure, which connects

combustor and turbine inlet. 2-D CFD results is the basis of 3D CFD study to design of the combustor and plenum as a whole.

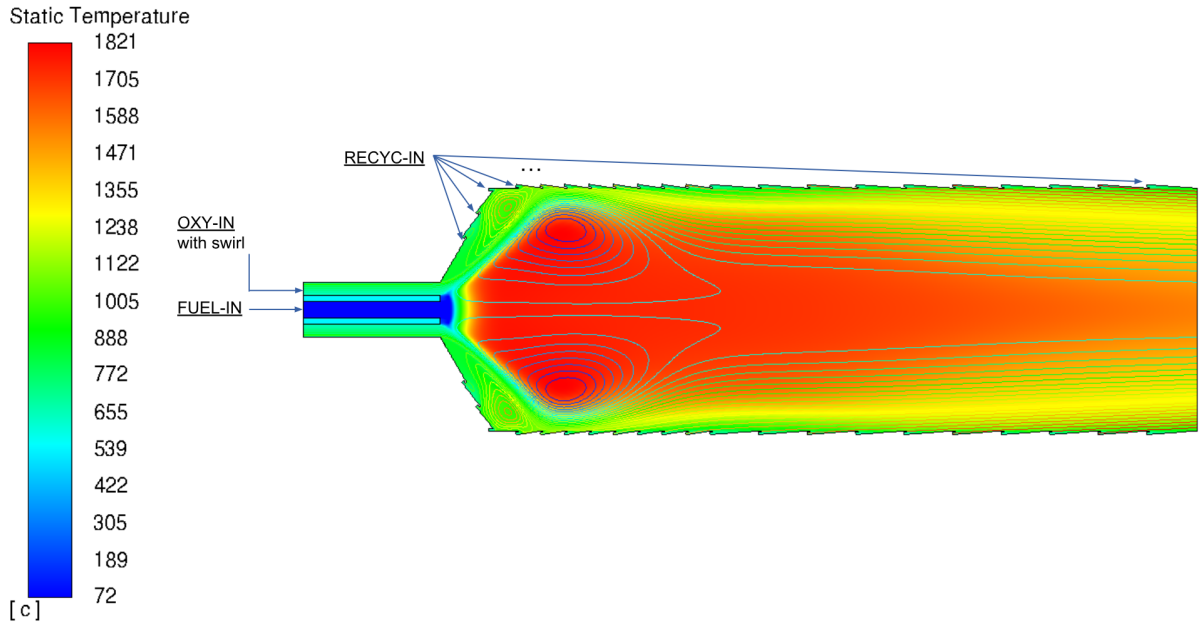

Figure 13. Case 8-2 Temperature and Velocity Streamline

For a back-to-back turbine configuration, four combustors are evenly spaced radially and connected to the transition plenum as shown in Figure 14 (a). Similar to 2D CFD cases, fuel is injected in the middle and the oxidizer is introduced in the annulus with swirl. Recycled flow is to keep the inner temperature of combustor liner and transition plenum below the limit. Half of quarter combustor is modeled for 3D CFD study. The combustor liner has 0.4 m of inner diameter and 1.2 m in length. Figure 14 (b) shows the boundary conditions for 3D CFD case. Main turbine cooling flow is relatively easier to be obtained at the bottom of transition plenum. For the first 3D simulation, 5% of main cooling flow is used in that section.

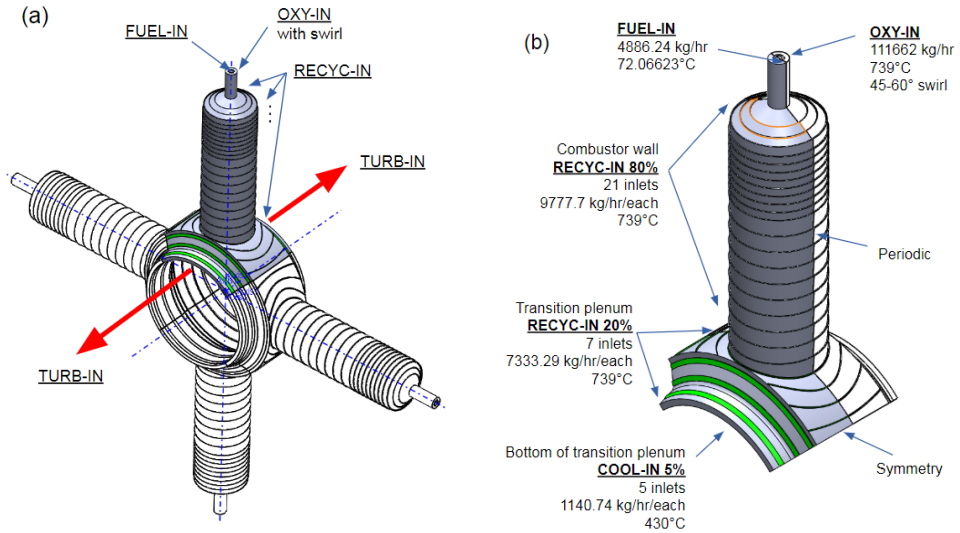

Figure 14. (a) ISO view of conceptual combustor geometry, and (b) 3D CFD fluid volume and boundary conditions

The reduced multi-chemistry reaction mechanism is used for this case same as 2D cases. Figure 15 shows the results of temperature profile, velocity magnitude and CO mole fraction at the turbine inlet. The overall temperature profile is consistent to the result from 2D cases. Although the velocity magnitude is relatively uniform at the turbine inlet, the temperature varies from 904°C to 1,330°C. Further optimization will be needed to make turbine inlet flow uniform.

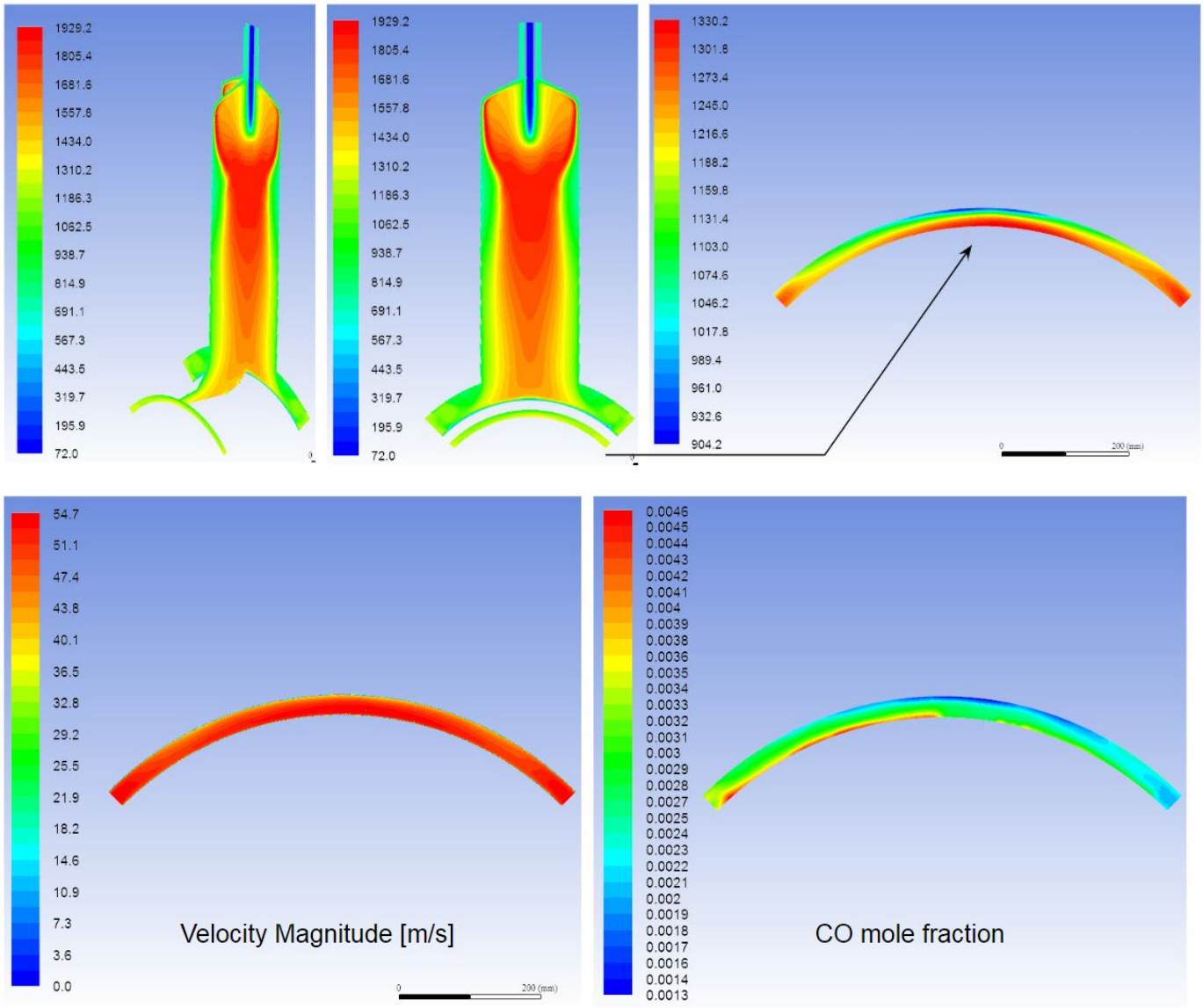

Figure 15. 3D CFD results: Temperature profile in degree C, and Velocity magnitude [m/s] and CO mole fraction at the turbine inlet

For this case, periodic and symmetric boundary conditions are applied for the half quarter of the combustor CFD for efficient computation (Figure 14b). Combustors are radially spaced, thus periodic is more realistic than symmetric for the transition plenum boundary. However, two periodic boundaries are not applicable in Fluent simulation as the model requires two axes. Therefore, a quarter of the combustor is simulated with a periodic boundary condition for one axis as shown in Figure 16 with the results. In the previous half geometry case, the periodic boundary acts as an additional constrain in the middle of the combustor so the middle methane

jet is forced to flow straight. Asymmetrical result is mainly because this boundary condition is not applied.

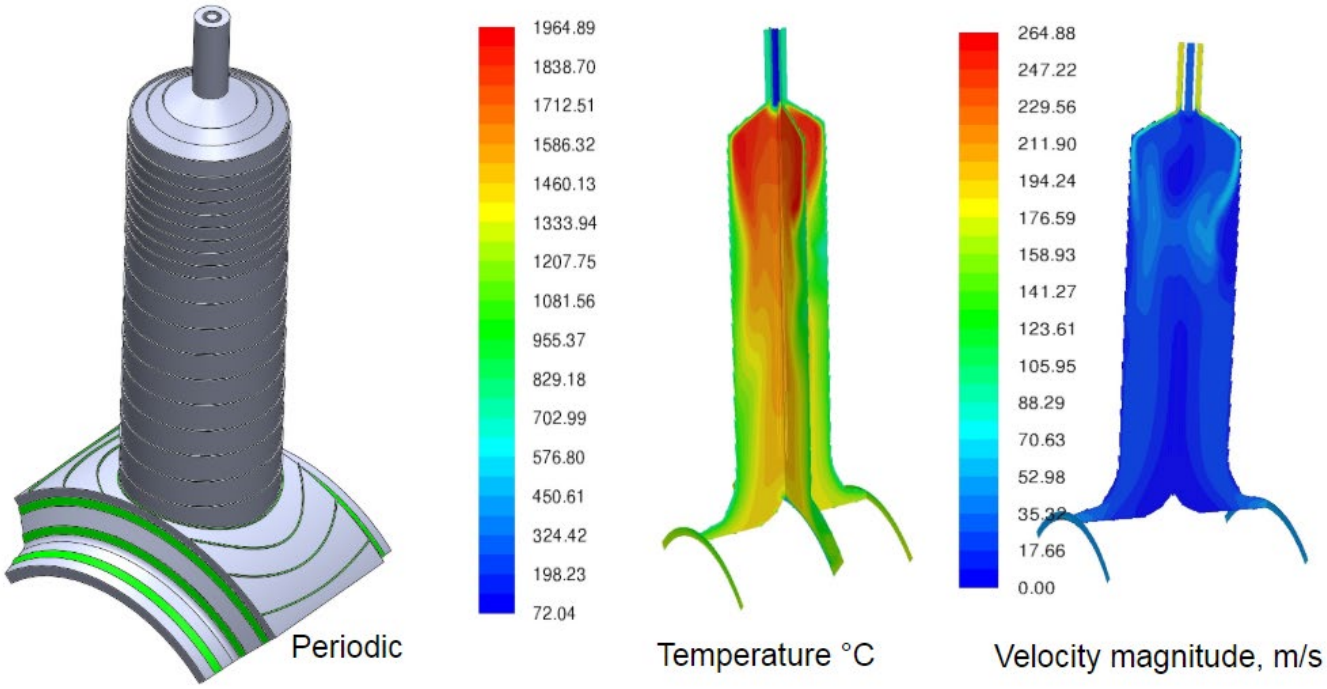

Figure 16. 3D CFD results: Temperature profile in degree C, and Velocity magnitude [m/s]

Fluent is a RANS simulation, therefore symmetrical results are expected.

Relatively larger inlet area of recycled CO_2 flow with mass flow inlet boundary condition creates non-uniform inlet velocity profile, although the mass flow rate inlet is conserved. This velocity fluctuation can be escalated to the larger perturbations with the combustion instability in the combustor can lead divergence of the entire calculation. The relaxation and turbulence chemistry interaction (TCI) factors have been modified to achieve a better convergence.

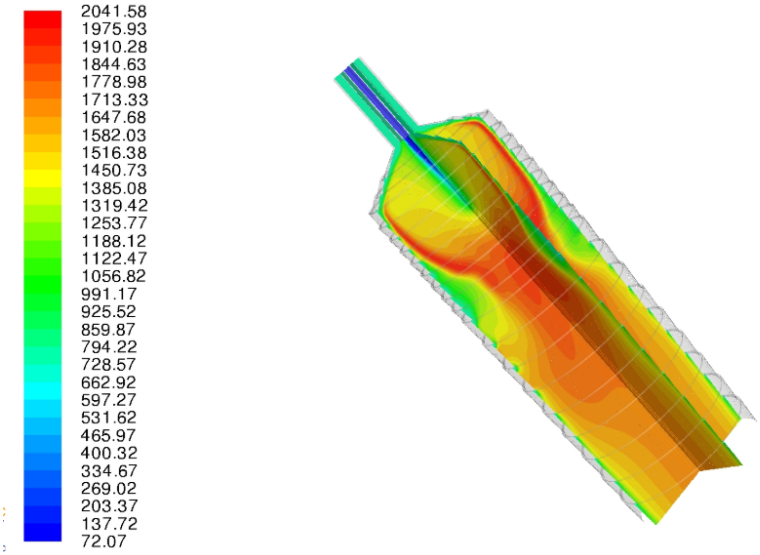

Figure 17 shows the result with smaller relaxation factors and using 20 (default is 5) as flow iteration per chemistry update in TCI setting.

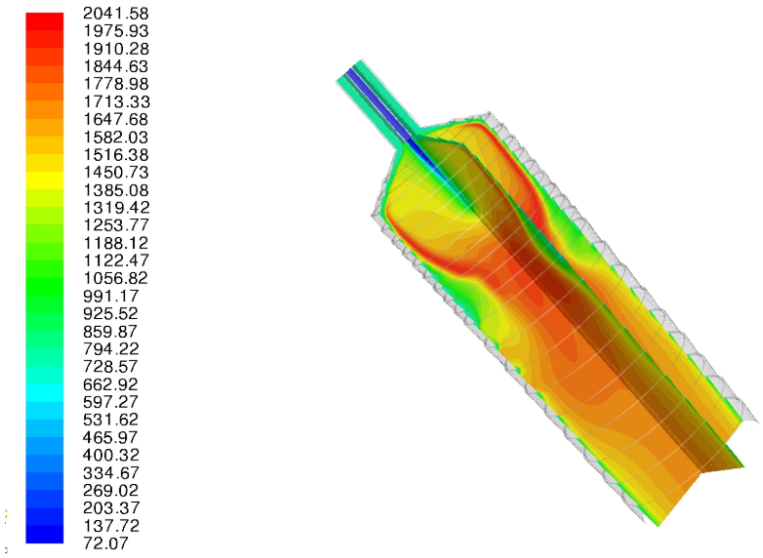

Figure 17. 3D CFD results of combustor can with manipulated relaxation and TCI factors

These modifications make the simulation much slower. The primary target is to screen the combustor can configurations. The simulations are conducted at the reasonable convergence to keep the computational efficiency. The following results are not fully converged like case 302 in Figure 17, but are calculated enough to make design decisions.

A new combustor for the straight through turbine design has been developed. Four combustor cans are investigated for an initial trial as shown in Figure 18 (case 303). The combustor cans have a 45 degree angle with respect to the axis of turbine shaft.

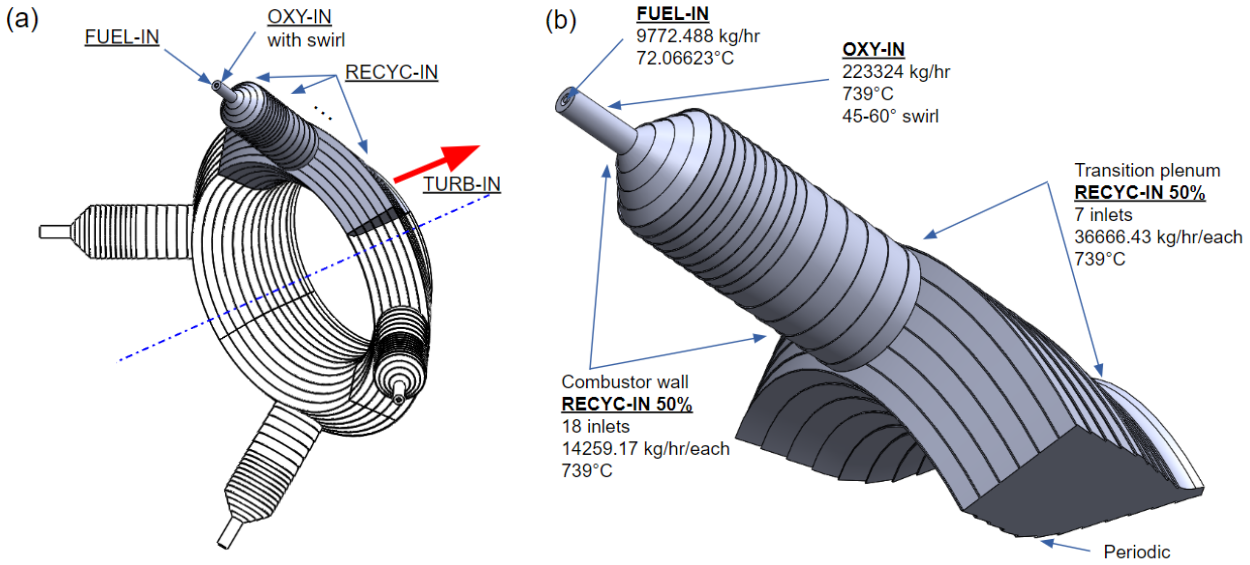

Figure 18. (a) ISO view of conceptual combustor geometry for straight through turbine design with 4 combustor cans, and (b) 3D CFD fluid volume and boundary conditions

Figure 19 shows the simulation results of case 303. Four combustor cans are not enough to generate uniform temperature and velocity at the exit of combustor plenum.

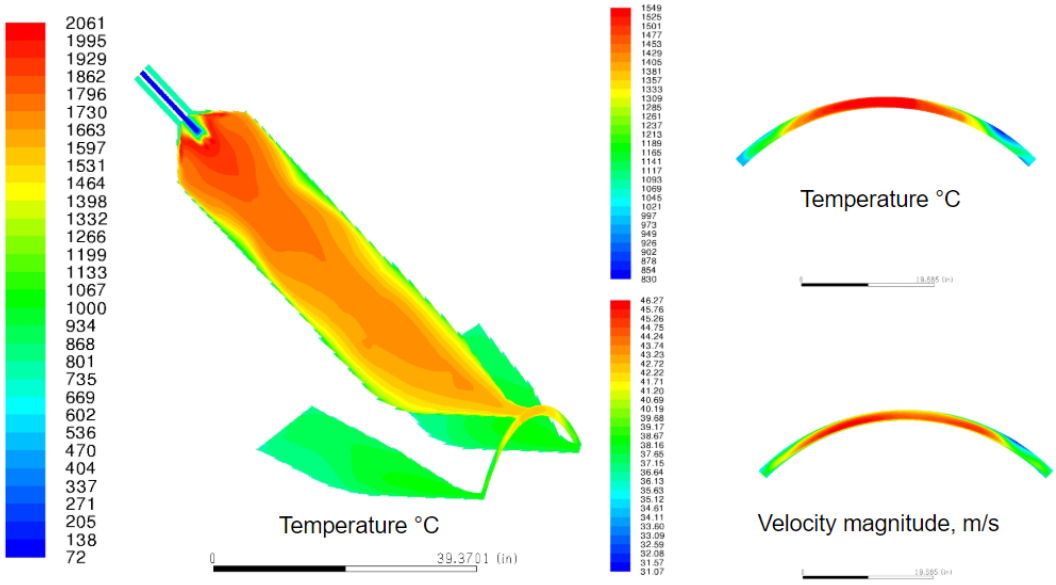

Figure 19. 3D CFD results (case 303): Temperature profile in degree C, and Velocity magnitude [m/s]

Six combustor can configuration (case 304) is studied to reduce the non-uniformity of turbine inlet conditions. The size of combustor can and flow rates of each stream are proportionally adjusted. Figure 20 shows the results. The velocity has a better distributed profile than 4 cans case and temperature differences between max and min value at the exit is also decreased compared to the 4 cans configuration.

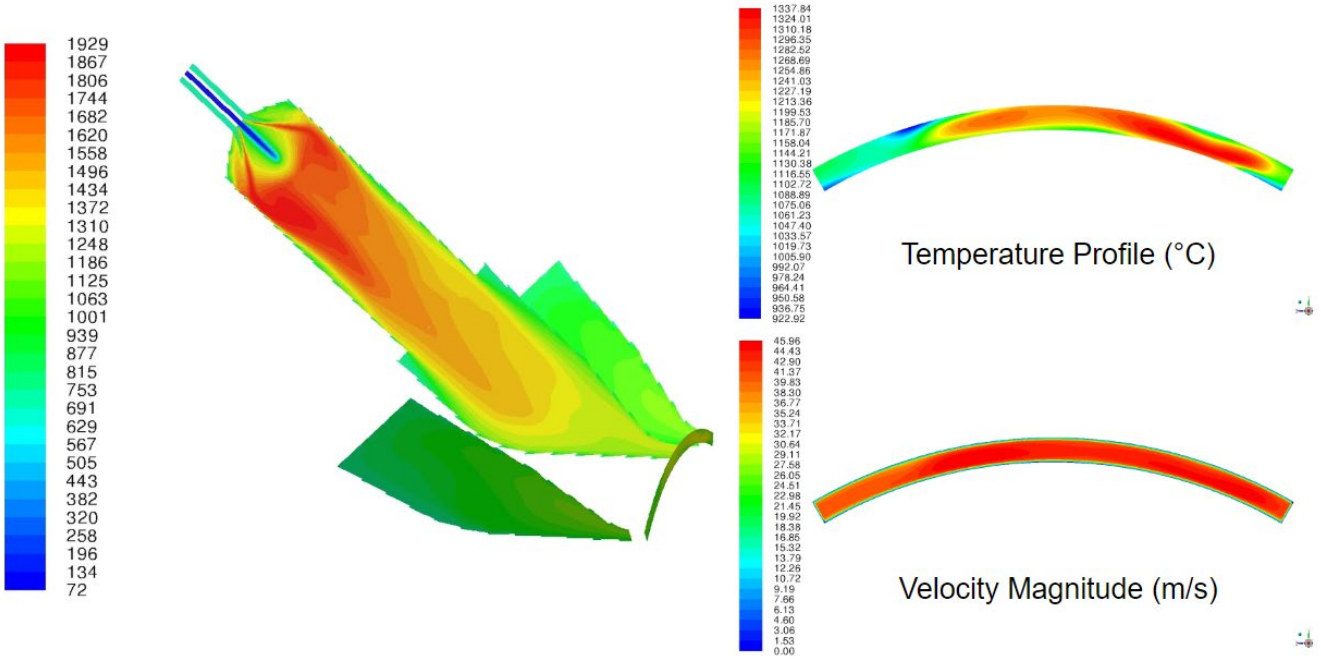

Figure 20. 3D CFD results (case 304- 6 cans): Temperature profile in degree C, and Velocity magnitude

To further reduce the temperature non-uniformity at the plenum exit, eight (8), ten (10), and twelve (12) combustion can geometries are investigated. The size of combustion can is

proportionally reduced as the number of combustion can increases while the transition plenum geometry is kept the same.

Figure 23 summarize the velocity and temperature profiles at the plenum exit. Uniform velocity profile was achieved for the case more than 6 combustion cans. As the number of can increases, the temperature profile became closer to uniform. For the case of 12 combustion cans, stronger mixing was needed to complete the reaction. 60 degrees of swirl was used for the oxidant flow instead 45 degrees.

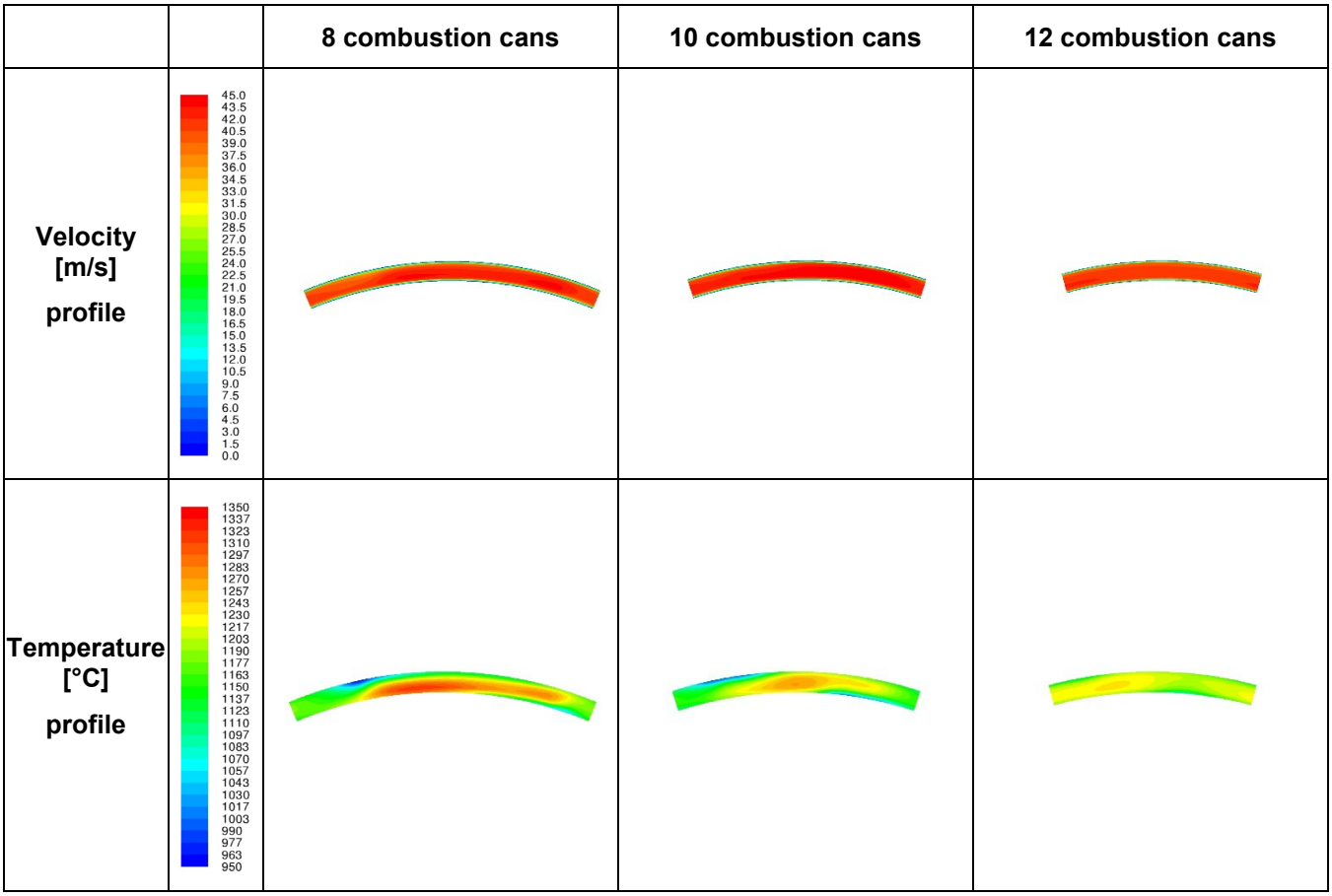

Figure 21. Summary of 3D CFD results at the transition plenum exit: Velocity magnitude and Temperature profile

Figure 22 shows the maximum and minimum temperature variation of each case normalized by the mass weighted average. More number of combustion cans generate less temperature variation difference at the transition plenum exit. Twelve (12) combustion can geometry has been selected as an overall combustor configuration.

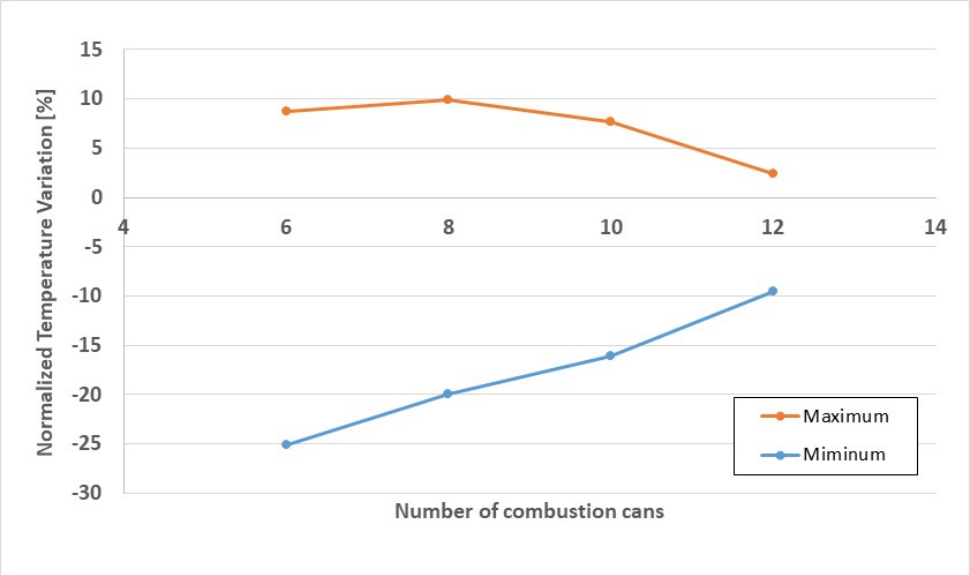

Figure 22. Maximum and Minimum Temperature Variation Normalized by the Mass Weighted Average

From the cycle modeling, extra O2 flow is expected at the combustor exit (Table 1). However, CFD results show certain amount of CO at the exit while mass fraction of CH4 and O2 are in the order of 10^{-6}. This discrepancy would be attributed from the kinetic model and combustor design which must be studied further in the next phase of the project.

The conceptual combustor design has been studied using commercial CFD software (Fluent) with reduced chemistry. Although modeling showed reasonable results, the experimental validation is needed at the operating condition. There are lack of experimental data and many estimations were made to perform the present CFD study such as turbulent models, turbulent chemistry interaction, relaxation, etc. Real gas effect can make changes of combustor performance by density deviation from the ideal gas leading local and bulk flow velocities. Chemical kinetic models are validated against only the ignition delay time and requires more experimental validation for the flame kinetics aspects. Since successful prediction of auto-ignition delays does not guarantee successful prediction on combustor performance, a small-scale flame experiment is planned for the validation of CFD results for the next phase of the project. The flame temperatures and speciation (CO, CO2, O2, CH4, C2H6, C2H4, etc.) will be measured and compared with numerical simulation. These experimental data will improve the accuracy of chemical kinetic modeling.

In addition, a Large Eddy Simulation (LES) modeling should be performed in future programs to identify the performance gap with the commercial RANS simulation software (Fluent). The simulation parameters in the commercial software can be properly adjusted to obtain similar modeling results from LES.

Task 3.3: Turbine 2-D Layout

During this quarter, there was more effort focused on laying out the conceptual case and rotor for the turbine. The previous quarter established operating conditions and initial aerodynamic layouts that would be used for some initial case calculations to help establish the design envelope. Key information needed to start the case layout:

- Inlet and Exhaust Flow Conditions

    - Temperature – Necessary materials and boundaries
    - Pressure – Wall thicknesses and case configuration
    - Volume Flow – Required flow area to keep velocities relatively low (<30 m/s)
- Aerodynamic Flowpath
    - Hub Diameter – Maximum diameter of the main shaft
    - Number of Stages – Required axial length for the turbine blades
    - Configuration – Overhung, straddle, straight through, back-to-back
- Combustor Can Geometry
    - Number of Cans – Radial spacing and organization around the case
    - Can Diameter – Required penetrations and connections to the case

Operating Conditions

Below are some of the key operating conditions that affect the overall design of the turbine:

	Inlet	Exhaust	Recycle	Cooling
Temperature [C]	1,200.0	778.4	739.0	430
Pressure [bar]	305.0	30.0	315.0	316.5
Flow [m^3/hr]	30,544	223,808	13,745	1,043.8

From these conditions, the key drivers will be inlet temperature and pressure and the exhaust temperature and flow rate. At 1,200°C, no material will have any significant strength if it can even survive the temperature. This leads to the necessity of cooling flow to cool the walls on the outside and provide film cooling. The turbine inlet flow is a mixture of fuel, oxidant, and recycle flow. The recycle flow will provide cooling mixed flow for the combustion and film cooling for the combustor cans. It is important to note that with a temperature of 739°C, the recycle flow will require high-temperature nickel allows for pressure containment.

For the exhaust, the 30.0 bar pressure is helpful in the overall design, but the high temperature and flow rate provides some significant challenges. At 778°C, material choices are limited and due to the low pressure and high flow rates, flow area will have to be large to keep velocities low to prevent significant pressure loss in the overall system. At this temperature and with a pressure ratio of 10 to 1, the exhaust flow will not be an ideal candidate for the pressure containment flow. This leads to the need for a high-pressure cooling flow to buffer the pressure vessel and also provide internal and film cooling to the hot blades and stators.

Two layouts were considered to determine which would be optimal for this application from a layout point of view. One design was a 12-stage back-to-back turbine (

Figure **23**) and the other was a straight through 5-stage turbine (Figure 24).

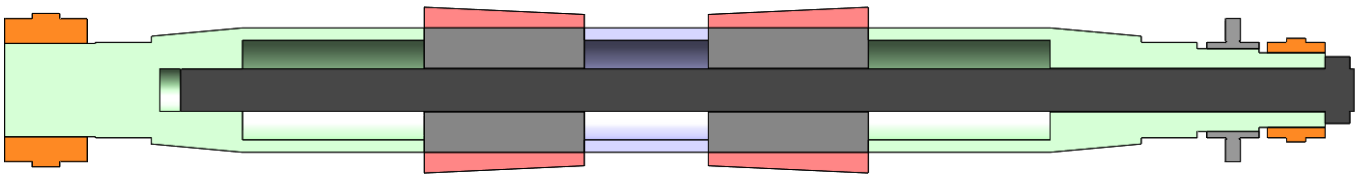

Figure 23. 12-Stage Back-to-Back Rotor Layout

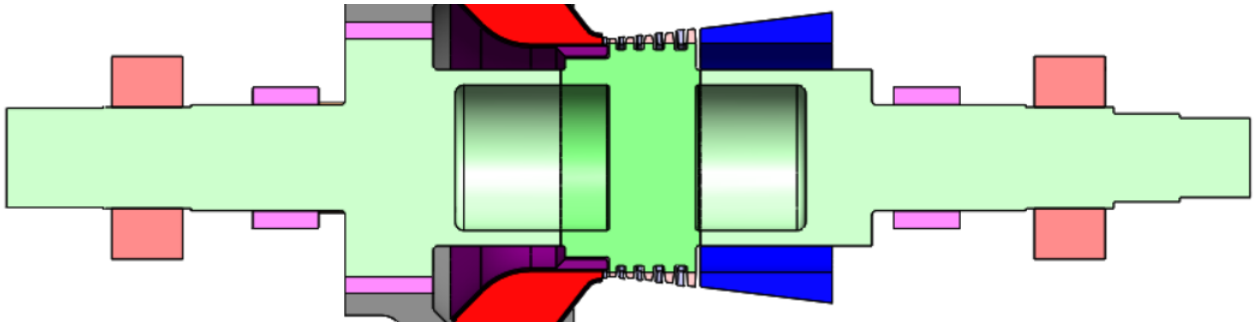

Figure 24. 5-Stage Straight Through Rotor Layout

The advantages for each design are as follows:

12-Stage Back-to-Back

- Smaller hub diameter
- In terms of mechanical design, a smaller hub diameter will lead to thinner casings and lower stresses on the turbine blades
- Due to the back-to-back design, the pressure is balanced and there is no need for a balance piston to balance the thrust
- A balance piston is a significant source of leakage

5-Stage Straight Through

- Fewer blades and overall shorter span
- Larger hub diameter
- While this is not advantageous for a case design, a larger hub diameter does lead to better rotordynamic stability
- Standard combustor layout
- No need to come in radially and split the flow in the middle
- This will lead to a potential hot section in the middle of the rotor

To decide between the two, a few items were considered:

- Total leakage
- Summarize all seals and total up all leakages to look at overall cycle performance
- Rotordynamic stability
- Rotor construction
- Case sizing
- Cooling requirements
- Combustor design

Between the two designs, the main advantage for the 12-stage back-to-back was that it would not require a balance piston. However, with the need for extra end seals, the leakage was actually more for the back-to-back design due to the cooling flow injection seals required on both

ends of the rotor to cool the rotor blades. In addition, due to the longer and skinnier shaft, the rotordynamics were marginal for the back-to-back design with no extra room for longer seals that could reduce overall leakage. Also, without a hole-pattern seal, there was no additional damping that would benefit overall stability. Because of this, the 5-stage design was selected.

Some of the main components for the straight through design are shown in Figure 25.

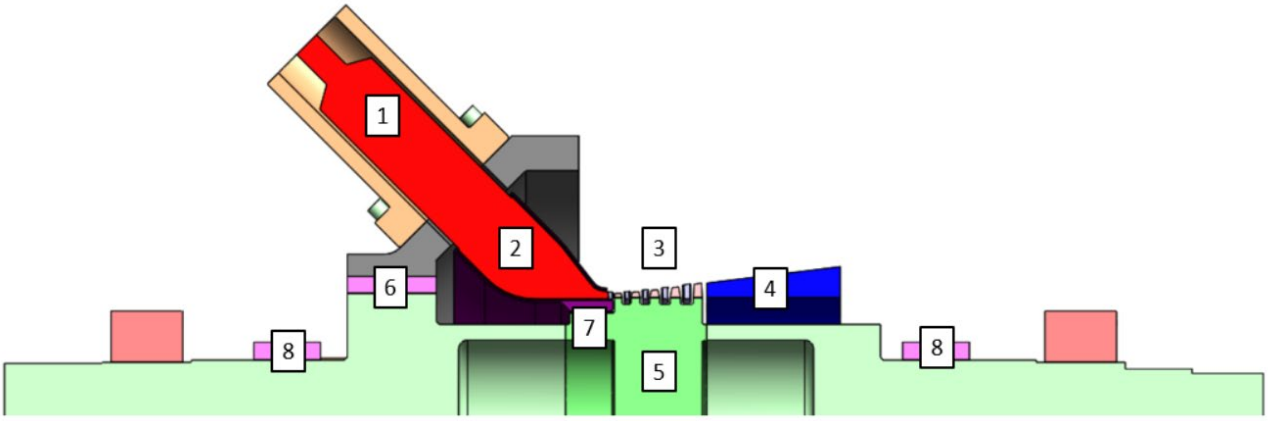

Figure 25. 5-Stage Straight Through Components

- Combustor Can (currently 4)
- Mix recycle flow and fuel
- Main can will contain recycle temperature and pressure that will be used to buffer the combustor liner (739°C at 305.0 bar)
- Cooled Inlet Plenum
- Double walled design – Combustor liner and additional liner to keep recycle flow from main case
- At temperatures below 400°C, the main case can be made out of 400 series stainless steel and have reduced wall thickness
- Aerodynamic Flowpath
- Cooled blades from the rotor
- Cooled stator vanes from the OD
- Turbine Exhaust
- Will be buffered by 30.0 bar cooling flow to maintain lower temperatures for 400 series case material
- Turbine disc and rotor
- Welded 3 piece rotor – two stubs shafts and turbine disc
- Turbine disc will be machined separately so that there will be access for cooling holes (axial and radial)
- Machine radial dove tails into disc to contain blades

- Balance Piston Seal
- Separation seal between cooling flow and stage 1 inlet
- End seals

The cooling flow through the turbine is shown in Figure 26.

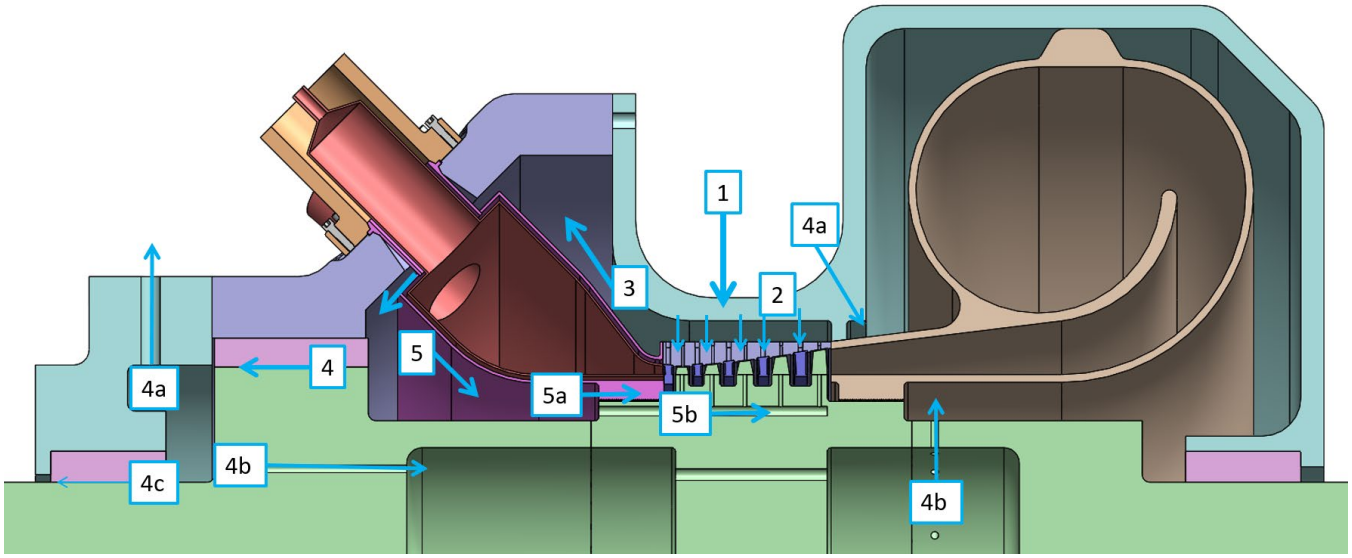

Figure 26. Cooling Flow Overview

- 1 – Main Cooling Supply to Turbine Case and Rotor
  - 400°C, 305 bar, 62.61 kg/s
- 2 – Main Cooling Supply to Stators and Blade Shrouds
  - 18.77 kg/s
- 3 – Remaining Cooling Flow that Cools Recycle Flow Liner
  - Going around the liner, this flow heats up by 3°C
  - 43.84 kg/s
- 4 – Balance Piston Flow
  - 305 bar to 30.0 bar at 19.50 kg/s
- 4a – Case cooling Flow
  - 13.6 kg/s
  - 4.53 kg/s will go to case. Remained will feed exhaust piping
- 4b – Rotor and Case Cooling Flow
  - 6.33 kg/s
- 4c – End Seal Leakage
  - 30.0 bar to atmosphere

- 1.8 kg/s. Same as other end of machine

- 5 – Remained of Cooling Flow to Buffer Recycle Flow Liner
  - 24.34 kg/s
- 5a – Stage 1 Buffer Flow
  - 5.40 kg/s
- 5b – Blade Cooling Flow
  - 19.94 kg/s

To verify needed flows, internal pipe flow calculations were performed on every section surrounding a hot liner. This was mainly focused on the recycle flow liner around the combustor cans and the exhaust liner. The goal of these cooling flows is to maintain a case temperature near 400°C to allow for high allowable stresses of readily available 400 series stainless steel for the main case. This will save overall cost and complexity of manufacturing. Figure 27 shows allowable design stresses for various materials.

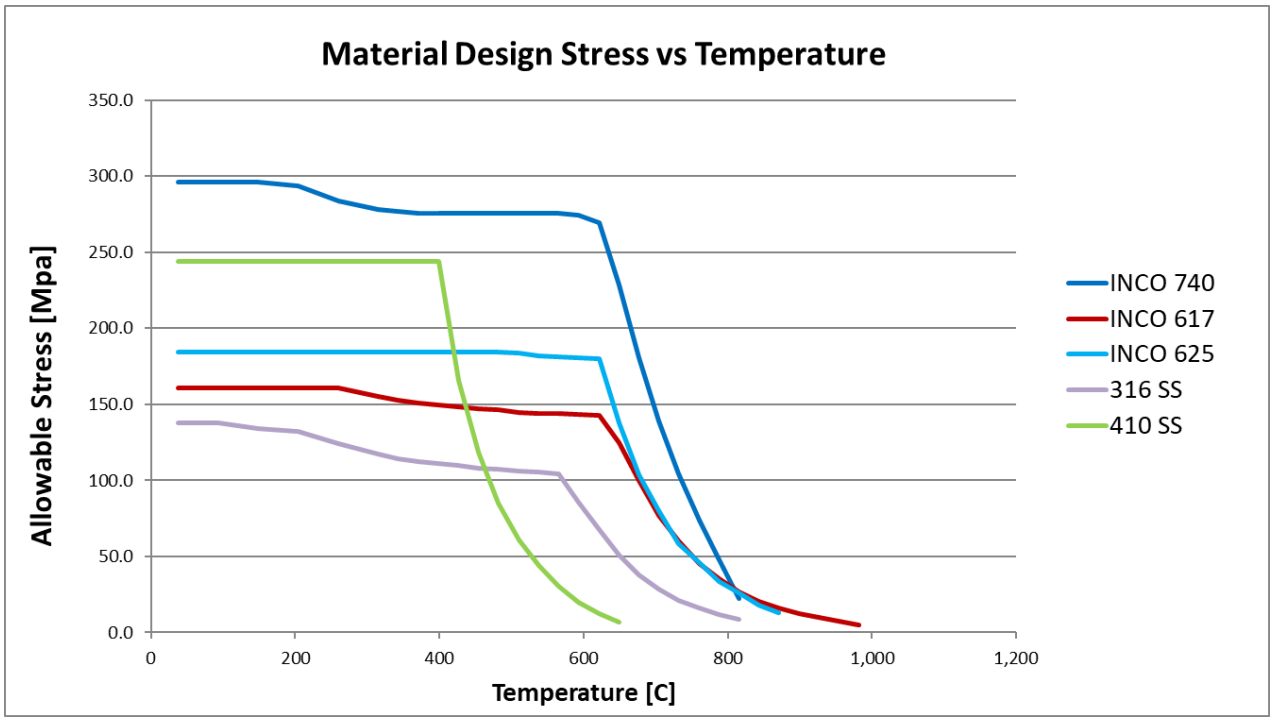

Figure 27. Case Material Design Stresses – ASME Section II, Part D. Section VIII-2 Applications

What can be seen in Figure 27 is that 410 SS maintains a relatively high allowable stress up to 400°C before the allowable stress begins to drop quickly. It rivals INCO 740, but is much cheaper and more readily available. SwRI has experience with using 410 SS for sCO_2 applications and it provides good corrosion resistance, while being easy to machine and forge, and also having high allowable stresses to reduce wall thickness and aid in transient performance of the case.

$$h = \frac{Nu_D k}{H_D} \quad (1)$$

$$Nu_D = \frac{f}{8}(Re_D - 1000)\left(\frac{Pr}{1 + 12.7\sqrt{\frac{f}{8}}(Pr^{\frac{1}{3}} - 1)}\right) \quad (2)$$

$$H_D = \frac{4A}{P} \quad (3)$$

$$Re_D = \frac{\rho U H_D}{\mu} \quad (4)$$

$$R = \frac{1}{hA} \quad (5)$$

$$q = \frac{\Delta T}{\sum R} = \dot{m}\Delta H \quad (6)$$

Where h is fluid heat transfer coefficient; Nu_D is Nuesselt Number; k is fluid thermal conductivity; H_D is hydraulic diameter; f is friction factor based on Reynolds Number; Pr is fluid prandtl number; Re_D is Reynolds Number based on Flow diameter; A is flow area; P is flow perimeter; ρ is fluid density; U is fluid velocity; μ is fluid viscosity; q is energy gain / loss; R is fluid resistance; ΔT is temperature difference across liner; $\dot{m}$ is mass flow; and ΔH is change in enthalpy of a fluid.

By using these equations, the heat pick up across the liner can be calculated based on the mass flow of the recycle flow at 740°C and the cooling flow at 400°C. This simple model assumes that the recycle mass flow is constant throughout the boundary. However, this flow will reduce to near zero as it will be used to buffer the combustor liner, which means the change in temperature of the cooling flow is on the conservative end.

Comparing the high pressure (inlet/combustor) and the low pressure (exhaust), there is much more temperature rise on the exhaust side due to a slightly larger ΔT and higher fluid velocities due to lower density flow. On the inlet side, the temperature rise is only 3°C compared to 25°C on the exhaust end. This is also due to the high mass flow required to supply the balance piston seal, stage 1 buffer seal, and blade cooling. Due to the low temperature rise, no extra flow is needed on the inlet side to cool the case. Since the exhaust casing will repurpose balance piston flow, the inlet to the case would need to be around 375°C to keep the exhaust case below 400°C. However, since the exhaust is only seeing 30.0 bar, a higher temperature will not lead to much thicker walls. At this size, there will most likely be a minimum wall thickness from a manufacturing perspective that would lead to extra design margin even with the case at a possible 425°C.

In addition to evaluating the turbine casing and cooling models, it is also important to look at the exhaust piping. One of the factors that limits the cycle is the maximum temperature of the exhaust. Due to the need for recuperation, the exhaust cannot be completely buffered by cooling flow like the combustor, blades, and vanes. This would lead to less effective recuperation and would hurt the overall cycle. By maxing the exhaust temperature at 778°C, the turbine inlet is capped at 1,200°C and limits the overall cycle efficiency. There are also options at increasing pressure ratio, but that will involve to need for more compression power in the loop. A few concepts were looked at to try and reduce the exhaust temperature before going into a more conventional printed circuit heat exchanger (PCHE) that can be compact compared to a shell and tube heat exchanger and also have high effectiveness leading to higher cycle efficiencies.

This particular concept looked into the possibility of having piping with internal recuperation. This would allow for low pressure and high temperature piping along with small tubing to contain the high pressure of the recycle flow. Figure 28 shows a sketch of the concept.

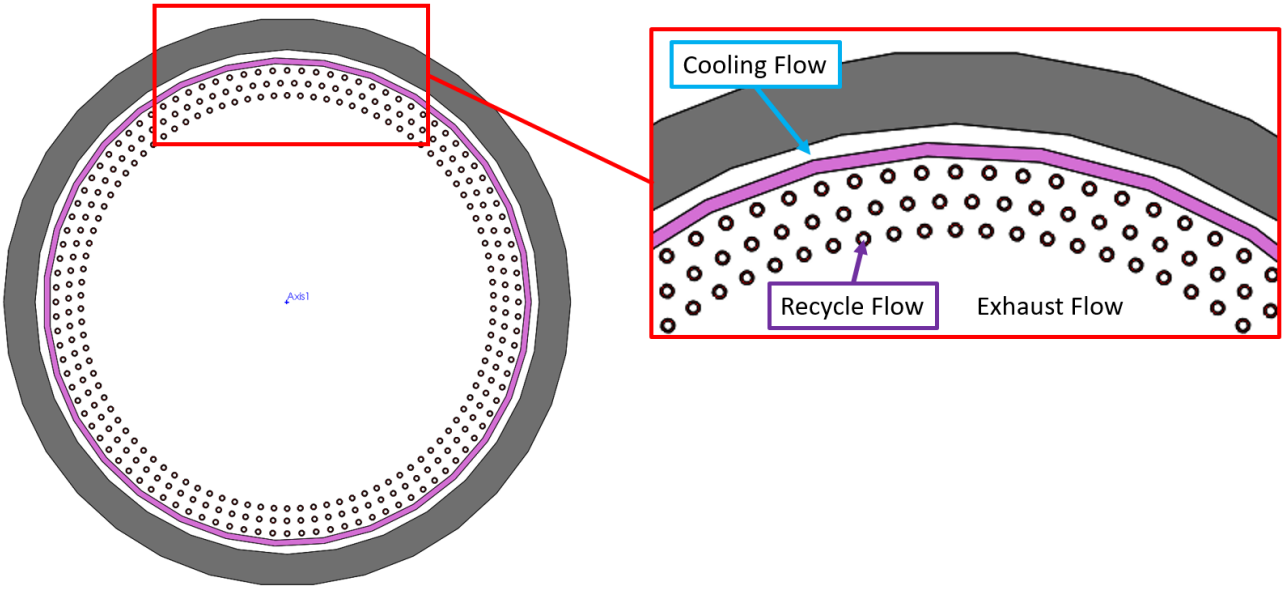

Figure 28. Recuperated Piping Concept

Using similar equations and relationships as used for looking at case cooling, it was determined that this design could be achievable with the following design requirements:

- 4 main exhaust pipes with an ID of 32” (812.8 mm)
- 1000X ¼” (6.4 mm) Tubes running in each pipe
- Internal liner for either cooling flow or insulation and using air natural convection to keep the pipe cool
- 25 feet (7.62 m) of length per section

This would allow the flow temperature to be reduced to 650°C which will allow for the use of 300 series stainless steel, which would reduce the cost of the recuperator significantly. Further design and analysis will need to be focused on optimizing this design and also looking at manufacturing methods to successfully make this system.

Task 3.4: Turbine Rotordynamic Analysis

Turbine Seal Leakage Estimations

Seals associated with secondary leakages will be required for both the inline and back-to-back turbine designs. Several iterations of seal leakage predictions evolved during the design process this quarter. The two main goals of the preliminary seal calculations are to estimate the secondary leakage rates (to aid in the cycle model efforts), and to help in the down-selection between the two rotor configurations (back-to-back versus inline designs).

This preliminary analysis considers annular seals, including both labyrinth and hole-pattern type seals. Labyrinth seals are quite common on many turbomachinery applications; however, their

impact on rotordynamic stability is often negative and must be considered in the lateral rotordynamic analysis. Hole-pattern seals are known for providing effect damping and improving rotordynamic stability, but usually sacrifice leakage.

Initial annular seal leakage estimations are performed with bulk-flow rotordynamic codes. Labyrinth seals are modeled with the XLLaby code within TAMU's XLTRC2 software. This is a bulk-flow code with single control volume assumption per cavity, and includes both real gas and ideal gas models. The hole-pattern seals are modeled with ISOT seal code in TAMU XLTRC2. This code includes two-control volume bulk-flow assumptions with an isothermal model. The ISOT seal code has the capability to predict frequency dependent force coefficients for hole-pattern and honeycomb seals, which will be later used in the lateral rotordynamic analysis. Only the leakage calculations are shown for the purposes here.

Shaft end seals will be required for both the inline and back-to-back designs. The end seals are assumed to be labyrinth seals and will experience flow at 30 bar at 400°C to atmosphere conditions. The end seal geometry assumes a 24" (609.6 mm) shaft diameter with varying length (up to 20" [508mm]) and clearances. The anticipated end seal leakage ranges from below 3 to over 4 lbm/s per end seal, calculated with the XLLaby seal code. Therefore, the total leakage for two end seals is estimated to be on the order of 6 to 8 lbm/s (2.7 to 3.6 kg/s).

For the back-to-back design, two cooling-flow injection seals will be required. This preliminary analysis assumes a 33" (838.2 mm) diameter, two seals at 10" (254 mm) long each, and a 33 mil (0.84 mm) diametral clearance. If hole-pattern seal is selected for the cooling-flow injection seals, the combined leakage for two, 10" (254 mm) long hole-pattern seals is predicted around 96 lb/s (43.5 kg/s) (or about 48 lb/s [21.8 kg/s] per 10" [254 mm] seal). If a labyrinth seal is selected, the combined leakage for two, 10" (254 mm) labyrinth seals is around 86 lb/s (39 kg/s) (or about 43 lb/s [19.5 kg/s] per 10" [254 mm] seal). While there is a marginal improvement in leakage with the labyrinth seal, it is expected that a hole-pattern seal will be needed for the lateral rotordynamics. In addition, lengthening the seal would improve leakage, however, the lateral rotordynamics cannot tolerate increasing bearings span.

For the inline turbine design, the balance piston will likely require a hole-pattern seal to add effective damping and improve rotordynamic stability. The balance piston calculations assume a hole-pattern seal at 54" (1.37 m) diameter, with varying length and clearances. Figure 29 shows the input parameters and predicted leakage rates for the hole-pattern balance piston seal associated with the inline turbine design. Assuming a 20" (508 mm) length hole-pattern, the predicted balance piston leakage ranges from about 43 to 69 lbm/s (19.5 to 31.3 kg/s) depending on clearance. Depending on the response amplitudes in the rotordynamic analysis, the 40 mil (1.02 mm) diametral clearance may have to be implemented.

Hole-Pattern Seal Parameters, Oxy-Turbine, Balance Piston					
Property	Units	L = 15"		L = 20"	
		30 mil cl	40 mil cl	30 mil cl	40 mil cl
Supply Pressure	psi	4445.4	4445.4	4445.4	4445.4
Exit Pressure	psi	435.1	435.1	435.1	435.1
Reservoir Temperature	Deg F	752	752	752	752
Seal Diameter	in	53.95	53.95	53.95	53.95
Seal Length	in	15.00	15.00	20.00	20.00
Inlet Clearance (radial)	in	0.0150	0.0200	0.0150	0.0200
Exit Clearance (radial)	in	0.0150	0.0200	0.0150	0.0200
Cell Vol to Area Ratio	in	0.044	0.044	0.044	0.044
Inlet Preswirl Ratio (de-swirl)	--	0.2	0.2	0.2	0.2
Entrance Loss Coefficient	--	0	0	0	0
Exit Recovery Factor	--	1	1	1	1
Absolute Viscosity	lbm/ft-s	2.394E-05	2.3944E-05	2.3944E-05	2.3944E-05
Molecular Weight	--	44.01	44.01	44.01	44.01
Specific Heat Ratio	--	1.3358	1.3358	1.3358	1.3358
Compressibility Factor	--	1.0269	1.0269	1.0269	1.0269
Predicted Leakage, ISOTSEAL	lbm/s	50.4	80.1	**42.4**	68.6

Figure 29. Hole-Pattern Balance Piston Seal Parameters and Predicted Leakage

In summary, the overall seal leakage rate of the inline rotor design is predicted to be improved over the back-to-back design for this preliminary analysis. This preliminary analysis suggests the leakage of the balance piston for the single flow turbine design is likely more manageable than the two cooling-flow injection seals for the back-to-back design for the provided assumptions. However, if the back-to-back turbine design is pursued, the axial length and clearance for the cooling-flow injection seals must be carefully considered as well as the impact on the rotordynamic analysis.

It is noted that all preliminary seal calculations assume annular seals for both inline and back-to-back turbine designs. Face seals were also considered have the benefit of a reduced axial length requirement, reducing rotor length and bearing span, theoretically improving the lateral rotordynamics. The leakage estimates and rotordynamic impact of the reduced length requirement of face seals were also evaluated.

Turbine Preliminary Lateral Rotordynamic Analysis

The oxy-turbine design team evaluated two main rotor configurations, including a back-to-back and inline turbine designs. Figure 30 provides the preliminary rotor geometry and beam models used in this preliminary lateral analysis. The back-to-back design includes a tie-bolt that connects the stub shafts and bladed sections. The inline turbine design also includes a tie-bolt with an overall shorter configuration. It is noted that the rotor geometry below reflects the assumed geometry for the preliminary lateral rotordynamic analysis in this quarter. The turbine design team is currently updating the lateral rotordynamic analysis, including the latest rotor geometry.

The turbine sections, thrust collars, and coupling hubs are modeled as lumped mass and inertia values for both designs. The journal bearings are assumed to be 23” (584.2 mm) diameter tilting-pad journal bearing (TPJBs) for both rotor configurations. For large machines of this class,

support and foundation flexibility will impact the rotordynamics. The preliminary lateral rotordynamic analysis assumes support or foundation flexibility at stiffness of 5e6 lb/in (8.8e5 N/mm) per bearing.

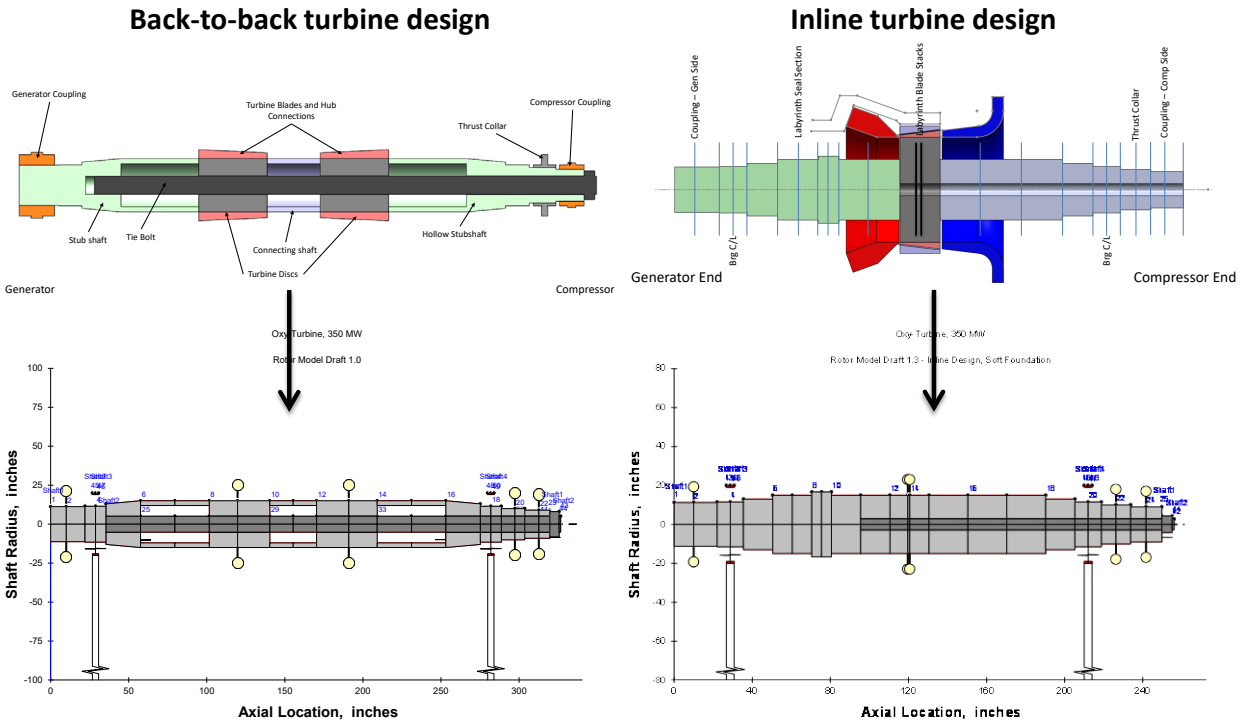

Figure 30. Preliminary Rotor Geometry and Rotordynamic Beam Element Models for the Back-to-Back Design (Left) and Inline Design (Right)

Figure 31 below shows the undamped critical speed (UCS) map for both the back-to-back and inline turbine designs, with and without foundation flexibility. This UCS calculation provides the predicted lateral modes, without damping, as a function of journal bearing stiffness. For the UCS maps with soft foundations (right plots in Figure 31), the foundation stiffness is held at a constant value of 5e6 lb/in (8.8e5 N/mm), while the journal bearing fluid-film stiffness is varied. With a rigid foundation, both the back-to-back and inline turbine designs are expected to operate near or slightly below the second mode. With a soft support or foundation, the bending mode (third rotor mode) for the back-to-back design is predicted to move near running speed, as denoted by a circle in Figure 31. The inline design with a soft foundation still maintains a separation margin with the bending mode.

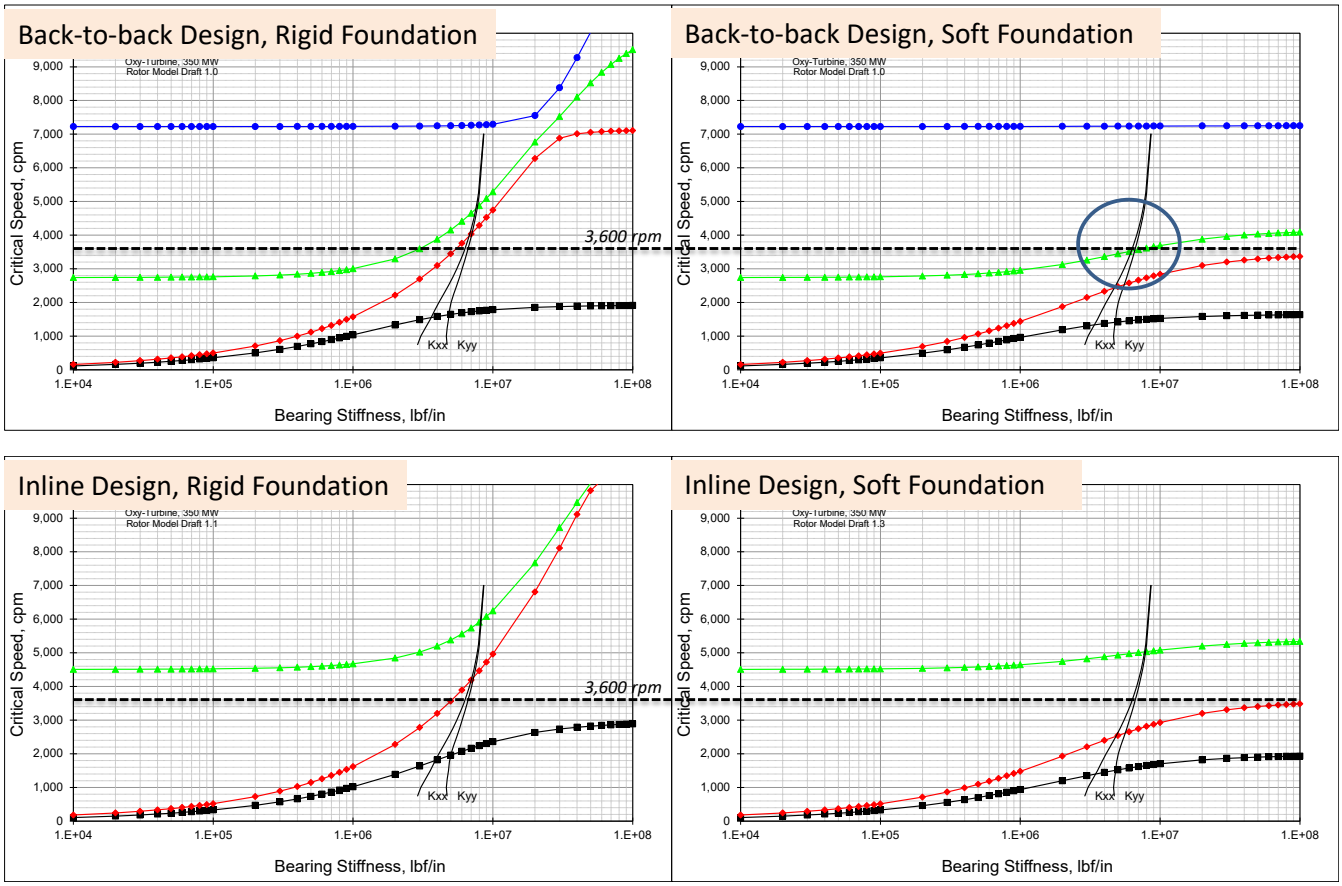

Figure 31. Undamped Critical Speed Map: Back-to-Back Design (Upper Plots) and Inline Design (Lower Plots)

The unbalance response analysis considers the synchronous excitation of the rotor due to unbalance with full bearing effects, including bearing damping. This analysis assumes an unbalance amount of approximately 277.59 oz-in, based on the criteria provided by API (American Petroleum Institute). An example of the unbalance response is shown below in Figure 32 for the predicted response at bearing 1, for both the back-to-back (upper plots) and inline turbine design (lower plots). The bearing response is calculated for both the rigid foundation (left plots) and soft foundation (right plots). As noted in the UCS analysis, the third critical speed, or bending mode, is placed on running speed for the inline design when considering a soft foundation. The response for the inline turbine rotor design shows good separation margins for both the second and third critical speeds.

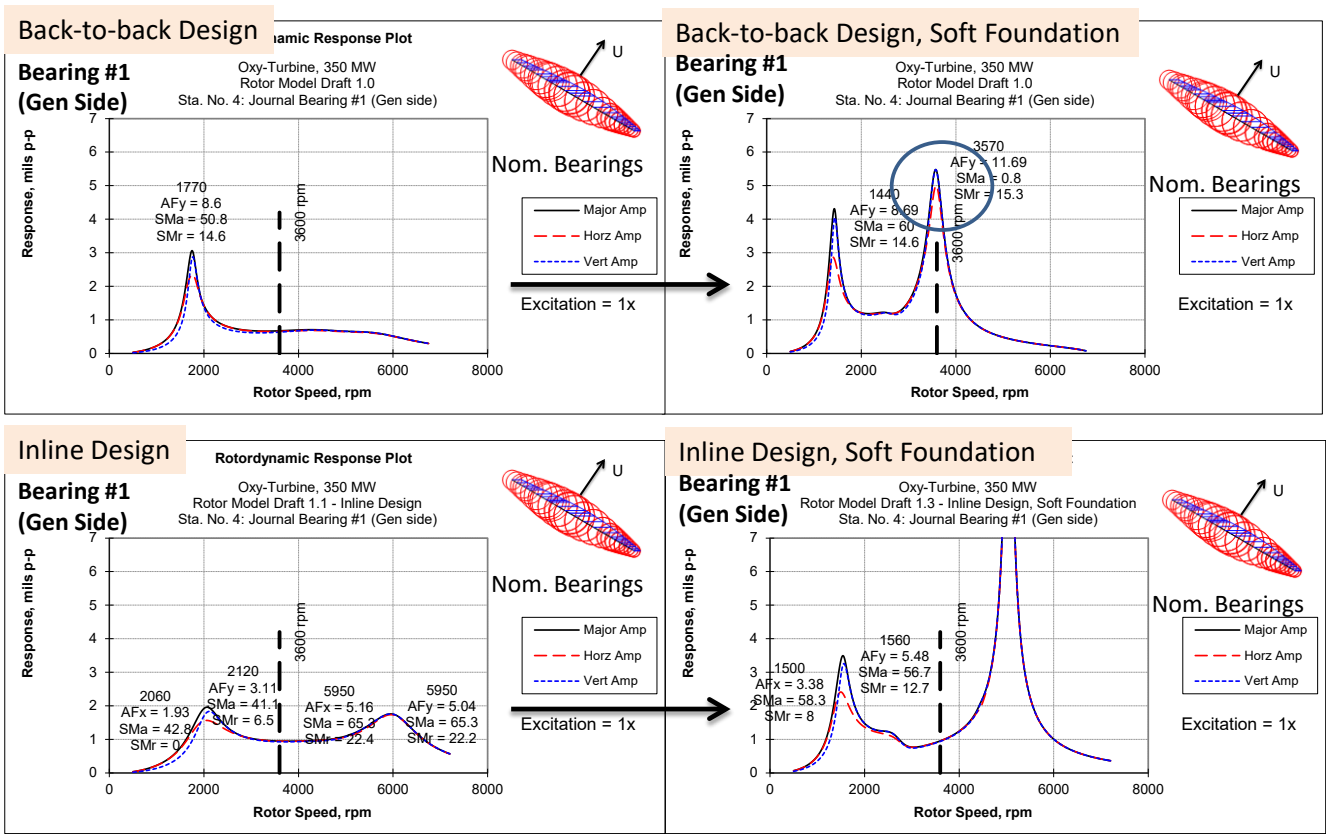

Figure 32. Predicted Response at Bearing 1: Back-to-Back Design (Upper Plots) and Inline Design (Lower Plots)

A preliminary lateral rotordynamic stability analysis was also conducted for both back-to-back and inline turbine designs. An Alford force calculation was applied to estimate the aerodynamic destabilizing force or cross-coupling from each stage. The Alford force was originally developed to quantify destabilizing forces of non-symmetrical clearances created by eccentric operation on gas turbines. Following the Alford force equation provided by API, the destabilizing cross-coupling for the back-to-back and inline designs are estimated at about 205,000 lb/in (35,900 N/mm) and 289,000 lb/in (50,600 N/mm), respectively. The rotordynamic stability analysis calculates the logarithmic decrement (log dec) values associated with the first damped mode to assess stability. Figure 33 below provides the log dec sensitivity plots for both the back-to-back and inline designs, including rigid and soft foundation stiffness effects. The dashed line denoted Qa refers to the nominal Alford force calculation by the API equation. Overall, the back-to-back design is considerably less stable (lower log dec). As expected, the soft foundation only lowers the log dec and reduces stability for both turbine designs.

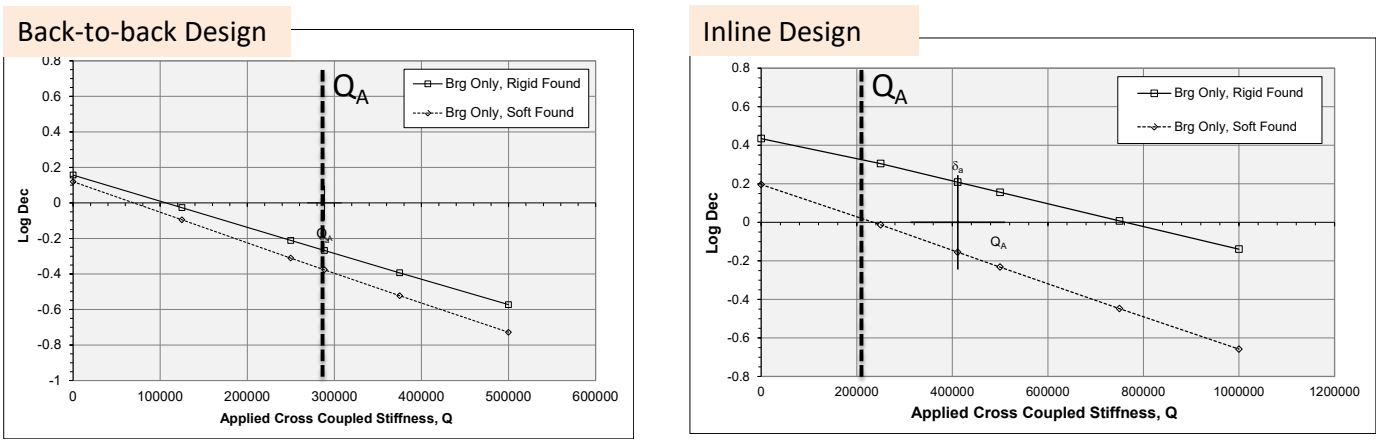

Figure 33. Rotordynamic Stability (Log Dec): Back-to-Back Design (Left) and Inline Design (Right)

Overall, the back-to-back turbine design has several rotordynamic challenges, including the placement of the third mode at running speed, and very poor rotordynamic stability (negative log dec). The back-to-back design would require significant design changes (such as reducing bearing span or increasing stiffness diameters) to improve the lateral rotordynamics. The inline turbine design shows to be promising at this point in the design process. While the unbalance response looks favorable, the rotor stability is still poor when including a soft foundation for the inline design. However, a hole-pattern seal at the balance piston is expected to add damping and improve the stability of the inline turbine design. Overall, the preliminary stability analysis clearly shows the need for the added damping associated with a hole-pattern seals.

Task 3.5: Turbine Blade Heat Transfer Modeling

The 1,200ºC turbine inlet temperature is beyond the working temperature of modern materials, and therefore, cooling is required. However, cooling fluid represents a loss of efficiency to the cycle and must be minimized. The objective of this task was to complete a conceptual design of the stage one turbine blade (S1B) and use this information to approximate the cooling flow used by the entire turbine. Additional goals of the conceptual design included identifying key risks and gaining a greater understanding of the differences of an oxy-fuel sCO_2 turbine cooling design relative to gas turbines, where there are decades of experience.

In gas turbine cooling, basic design and cooling flow estimation can be performed with relative ease using cooling technology curves, as described by Bunker (2005). These curves relate gross cooling effectiveness (Φ) to a heat load parameter (*HLP*), which are shown in Figure 34. Heat load parameter is a function of coolant mass flow rate, coolant specific heat, hot gas wetted surface area, and the average external heat transfer coefficient (taking thermal coatings into account). These curves are typically developed for gas turbine cooling using engine experience data points, and they are a function of cooling technology (e.g., a turbine component with film cooling and thermal barrier coating (TBC) will have a higher efficiency relative to one that does not). Therefore, given a target cooling effectiveness, trades can be conducted with respect to cooling flow and design complexity. The challenge of this investigation was that no technology curves existed for sCO_2 turbine cooling design, making conceptual design considerably more complex and less accurate.

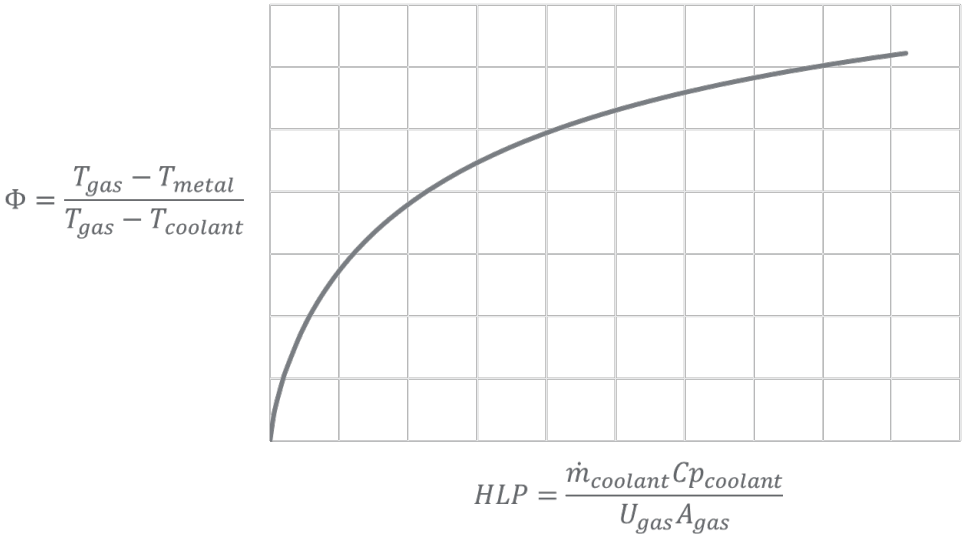

Figure 34. Example of a Cooling Technology Curve

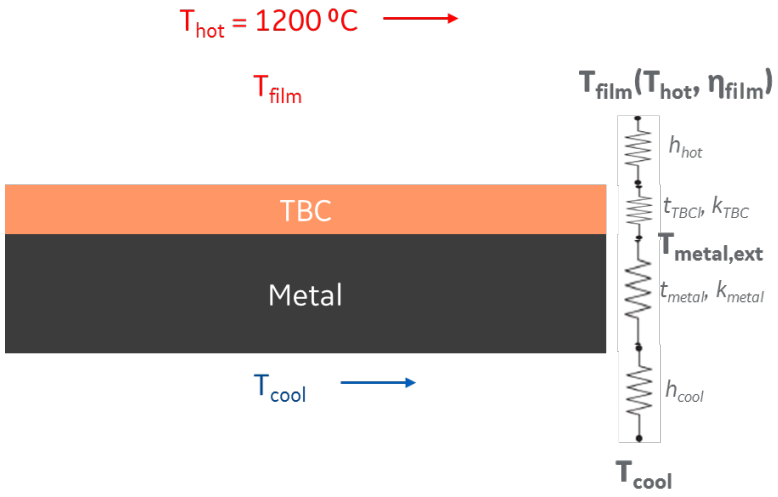

Figure 35. Schematic of the 1-D Thermal Circuit

There were two main parts of the conceptual cooling design. The first involved a 1-D heat transfer analysis of the S1B using a thermal resistance network. The main output from this analysis was a sCO_2 design curve that was used to calculate approximate cooling requirements for the turbine and perform basic trades early in the design process. The tool was primarily leveraged to compare single and double flow designs with various stage counts so that the team could efficiently down-select a layout. This analysis was clearly rudimentary; however, it was deemed sufficient for gauging relative performance of different concepts.

The hot gas and coolant conditions for the 1-D analysis were provided the cycle analysis, and the blade cross-section was prescribed from aero design. Heat transfer correlations were used to provide boundary conditions on the outer and inner walls, where the inner wall correlation was a function of coolant mass. The Reynolds number was out of the correlation's range for many heat transfer calculations, introducing additional uncertainty in the analysis. Developing correlations that are within the expected Reynolds number range (>200,000) should be a focus of follow-on work. Initial design trades were performed targeting a maximum metal temperature

of 750ºC, above which the mechanical properties of nickel-based superalloys begin to swiftly degrade. Following a preliminary analysis, multiple serpentine passages with turbulators were selected to be the foundation of the design, which is typical for a gas turbine S1B.

The most obvious difference of the oxy-fuel sCO_2 environment with respect to modern gas turbines is that the first stage hot gas path temperature of ~1,200ºC is considerably lower than gas turbines. Assuming a coolant temperature of 430ºC (from the cycle analysis) and a metal temperature of ~750ºC, the required cooling effectiveness was ~0.6, which was also lower than modern gas turbine S1Bs. Another difference that was not as immediately obvious but was quickly identified in the 1-D analysis was the disproportionate thermal resistance of the component wall and heat transfer coefficient. Relative to gas turbines, the heat transfer coefficient had a very low thermal resistance compared to the wall, indicating that the external surface temperature would be very close to the hot gas temperature. Therefore, TBC was mandatory to reduce maximum metal temperature to 750ºC. Moreover, cooling flow requirements were heavily dependent on TBC thickness, even more so than in a gas turbine, making it a key design consideration. Film cooling was also evaluated into the analysis in this stage. It was found that film cooling effectiveness was quite low with any practical quantity of cooling flow (≤ 15% of the recycle-in flow), owing to the relatively large wetted surface area of the turbine. Therefore, it was concluded that airfoil film cooling was not worth the additional complexity and cost.

The results of flow path analysis are given in Table 6. As discussed above, the objective of this analysis was to perform trades. Cooling flow increases with stage count, as expected. An unexpected outcome was that the double flow design consumed less coolant than a single flow design with the same stage count, which was due to several reasons. For one, although the airfoil stage count was similar between both designs (so the double flow had twice the airfoils), the single flow blades had significantly larger wetted surface area, nearly twice as large in some stages. Thus, the total wetted surface area was similar between the two. In addition, the single flow Mach numbers were higher, resulting in larger external heat loads. Lastly, heat transfer is generally greater in smaller channels. Therefore, the smaller airfoils in the double flow design had more efficient cooling and required less mass. The cooling flow estimates in Table 6 were added to the seals flows and traded against aerodynamic efficiency, which generally increased with stage count. The most efficient design was determined to be the 5-stage single flow layout.

Table 6. Turbine Cooling Flow Estimates for Various Stage Counts of Single and Double Flow Designs. Estimates are based on a 1-D Analysis

Flow path	Stages	Cooling (% of Recycle-In)
Single	4	4.2
Single	5	5.6
Single	6	7.5
Single	8	11.2
Single	10	15.9
Double	8	8.0
Double	10	9.2
Double	12	12.4

Once the layout was selected, the cooling analysis proceeded to the next level of detail, a finite-element thermal analysis of the S1B airfoil. Mass flow rate was calculated with a set of equations

that represented the flow network and pressure loss through the blade was determined using correlations and assuming hole discharge coefficients. Back flow and outflow margin constraints were imposed on the design. An interesting difference of this environment relative to a gas turbine is that typical cooling features (e.g., turbulators) create a smaller relative pressure drop, given the large inlet pressure. The present analysis was limited by the range of existing correlations, but there is a lot of space to improve the cooling design leveraging larger (high pressure drop) heat transfer features.

Heat transfer correlations were also used to calculate thermal boundary conditions that were mapped onto an Ansys Workbench thermal model. The thermal model was an extrusion of a mid-span S1B cross-section that was ~5% of the total span and had periodic boundary conditions on the sides. The TBC was included in the model as a separate body, but the bondcoat was not, as it typically has a second order effect on cooling. The impact of rotation on heat transfer was neglected in this analysis.

The final Phase I conceptual design is shown in Figure 36, which was the result of several design iterations. The blade has a single inlet at the leading edge and numerous serpentine passages where the flow travels radially (up and down) within the blade. The 2-D extrusion shown in Figure 36b is simplified, but adjacent passages would be connected at the top or bottom of the final design. The second cavity from the trailing edge has an array of fins that the flow passes radially through. The purpose of the fins is to enhance heat transfer and provide structural support. The walls begin to taper in this region to enable the cooling cavities to extend as far aft as possible and to provide line of sight for the final cooling feature, holes through the trailing edge of the airfoil. The TBC thickness also tapers from 25 to 10 mils (0.64 to 0.25 mm) in this region. This thickness was a trade between aero and cooling, as a thicker trailing edge consumes less cooling, but has lower aerodynamic efficiency. A preliminary aero analysis indicated that 10 mils (0.25 mm) in trailing edge thickness was worth ~0.15 in stage efficiency, and the cooling analysis suggested that cooling flow went up steeply as TBC thickness dropped below 10 mils (0.25 mm). The value chosen for the current phase of the design should be regarded as preliminary and optimized in the next phase.

Figure 37 shows metal temperature contours. The spanwise thickness of the model corresponds to the pitch of a trailing edge hole. The simulations revealed that the trailing edge is the hottest region of the airfoil cross-section, further demonstrating the challenges imposed by this region. Moreover, the heat transfer coefficient calculated for this region had the highest uncertainty as a result of the unknown surface roughness, which was presumably a significant proportion of the relatively small hole diameter. The hole roughness was estimated based on Suchánek (2015) and incorporated into the heat transfer correlation using the method in Adams (2012). Reducing the uncertainty in the trailing edge hole heat transfer correlation and more detailed design of this region should be a focus in future programs.

Blade tip cooling was considered in this effort, but not studied in detail. The tip rail will likely not have TBC on the upper surface and will therefore be subjected to very high heat loads. A 3D thermal analysis conducted by Southwest Research Institute suggested that metal temperatures may be high enough that oxidation could be of concern. However, there are no known data of material oxidation in a high temperature, high pressure oxy-fuel combustion sCO_2 environment. Given the uncertainty in the target design temperature and the limited scope of Phase I, tip cooling design was not included in this effort, but should be looked at in more detail in

subsequent phases. If tip cooling is required, initial efforts should be focused on internal cooling. If the tip requires dedicated external cooling holes, total cooling flow will rise sharply.

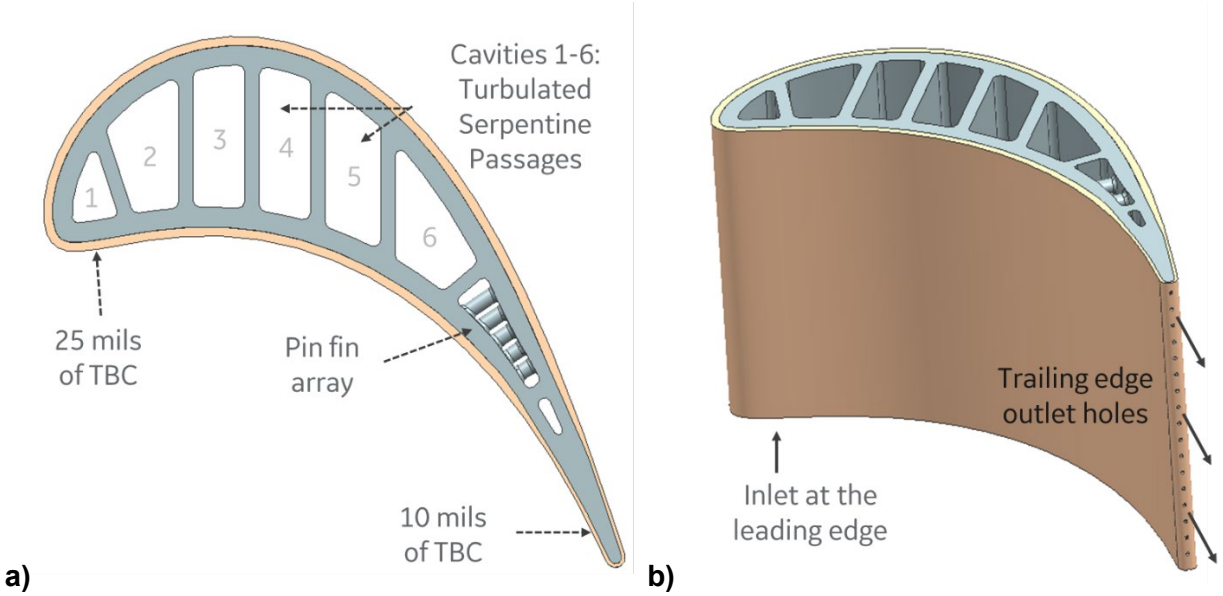

Figure 36. 2-D Conceptual S1B Cooling Design shown in a) side and b) isometric views

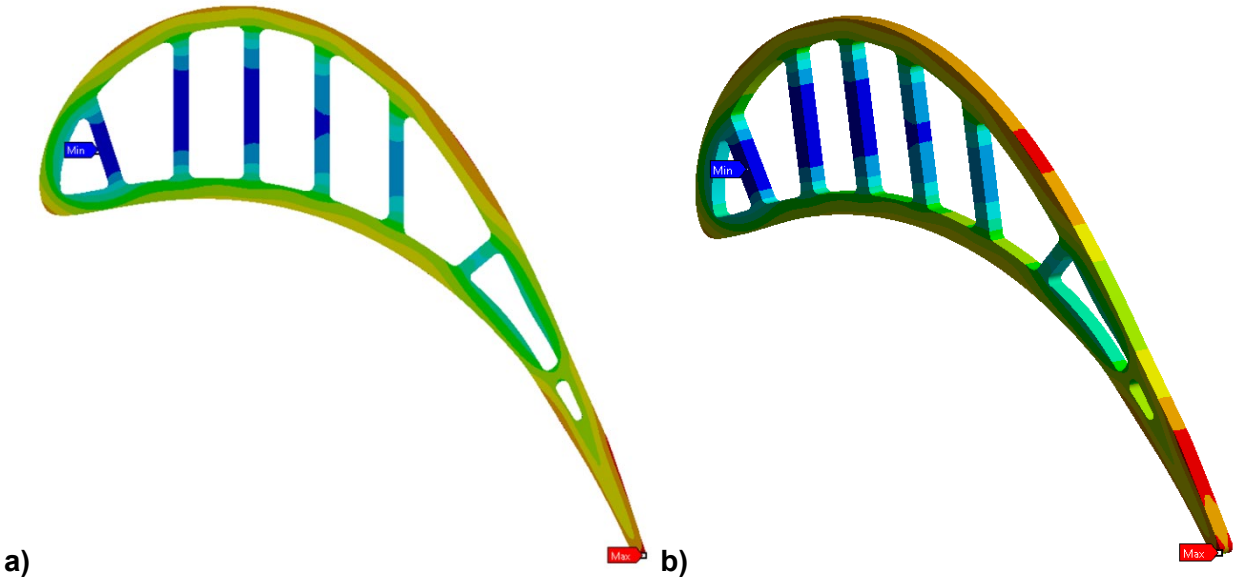

Figure 37. Metal Temperature Contours from the S1B Thermal Model

The total S1B airfoil cooling flow calculated from this analysis was 0.52% of the recycled flow. The final step in the conceptual Phase I design was to extrapolate this cooling flow to the entire turbine. The initial plan to accomplish this was to utilize gas turbine data, but ultimately the decision was made to use the design curve method discussed above. An updated blade airfoil design curve was obtained by running finite-element thermal simulations over a range of inlet mass flow conditions. Design curves for blade endwalls and shrouds were calculated assuming a 1-D thermal circuit. The shroud design, in particular, is sub-optimal at this time and could be significantly improved with further analysis. The nozzle and blade airfoils utilized the same design curves. One additional detail that needed to be considered was if radially cooled blades

were feasible in downstream stages, as opposed to blades cooled with serpentine passages (following the analogue to a gas turbine) as previously discussed. Radially cooled blades are a cheaper, but less effective alternative to serpentine cooled blades. For Phase I, it was assumed that only the 5th stage would be radially cooled, and the design curve cooling effectiveness was reduced accordingly. Another interesting take-away from this analysis was that the cooling flow did not decrease as sharply over each stage compared to a gas turbine, due in part to the lower temperature ratio per stage. In fact, many of the downstream stages consumed similar cooling flows as the first stage (since the airfoils are quite a bit larger), which will place additional scrutiny on these components in a more detailed design.

The turbine cooling flow was estimated to be approximately 6.2% of the recycled flow based on the conceptual analysis. This increased by 0.7% from data in Table 2 since the more accurate 2D analysis was performed over the 1D design tool used when down selecting designs. However, there are several uncertainties and key risks that need to be addressed as part of future efforts, as indicated in Table 7. Depending on the outcome of this future work, the total cooling flow could significantly change. The greatest risk identified in Phase I is the prime reliance on TBC. TBC spall could lead to catastrophic failure, and cooling flows without a prime reliant TBC are likely unpractical as shown in this study. Material oxidation is another large unknown, as it will guide the design temperature in certain situations. Furthermore, significant risk is currently being carried in the heat transfer and friction factor correlations. The Reynolds number is out of range in many cases and rotation is not being considered, the latter of which may be very important for this sCO_2 environment (based on rotation number calculations). Lastly, the details of a turbine cooling design can often be the most problematic. A more detailed heat transfer design of the S1B, particularly in the tip and trailing edge regions, as well as designs of components in both the first stage and downstream stages is required.

Table 7. Key Risks of Turbine Cooling Design

Risk	Mitigation
Prime reliant TBC	TBC testing at relevant conditions
Material oxidation in high temperature sCO_2	Oxidation testing of candidate metals at relevant conditions
Heat transfer correlations are out of range	Heat transfer testing at relevant conditions
Conceptual analysis lacks important details	Preliminary design of stage one blade, nozzle, and shroud as well as design of other stages

Blade Analysis

With the rotor layout defined and the main case waiting on final combustor count to move forward with more detailed design, the mechanical design has been focused on the feasibility of the turbine blades. Focus has been placed on the stage one turbine blade shown in Figure 38, since it will be seeing the highest temperature and pressure load.

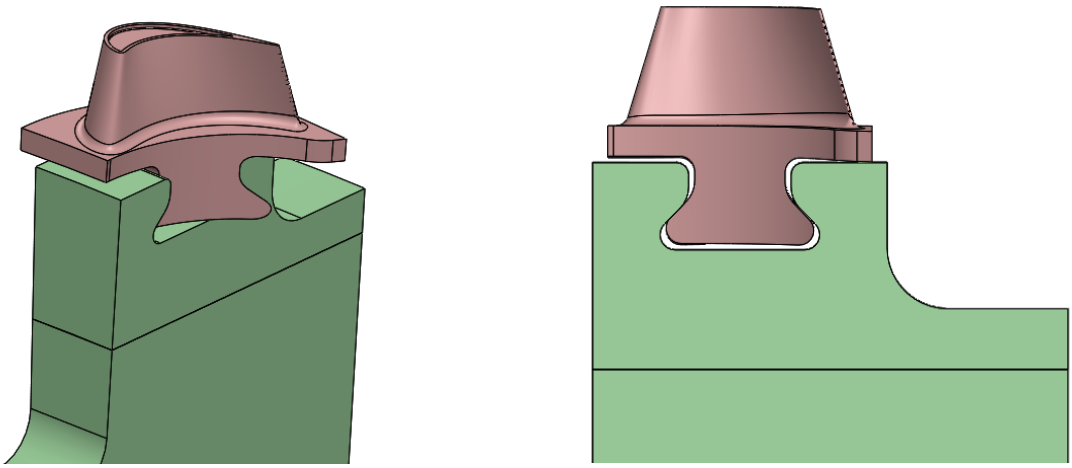

Figure 38. Stage One Blade

Design Conditions:

- Blade Inlet
  - 2,166 lbm/s (982.5 kg/s)
  - 3,270 psi (225.5 bar)
  - 2,083°F (1,139ºC)
- Blade Exit
  - 2,563 psi (176.7 bar)
  - 2,011°F (1,099ºC)

In addition to the external forces and features of the blade, the internals are also modeled to roughly represent the internal cooling cavities that will be required for thermal management. Two analysis will be looked on the blades. One that will look at load based stresses from pressure load, torque, and rotational forces. This will be focused on ensuring the root stresses are acceptable as these will be heavily influenced by bending loads for aerodynamic forces and also rotational pull loads. With the internal cooling cavities, the blade will be acting as a pressure vessel since the internal pressure will be higher than the external pressure.

In additional to structural loads, strain based stresses will also be looked at in a thermal stress only analysis. This will include effective heat transfer coefficients (HTCs) acting on the internal and external surfaces of the blade. These blades will be coated with a thermal barrier coating (TBC), however this coating will not be modeled. The HTCs used will be based on what the surface of the blade is seeing due to the effect of the TBC. Internal cavities are shown in Figure 39.

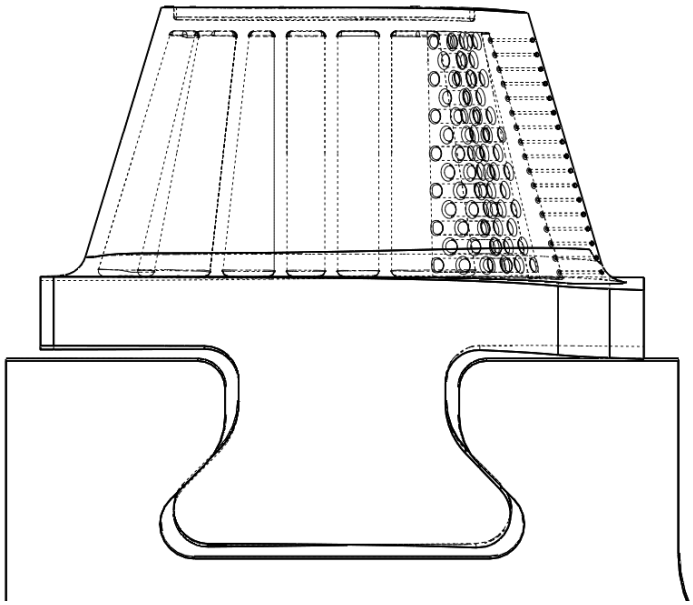

Figure 39. Blade Internal Cooling Cavities

It is important to note that the current internal cavities are merely representative of what the final model would like. These are based on a 2D cross section taken at the mid span of the blade and lofted to the hub and shroud. A much more advanced effort will need to be conducted in a detailed design phase based on these initial stress results. This would involve the actual serpentine passages with proper connections between cavities. This would also involve a properly modeled supply hole from the ID of the blade. The relative sizes of the cavities and accurate along with the trailing edge cooling holes and support pins towards the trailing edge of the blade. Wall thicknesses are kept constant from Hub to shroud, which might not be needed in a final design. Figure 40 shows the structural loads acting on the blade.

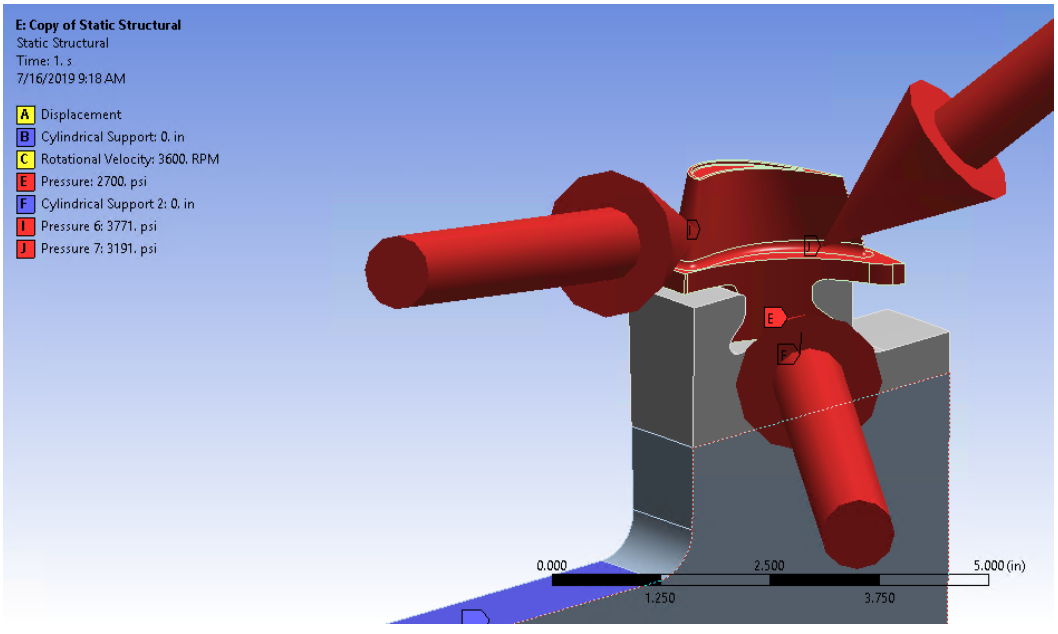

Figure 40. Static Structural Boundary Conditions

The stress model is using INCO 738 material properties at 1,380°F (749ºC). Figure 41 shows allowable stress properties for cast INCO 738. These stresses are used for load controlled stresses only. This includes rotational pull loads, bending loads from torque and pressure, and also internal pressure loads on the blade due to the internal cavities. For these values, 100 hr and 1,000 hr test data are compiled and a Larson miller parameter plot is established so that 100,000 hr rupture data can be calculated at various temperatures. For an initial analysis, a safety factor of 1.5 is applied to the resulting creep rupture data. With more accurate minimal data, this safety factor can be decreased to 1.25 along with diving into more detailed properties for 0.1% and 0.2% creep rate data.

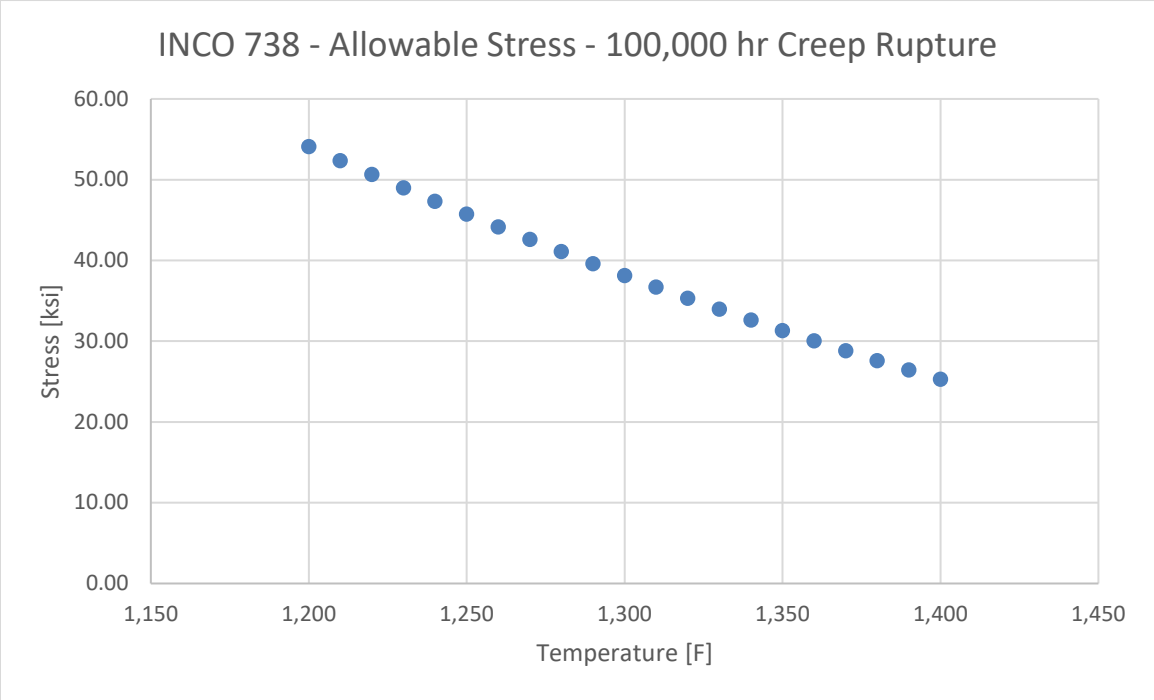

Figure 41. 100,000 hr Creep Rupture Allowable Stress for Cast INCO 738

Figure 42 shows initial stress results with the 100,000 hr creep rupture allowable of 25 ksi (172.4 MPa) as the limiting stress. From these results, it can be seen that a bulk of the stresses are below the rupture allowable. This indicates there is sufficient wall thickness to contain internal cooling pressure and also enough surface area at the hub for bending and pull loads acting on the blade. There are some areas near the hub fillet that are higher than the allowable, but these are more localized and can be reduced with some more refined design or allowing for higher loads due to location.

In the blade attachment region, the stresses are higher and this would be a concern, but the temperature in this area needs to be taken into account to determine what the allowable stresses are. Since this is the area that will be cooled, the allowable stresses will most likely be closer to yield, which are above 100 ksi (689.5 MPa).

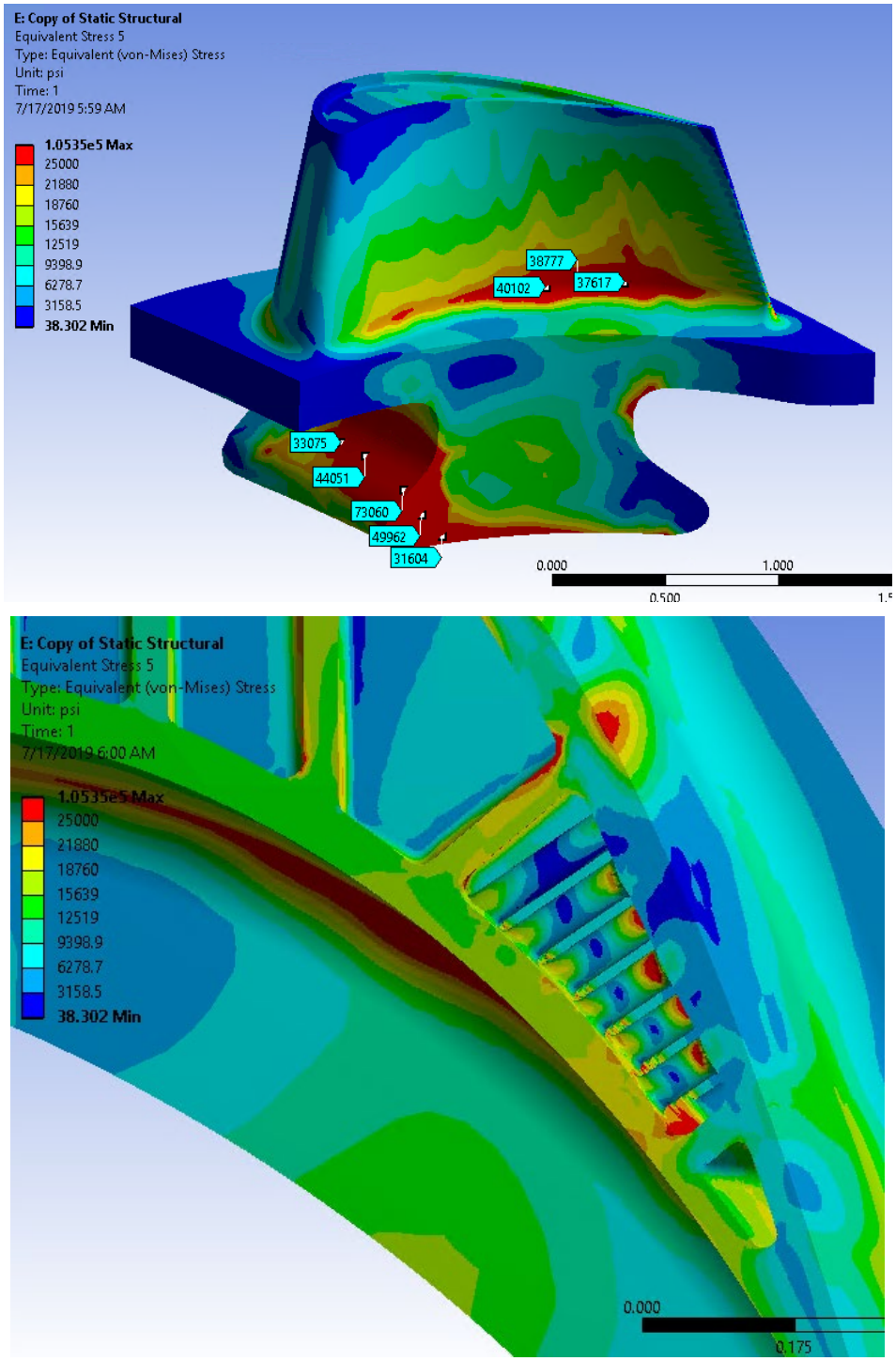

Figure 42. Structural Stress Results (Torque, Rotation, Pressure)

Based on a 2D thermal model, the HTCs are applied to the 3D model to get a first look at thermal stresses acting on the blade. Figure 43 shows the thermal boundary conditions acting on the blade.

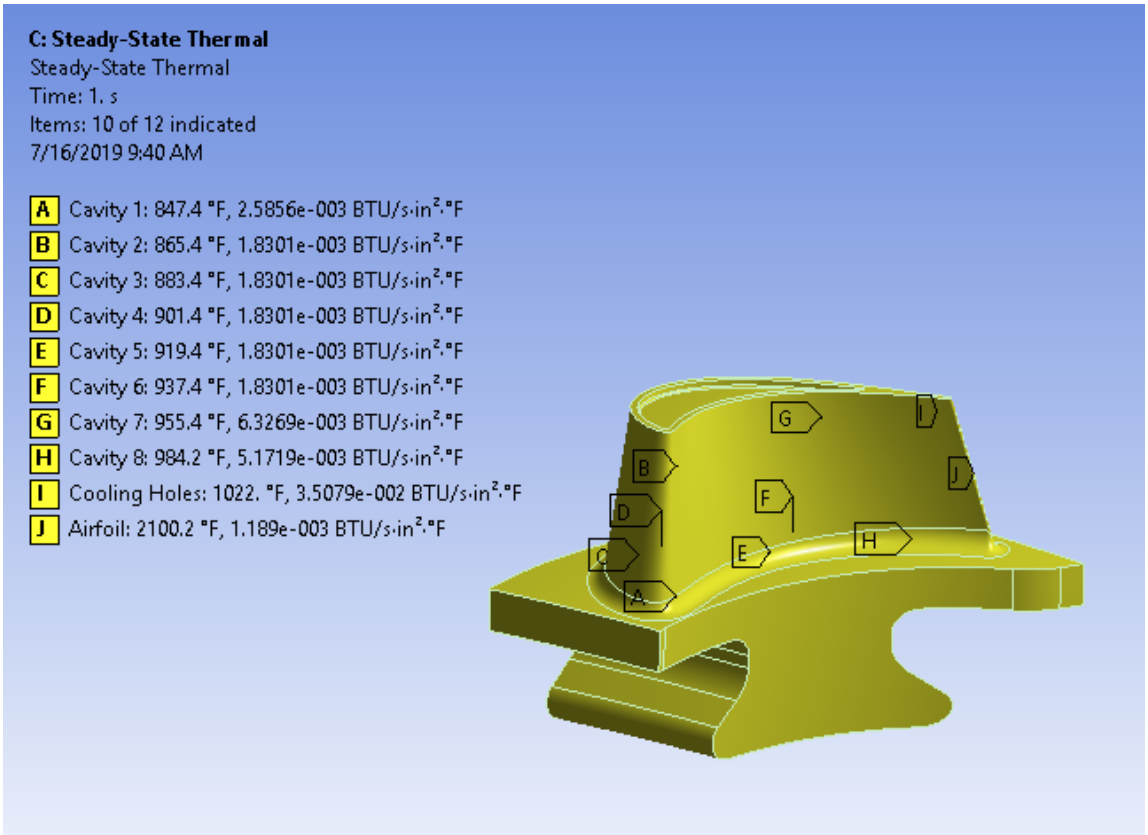

Figure 43. Thermal Boundary Conditions

It is important to note that the majority of the airfoil (blade, hub, and tip cavity) are seeing a uniform temperature and HTC for this initial analysis. Based on the varying speeds and varying TBC thickness, this HTC will actually be different around the blade. In addition, the temperature will also decrease from inlet to exit of the blade. This analysis should represent a worst-case scenario. Also, the very tip of the blade, the tip rails, will have no TBC and are currently seeing the max temperature along with an HTC 10X greater than the coated areas.

All the internal cavities are seeing a relatively uniform temperature and HTC, but the temperature does increase slightly between cavities. The HTC is the cavity with pins is much higher due to increased HTCs from flow around the pins, and a much higher HTC in the trailing edge holes due to higher velocities through the holes. Figure 44 shows the resulting temperature distribution on the external and internal of the airfoil. Material is INCO 738 will full thermal properties.

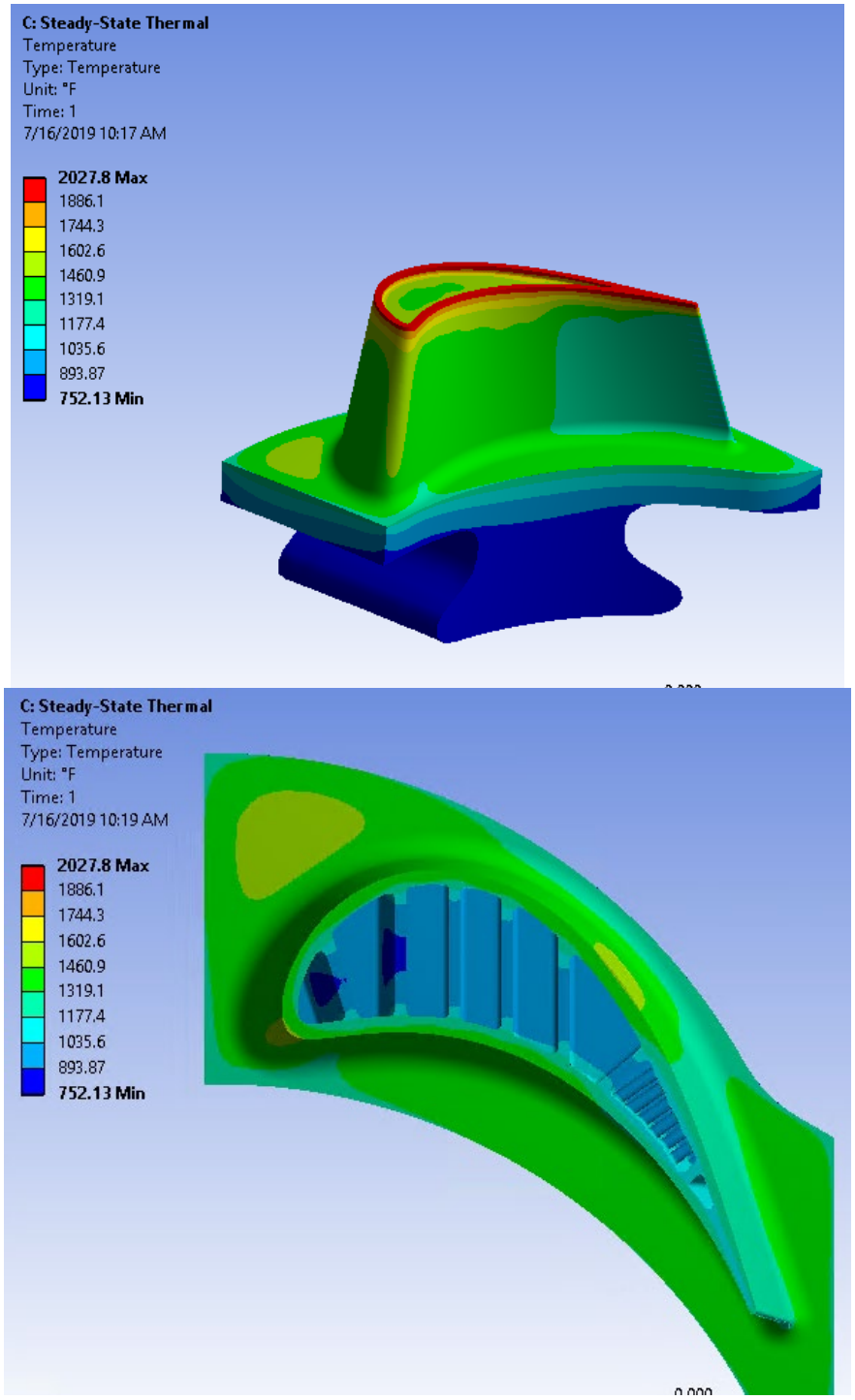

Figure 44. Temperature Results

For a bulk of the blade, the temperature is peaking at the design temperature of 1,350°F (732.2°C), with the internal cavities <1,000°F (537.8°C). This shows that the wall thickness is not too thick to prevent effective cooling of the external surface of the blade. With the hot external surfaces, and the cooler internal surfaces there will be stresses from differential thermal expansion as shown in Figure 45.

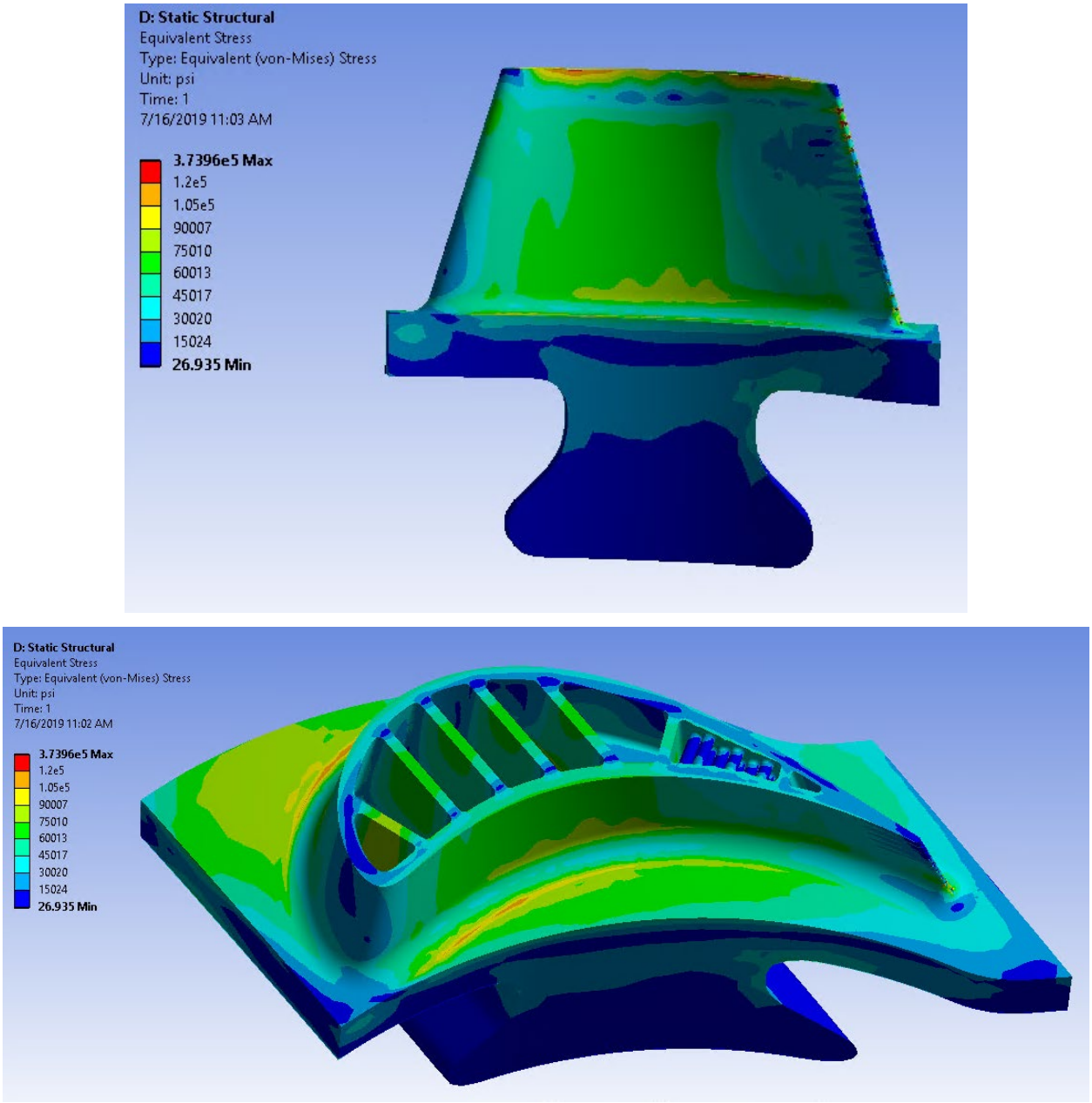

Figure 45. Blade Thermal Stresses

Based localized high stresses at the tips of the airfoil, most of the stresses are below 100 ksi (689.5 MPa), which is around the yield strength at 1,380°F (749.9°C). A more in-depth analysis of various material properties will need to be investigated to determine proper allowable stresses in future programs. More advanced design in the interior cavities will allow for reduced stresses in struts by allowing for more thermal growth.

Task 3.6: Turbine End Seals Development

The objective was to develop a conceptual design for turbine end seals and balance piston seals. Estimates of leakage performance were to be developed and compared to baseline leakage rates based on conventional labyrinth seal designs. Once boundary conditions were established, a set of baseline designs based on conventional labyrinth seals were developed. Design tools and

experience from the sCO_2 seals [6] and steam turbine seals [7] programs were leveraged to generate a conceptual design for large diameter, high-temperature face shaft end seals.

Baseline labyrinth seal designs were developed. For both the end seals and for the balance piston seal, a 0.3" (7.62 mm) tooth pitch and height was assumed. A range of radial clearances of 0.015 to 0.024" (0.38 to 0.61 mm) was studied for the 24" (610 mm) diameter end seals, and of 0.015 to 0.020" (0.38 to 0.51 mm) for the 53.95" (1370.3 mm) diameter balance piston seal. The latter was based on the expected rotor deflections predicted by the rotor dynamics model; rotor deflections at the end seals will be no larger and likely somewhat smaller. The TAMU XLTRC2 code was used for leakage flow predictions (XLLABY for the end labyrinth seals and ISOT for the balance piston hole-pattern seal). The inlet conditions and flow predictions are summarized in Table 8. The associated effective clearances were calculated and are shown in blue. Effective clearance can be thought of as the clearance of a single tooth labyrinth seal with a flow coefficient of one; this becomes a useful metric to compare different sealing technologies. Estimated face seal flows are shown in Table 9 in terms both of effective clearances and mass flow. Both are shown graphically in Figure 46 where the range of possible values is shown along with the actual expected performance, plotted against the axial rotor length required. The end seal leakage flow can be reduced by 2 to 3½ lb/s (0.91 to 1.59 kg/s) and the rotor shortened by 6 to 11" (152 to 279 mm), and the balance piston leakage flow could be reduced by 30 to 50 lb/s (13.6 to 22.7 kg/s).

The rotor dynamics model developed in Task 3.2 indicates that frequency margins are such that shortening the rotor by 6" (152 mm) for each of the end seals results in no significant benefit. Consequently, the benefit of better sealing at the end seals will be mostly from the value of the reduced flow and also from the material cost savings of a shorter rotor and casing.

According to the same rotor dynamics model, the need for a hole-pattern damper seal at the balance piston depends entirely on the assumptions made for foundation stiffness. If a hole-pattern damper seal is needed, it is likely that a minimum flow will be required, and this will drive the seal's design or even whether a face seal should be used.

Table 8. Labyrinth seal inlet conditions and flow predictions, and estimates for face seal flows

End Seals						Cp/Cv	1.2183					
Case	*Tooth height*	*Pitch*	*# teeth*	*Length*	*Diameter*	*Radial clearance*	*Inlet swirl*	*Pin*	*Pout*	*Tin*	*Flow (Ideal)*	*Effective Clearance*
	[in]	[in]		[in]	[in]	[in]		[psia]	[psia]	[F]	[lb/s]	[mil]
1	0.3	0.3	33	10	24	0.015	0.6	435.1	14.5	752	2.68	4.8
2	0.3	0.3	33	10	24	0.018	0.6	435.1	14.5	752	3.36	6
3	0.3	0.3	33	10	24	0.024	0.6	435.1	14.5	752	4.8	8.6
4	0.3	0.3	50	15	24	0.015	0.6	435.1	14.5	752	2.27	4
5	0.3	0.3	50	15	24	0.018	0.6	435.1	14.5	752	2.86	5.1
6	0.3	0.3	50	15	24	0.024	0.6	435.1	14.5	752	4.12	7.4
Balance Piston Seal						Cp/Cv	1.3349				*Flow*	
7	0.3	0.3	50	15	53.95	0.015	0.2	4445.4	435.1	752	50.4	3.8
8	0.3	0.3	50	15	53.95	0.020	0.2	4445.4	435.1	752	80.1	6.2
9	0.3	0.3	66	20	53.95	0.015	0.2	4445.4	435.1	752	42.4	3.2
10	0.3	0.3	66	20	53.95	0.020	0.2	4445.4	435.1	752	68.6	5.2

Table 9. Estimated Face Seal Flows for Various Effective Clearances

End Seals		Balance Piston Seal	
Effective Clearance	*Flow (real)*	*Effective Clearance*	*Flow (real)*
[mil]	[lb/s]	[mil]	[lb/s]
0.5	0.28	0.5	6.6
0.75	0.42	0.75	9.9
1	0.56	1	13.3
1.5	0.84	1.5	19.9
2	1.12	2	26.5
		4	53.1

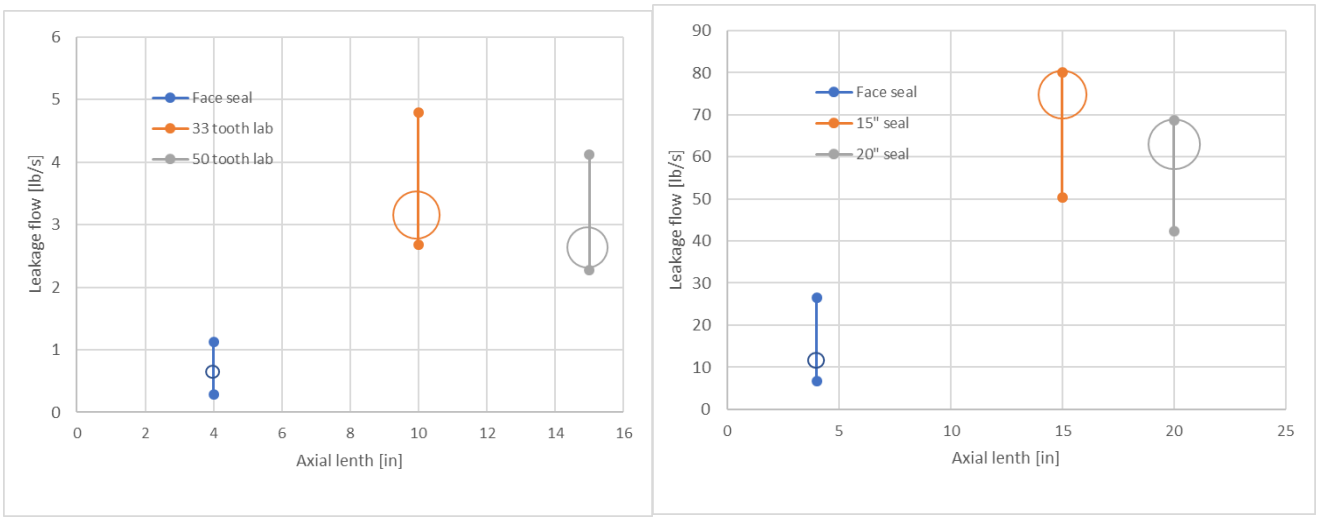

(a) *(b)*

Figure 46. (a) End seal leakage flows for face and labyrinth seals and (b) balance piston leakage flows for the face and hole-pattern seals, all versus axial length

Seal Conceptual Design: The proposed shaft end face seal is based on the design being developed in [6] and which is described partially in [9]. The seal shown in Figure 47, is a split 24” (610 mm) diameter seal. The split is necessary to allow for assembly on a shaft with an integral coupling on the end. In the figure, the seal in grey is allowed to float axially on springs and guide pins to follow the rotor’s axial travel and maintain a tight clearance to the rotor face. In the sCO_2 application of [6], the seal will operate with a pressure drop 1,100 psi (75.8 bar) at 400°F (204°C), and the supply pressure for the hydrostatic ports may exceed the upstream pressure. In the steam turbine version, a similar seal will be developed to operate at higher temperatures at diameters ranging from 18 to 25” (457 to 635 mm) and tested at a diameter of approximately 15” (381 mm). The technology will be an excellent fit for the oxy-fuel combustion turbine shaft end seals.

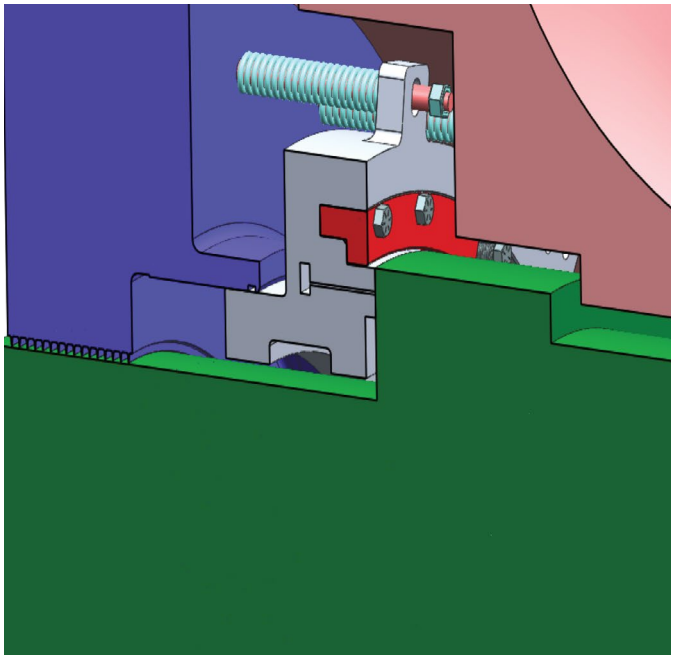

Figure 47. Proposed Face Seal Design

The proposed balance piston face seal is also based on the design being developed for the sCO_2 and steam turbine applications. The larger diameter is not expected to pose a significant challenge: GE has face seals in production at a 3' (0.91 m) diameter, and a prototype have been manufactured at about a 6' (1.83 m) diameter. A significantly simplifying detail for dimensional control is that the seal does not need to be split. The pressure drop however is significantly higher than has been tested in large diameter seals. At this stage of the evaluation, it is presumed that the preliminary design tools used to design for pressure-based deformations will work as well as the balance piston pressures. Deformations due to temperatures and temperature gradients can be resolved with design details similar to the shaft end/steam turbine seal designs. To determine how best to scale the seal design at a conceptual level, hoop stresses were evaluated.

Hoop stresses in the shaft end seal with 1,100 psi (75.8 bar) across it are calculated via finite element analysis (FEA) to be 7 ksi (48.3 MPa) away from the horizontal joint. The stress field near the joint is quite complex and can be as high as 30 ksi (207 MPa). The hoop stresses were also calculated for a simplified two-dimensional cross section with ring theory equations described in [3]. Hoop stresses were thus calculated to be 8 ksi (55.2 MPa). The calculations based on ring theory were repeated for the balance piston seal by scaling the seal up to a 54" (1.37 m) diameter with 3,965 psi (254.8 bar) across it. The cross-section dimensions were increased by factors of one through four; the resulting hoop stresses are shown below:

- Same cross section: 76 ksi (524 MPa)
- 2x cross section: 40 ksi (276 MPa)
- 3x cross section: 27 ksi (186 MPa)
- 4x cross section: 21 ksi (145 MPa)

Increasing the cross-section dimensions reduces hoop stress, though with diminishing returns. Tripling the seal's size brings the hoop stresses below those seen near the joint in the segmented

seal, so this is proposed as a design starting point. The stress results do suggest that the seal should not be segmented.

To see how the seal might find on the rotor, the triple-sized seal is sketched below in Figure 48. In order to remain unsegmented, the seal must be fitted on the bearing side of the balance piston. The seal must be slid onto the rotor prior to the rotor being lowered onto the bearings, and the seal stator assembled onto a flange on the combustor casing (shown as a bolted joint in the figure). The casing portion over the shaft ends can then be installed. The seal as shown measures approximately 4” (101.6 mm) radially and 8” (203.2 mm) axially. It should be noted that the axial dimension will be affected by the range of relative rotor stator motion at the seal location.

This result suggests that a viable seal design can be developed. The next steps in the design will be to establish rotor and stator relative motions, and to determine the pressure at which the seal must become operational. Detailed structural, fluid and heat transfer simulations will then be required to refine the design to achieve acceptable stresses and deformations.

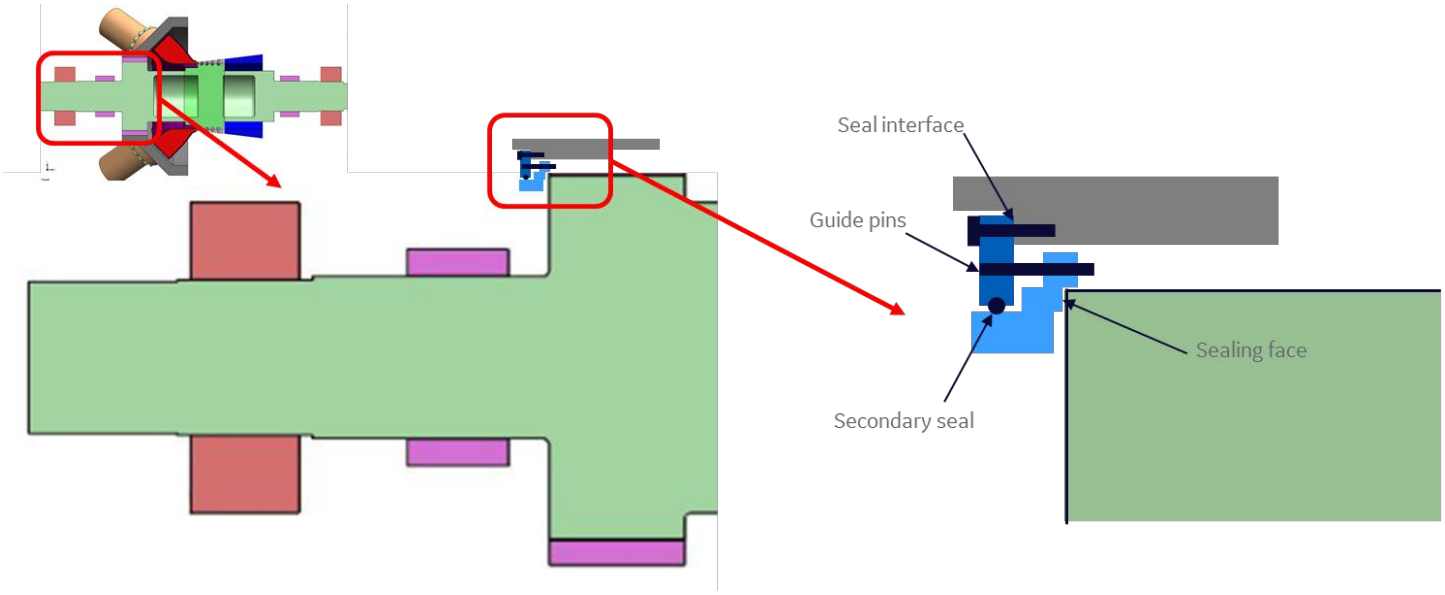

Figure 48. Proposed Face Seal Design Shown in Turbine Cross-Section

Cost/Benefit: The shaft end face seal cost estimates start from the first part costs estimated in [7], which were $75k for a split seal. A number of factors is expected to bring the cost down, including the experience of fabricating multiple seals and the simplification of some key complex features. If a material change from IN718 to a stainless steel is to become possible, a substantial cost savings will result. The balance piston face seal cost, and the cost savings listed for the end seals, would scale roughly with diameter. Fabrication trials of a similarly large diameter seal on another GE program confirm this assumption. One additional cost savings comes from the fact that the balance piston seal does not need to be split.

The face seals are axially more compact than the labyrinth seals they would replace. The 15” (381 mm) end labyrinth seals could be shortened to about five inches each, shortening the rotor by 20” (508 mm) on a 24” (609.6 mm) diameter. Based on the cost estimates of $3/lb ($6.61/kg) for typical chrome steel alloys, the shorter end seals will result in rotor material cost savings of $25k-$30k, with the associated machining cost impact being small. Assuming the value of the

casing cost savings at a third that of the rotor per inch of rotor length, the total savings will be on the order of $35k-$40k. Similarly, the balance piston seal could be reduced by 15” (381 mm) from 20” (508 mm) at a 54” (1.37 m) diameter. The total savings could be as much as $130k for rotor and casing; this is only possible if the hole-pattern seal is not required to its full length for rotor dynamic reasons and if the packaging of the inlet and combustor does to drive rotor length. The cost savings from the shorter rotor will not completely balance the seal cost, but will offset it partially.

The performance benefits of the face seals’ reduced leakage were estimated and the results are shown below in Table 10. On the basis of fuel cost savings alone, the cost of the shaft end face seals will be recovered sometime in the second year of operation depending on the part cost savings realized. If the full leakage reduction can be taken across the balance piston, the cost of the face seal will be recovered in the first year. Even if a substantial fraction of the flow must be maintained for rotor dynamic purposes, the face seal appears economically viable. It should be noted that, in addition to performance benefits while the seals are new and clean, a successful face seal design will not be vulnerable to rubs and the associated performance degradation that is typical of labyrinth seals.

Table 10. Performance impact of face seals over baseline labyrinth seals for a 550 MW turbine operating with an 85% capacity factor with gas price at $2.33/mmBtu

	End seals	Balance piston	
Reference mass flow:			
Labyrinth seal	2.27	68.6	[lb/s]
Configuration	15" seal, 0.015" clearance	20" seal. 0.020" clearance	
Face seal	0.42	13.3	[lb/s]
Efficiency impact	0.06	0.37	[%]
Output impact	0.70	4.09	[MW]
Heat rate impact	20,973	122,194	[mmbtu/yr]
Fuel cost savings	41,537	242,004	[$/yr]

Design validation: A full development effort to achieve TRL 5 will include detailed design with validation on a large sub-scale rig. The areas of focus include seal flows in terms of face pressure distributions, film thicknesses and forces; seal temperatures and thermal gradients; the accuracy of scaling approaches; seal slider to stator attachment and guide system; and secondary seal performance.

The scaling approaches will be important as results on smaller diameter seals designed and tested at lower pressures will be important starting points. Flow pressure distributions and thermal gradients will drive seal deformations, which must be characterized and controlled for a successful seal design. Seal attachment and guide design must be developed with a good understanding of the engine transients to which the seal will be subjected. The secondary seal is both a significant source of leakage and friction associated with the seal can also significantly affect the operability of the seal.

In a staged development effort, the secondary seal should be the first area of focus. A three-step approach will be used to develop the balance piston seal secondary seal. First, a seal conceptual design will be developed, including a bearing face design, a seal cross section, and a secondary seal. This will quantify pressure- and temperature-driven deformations and the overall force balance. The starting point for the secondary seal design will be a piston ring. Expected leakage performance and ring loading will be determined. Second, a test rig will be designed to characterize the secondary seal leakage performance ad drag loads. Third, a test campaign will be executed to validate the secondary seal design. The intent is to test the secondary seal at sub-scale in a rig approximately 8 to 14" (203 to 356 mm) in diameter. The testing will be at full temperature and pressure with nitrogen: high pressure nitrogen can be obtained in bottles to enable series of short tests. The concept for the rig is shown in Figure 49. Nitrogen will flow through a flow meter into a plenum between two test seals, and then will leak out to the test cell. A ceramic heater will be used to heat the vessel to temperatures up to 750˚F (399ºC). An actuator and load cell will be used to characterize drag loads under pressure.

With the secondary seal design addressed, the next stage will be the detailed design of the seal bearing face and cross section. A successful design must maintain the bearing face and rotor face geometry through all engine operating conditions. Once a design is completed, it should be validated at a scale large enough to capture the effects of deformation both across the cross section and along the circumference.

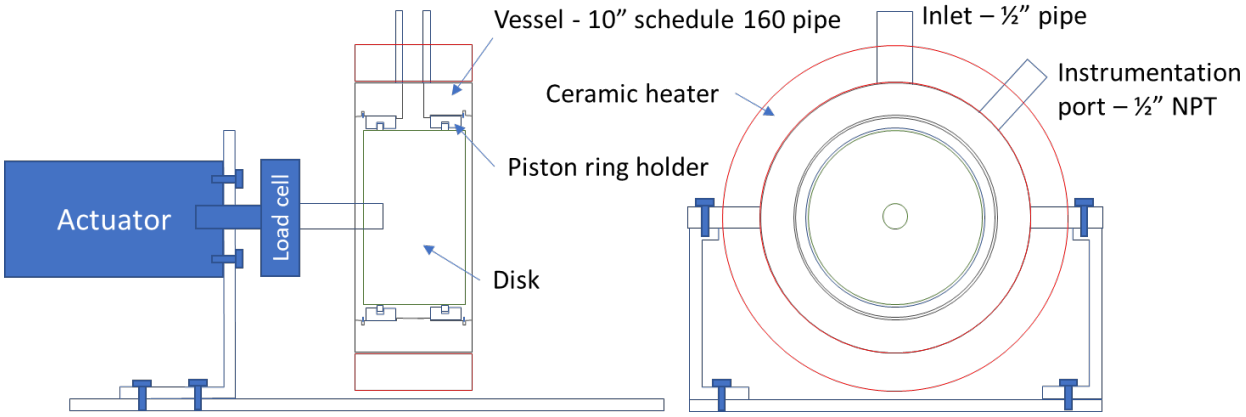

Figure 49. Proposed Secondary Seal Test Rig

Task 4.0: Turbine High-Temperature Materials Evaluation

Over Phase I, EPRI prepared a preliminary compilation of publicly available literature data on common high temperature alloys for combustion and steam turbine service, specifically those nickel-based alloys with some promise for relevant high temperature duty. This search was not intended to be exhaustive, nor sufficient for a detailed design, but provide a good estimate of creep rupture strength that the candidate alloys may be ranked and a few down selected for further research. EPRI expanded this compilation to include high temperature creep-strength enhanced steels, specifically a detailed analysis of a series developed under the Consortium of Science and Technology in Europe, COST, actions 501, 522, and 537. These steels have found application in ultra-supercritical steam turbines and would be suitable for service in sCO_2 environments as well, provided metal temperatures remain below 650ºC [12]-[50].

The research to this date focused on finding at least two corroborating articles for the following materials:

- Blade Alloys: GTD-111 (a.k.a. Rene80), “Inconel” 738, “Inconel” 939, “Nimonic” 105, “Rene” N5, “Rene” N6, and “Udimet” 500, 520, 700, and 710.
- Rotor Forging Alloys: “Haynes” 282, “Inconel” 617, “Inconel” 706, “Nimonic” 105, Toshiba TOS1X-2, and Waspalloy.
- Casing (Casting) Alloys: “Haynes” 282, “Inconel” 617 and 625.

At this time, some of these common alloys are compared in the following figures. As a first look at this variety of nickel-based alloys suitable for high temperature service, the investigation focused on readily available, relatively common alloys in the industry. As these materials are not standard ASME B&PVC code materials, they do not have a strict “allowable” stress limit. The comparisons included here are average properties based on public data – no significant statistics have been performed.

The blade alloys listed are currently in use in the land-based high efficiency gas turbines for power generation or in aircraft jet engines. Manufacturers are familiar with and comfortable working with these alloys, be they for equiaxed (EQ), directionally solidified (DS), or single crystal (SX) components. Preliminary conceptual design of these components has produced small blades, more akin to aviation engines than power generation turbines. This will simplify the manufacturing challenges for SX designs.

With respect to commercial viability, the rotor alloys are a challenge. Today’s disk forgings in land-based gas turbines are commonly Alloy 706 or 718 and operate cool relative to the blades. These disks are 2-3,000 kg due to several metallurgical concerns melting a larger ingot. The other alloy candidates are further away from market. Alloy 105, while very strong, may be impossible to create in a large forging, even as the conceptual design looks at larger forgings than the disk size.

Due to the extensive research for advanced ultra-supercritical steam turbines, Haynes 282, a relatively new alloy, may be the most viable option. It has been produced in a bar forging, pancake forging (akin to a wheel), and is slated for a large rotor forging under the continuation of the AUSC project, ComTest Phase II, DE-FE0025064.

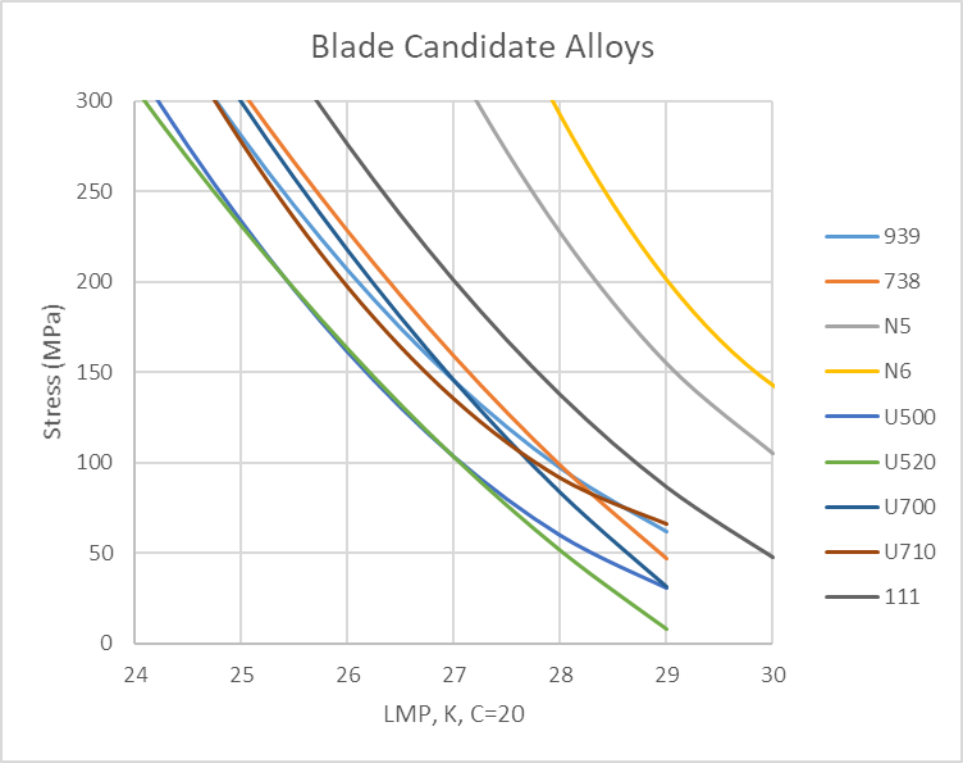

Figure 50. A Larson-Miller Parameter Versus Rupture Stress Plot of Several Blade Candidate Alloys

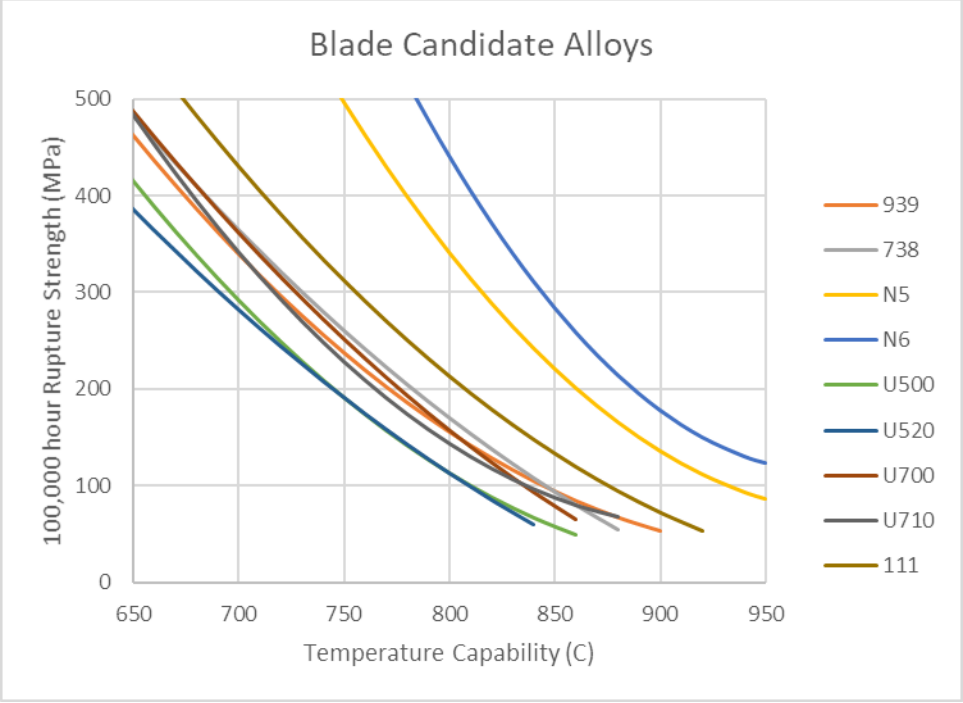

Figure 51. A Larson-Miller Parameter-Derived Isochronal (100kh) Comparison of Several Blade Candidate Alloys

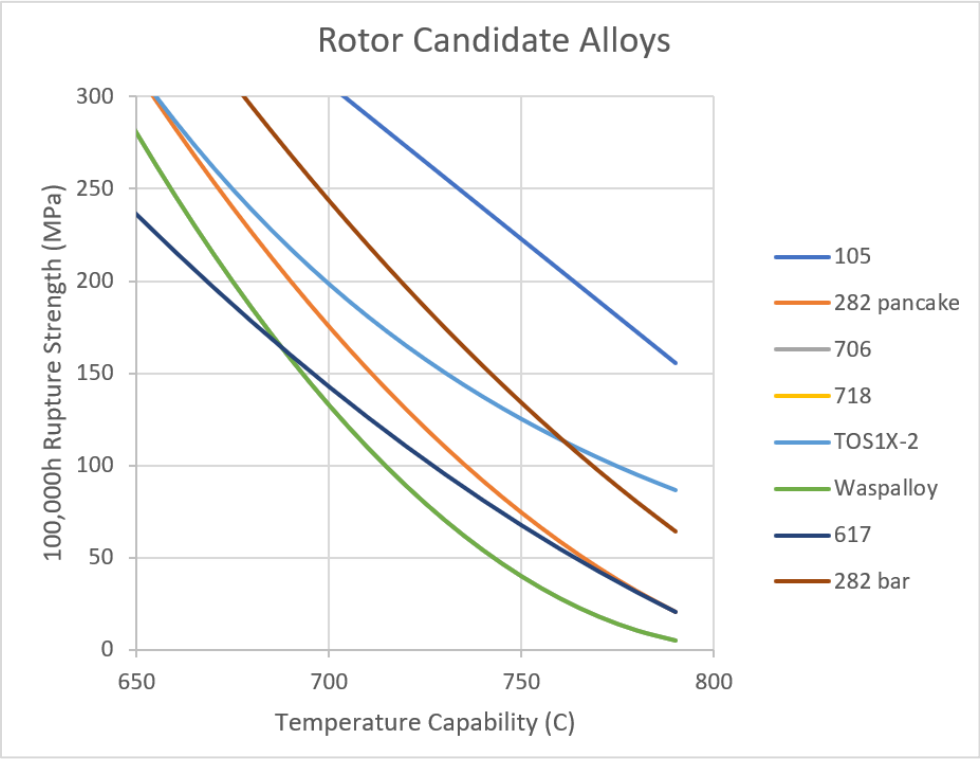

Figure 52. A Larson-Miller Parameter-Derived Isochronal (100kh) Comparison of Several Rotor Candidate Alloys. Note: Due to Differences in Reported LMP C Values for Some Alloys, a Direct LMP Comparison Was Not Viable

On casings, cast alloys may still be able to offer desirable properties for relatively thin-walled components. Currently the conceptual design accommodates a significant amount of cooling of the shell and this may enable use of steels; but even at cooler temperatures, there are advantages in considering thinner designs made of a stronger material. Research is not complete in this area, but for the 1,300°C THERMIE/AD 700 project, Alloy 625 was selected for valve body and turbine casing. Haynes 282 was the strongest candidate out of the US/DOE AUSC project (2005-2015) and a full-sized nozzle box casting is being prepared as part of ComTest (DE-FE0025064). In-air casting of >1,000 kg pours has been successful. As always, casting upgrade (e.g., repair welding) is still required, but with advanced foundry modeling it can be minimized. Of note, extensive homogenization heat treatments (in excess of 4 days) were used previously and would be recommended for future castings.

For reference, existing steam turbine casings (valve and turbine shell) and gas turbine casings are mostly cast low-alloy 1.25 Cr, 1 Mo, 0.25 V steels up to about 560°C and 10Cr creep-strength enhanced ferritic steels (containing a variety of Co, Mo, W, Nb, V, N, and B) up to about 620°C. Austenitic steels (such as 300-series stainless steels) have not found use in power generation castings outside of nuclear (and lower temperatures).

Consortium of Science and Technology programs 501, 522, and 538 were a European effort from 1998 through 2012 to produce iron-based alloys for castings and rotors for steam turbines operating above 600ºC; they are all creep strength-enhanced ferritic steels. Table 11 describes the nominal chemical composition of the several alloys out of these programs that are being used in USC steam applications. Five alloys saw strong adoption in the industry after several rounds of down select: B2 (blades and bolting), E, F, FB2 (rotor forgings), and CB2 and to a lesser degree E (castings). EPRI [38] has just completed a thorough literature survey of these

alloys and their properties - especially rupture. These curves below were produced after extensive analysis using an ASME (Swindeman) approach [47].

Table 11. Nominal Composition of COST Steels

Comparison Alloys		**C**	**Cr**	**Ni**	**Mo**	**W**	**Co**	**V**	**Nb**	**N**	**B**
Grade 91 / cast C12A		0.1	8.7	0.1	**0.9**	**--**	**--**	0.2	0.05	0.05	--
Grade 92		0.1	9	0.1	**0.4**	**1.8**	**--**	0.2	0.07	0.05	0.002
	EN Designation										
A	--	0.12	9.5	0.5	**1**	--	--	0.25		**0.2**	--
B	--	0.12	9.5	0.5	**1.5**	--	--	0.25		0.05	**0.01**
B2	X17CrMoCoVNbB10-1-1	0.17	9.5	0.12	**1.5**	--	**1**	0.25	0.06	0.015	**0.01**
CB2	GX12CrMoCoVNbNB9-2-1	0.12	9.5	0.2	**1.5**	--	**1.2**	0.25		0.05	**0.01**
D	--	0.16	11.3	0.8	**0.3**	**1.8**	--	0.25	0.06	0.06	--
E	X12CrMoWVNbN10-1-1	0.12	10.3	0.75	**1**	**0.9**	--	0.18	0.05	0.05	--
F	X12CrMoVNbN10-1	0.12	10.3	0.6	**1.5**	--	--	0.18	0.05	0.05	--
FB2	X13CrMoCoVNbNB9-2-1	0.13	9.3	0.15	**1.5**	--	**1.25**	0.2	0.05	0.025	**0.01**

The Swindeman approach is a complex exploration of the original Larson-Miller concepts to dynamically calculate a LM relationship with any given set of data. ASME developed a spreadsheet-based tool for rapid, semi-autonomous assessment of a given data set. This tool was exercised for the above data sets. The key outputs are described in Equation 7 and Table 12. For consistency, all data fits were calculated as third-order fits with lot centering and were used to produce the comparison in Figure 53 for steam turbine alloys up to 650°C use temperatures.

$$LMP = A0 + A1 * \log stress + A2 * (\log stress)^2 + A3 (\log stress)^3 \quad (7)$$

$$LMP = \text{Absolute Temperature} * (C + \log time) \quad (8)$$

where LMP is the Larson-Miller Parameter for the given C, and for these calculations stress was calculated in MPa, and Temperature/Absolute Temperature was calculated in C/K.

Table 12. Parameters to fit the Swindeman Equation, Equation 1, for Several ST Steels. Standard Deviation, σ, is on log(stress)

	Wrought							**Cast**	
	CrMoV	Grade 91	B2	E	F	FB2		CB2	Cast E
A0	22468	38272.64	69789.65	96481.49	101159.7	83974.05		97272.72	69471.5
A1	-13.549	-15640.7	-60699.4	-103136	-116775	-82330.8		-105982	-57267.9
A2		8106.709	29551.01	49183.92	56523.31	40033.09		52793.36	27721.52
A3		-1853.97	-5200.25	-8099.6	-9360.57	-6827.97		-9304.25	-4945.27
C	20	23.64199	23.23433	20.4409	16.72038	22.92387		20.33499	25.28025

σ			0.01995	0.02852	0.0309	0.03131		0.03727	0.02687

This comparison is intended to inform the boundary conditions for a suitable turbine design. The Allam cycle oxy-fired sCO_2 conceptual turbine design shares some characteristics of a conventional gas turbine (high temperature) and other characteristics of a steam turbine (high pressure) and identifying materials that can survive the combination of both will prove challenging.

Overall, this assessment sought to provide a look at commercially viable alloys at a high level. Many additional factors (design, environment) may influence the material selection and further research may be required to properly down select.

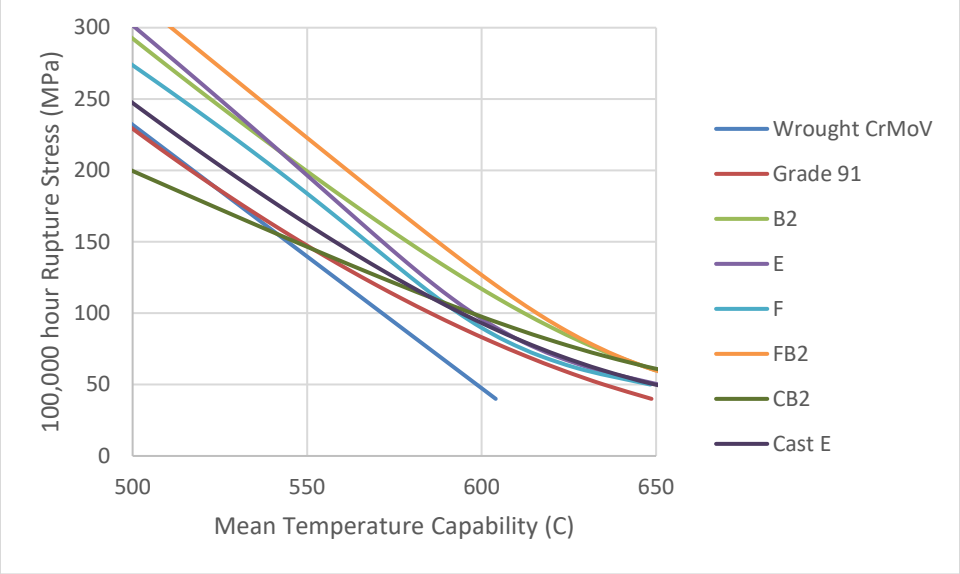

Figure 53. A Larson-Miller-Derived 100,000h Isochronal Comparison of Various High Temperature Creep Strength-Enhanced Ferritic Steels used in Commercial USC Steam Turbines

Task 5.0: Combustion Kinetics Evaluation

The combustion chemical kinetics of fuels has significant influence on the performance of every combustion system. Furthermore, combustion chemical kinetics is strongly dependent on temperature and pressure variations. Therefore, the kinetic models have to be carefully studied and validated at the conditions under which combustors operate. The well-developed kinetic models presented in the literature are calibrated for combustion in air (N_2 diluent) at pressures less than 20.3 bar and normally have to be validated by both ignition and flame properties. However, in the region where combustion chemical kinetic models have not been validated by experiments, the kinetic models cannot be applied. This point is demonstrated by recent work by the measurement of CH_4 auto-ignition delays. Figure 54 shows auto-ignition delays of CH_4 in CO_2 diluent at 0.62 bar [2] and 200 bar (200 bar results from Georgia Tech [3]). It can be seen that at 0.62 bar, experimental measurements agreed well with simulation using GRI Mech 3.0 [4] and Aramco Mech 1.3 [5]. However, at high pressure conditions, significant deviation between experiments and prediction from GRI Mech 3.0 was observed as shown in Figure 54 (bottom), indicating the failure of GRI Mech at elevated pressure conditions. As shown in Figure 54, Aramco 2.0 has good agreement with experiments. However, recently developed FFCM-1 kinetic model fails to predict the auto-ignition delays at 200 bar because it was not validated by high pressure data. Detailed kinetic analysis showed that the deficiency of FFCM-1 on the prediction of auto-ignition delays is owing to the missing of CH_3O_2 kinetics. Once CH_3O_2 kinetics is added into FFCM-1, the revised FFCM-1 kinetic model can predict auto-ignition delays at 200 bar very well as demonstrated in Figure 54 (bottom). However, successful prediction of auto-ignition delays does not guaranty successful prediction on combustor performance. This can be clearly demonstrated by simulating identical combustors using both revised FFCM-1 and Aramco 2.0, respectively. This is accomplished by simulating a conceptual step combustor with JICF (Jet in Crossflow) feature using these two kinetic models, respectively.

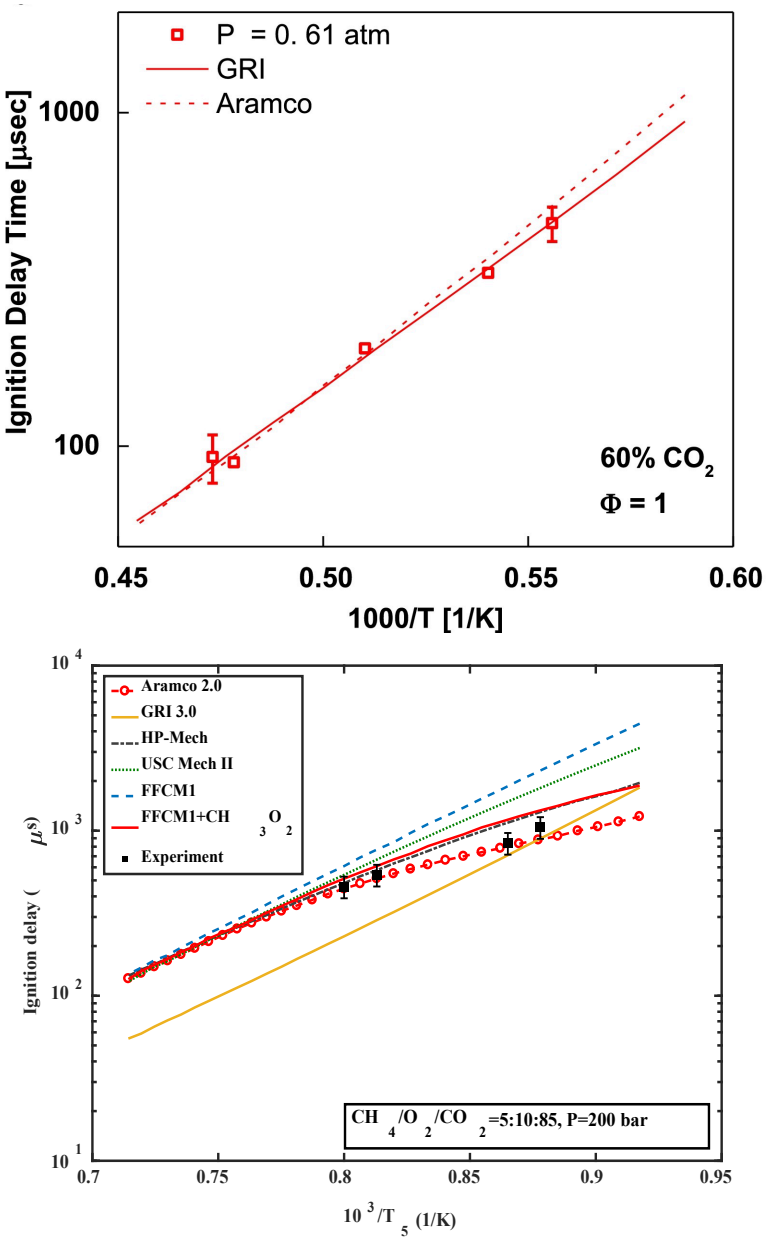

Figure 54. Ignition delay time measurements of stoichiometric $CH_4/O_2/CO_2$ mixtures at (top) 0.61 atm [1] and (bottom) 200 bar

The conceptual combustor has hot CO_2 cross flow and circumferential CH_4 and O_2 jets. The simulated temperature profiles and CO distributions are compared in Figure 55. It can be seen clearly that very different results are obtained using two different kinetic models even through both kinetic models that can predict auto-ignition delays well. Clearly, this is indicating that shock tube data (fuel to CO) is not adequate to validate the entire region where kinetic models work without validation of flame experiment (CO_2 and H_2O formation). Therefore, without experimental validation at the conditions of interest, it is meaningless to claim the comprehensiveness of any models developed.

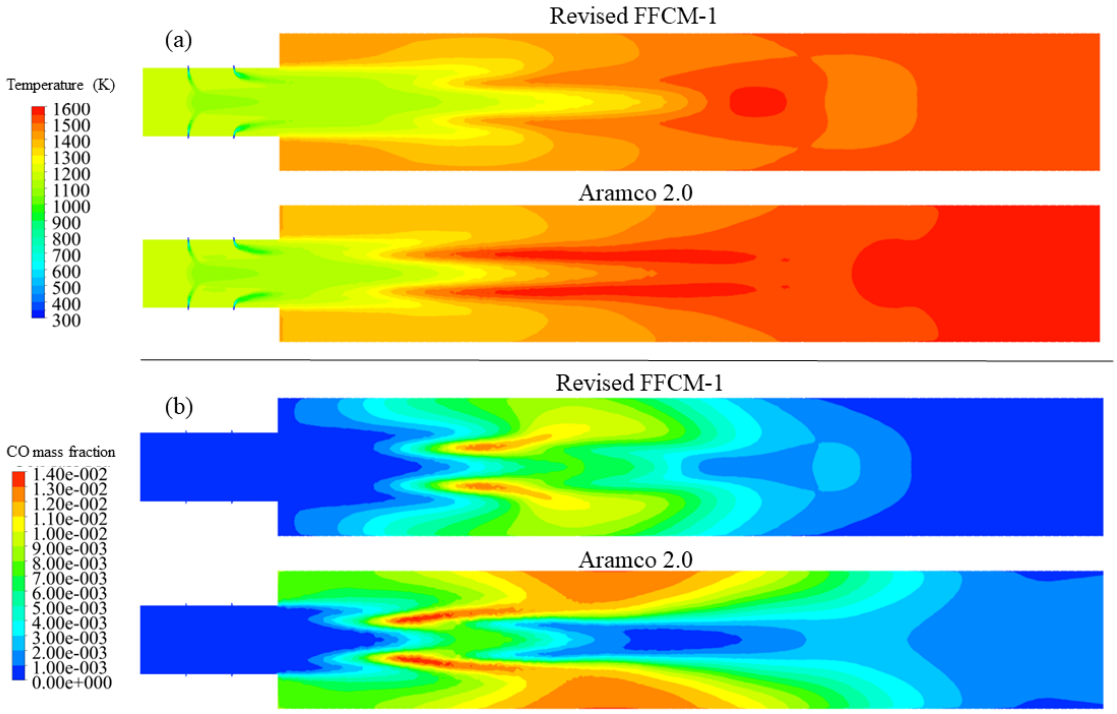

Figure 55. Fluent simulation of a model combustor using revised FFCM-1 and Aramco 2.0 kinetic models, comparison of (a) temperature profiles (b) CO profiles

On the experimental side, one striking feature of high-pressure flame is soot formation. Figure 56 shows direct photograph of CH_4/air diffusion flames at different pressure conditions. It can be clearly seen that CH_4/air flame produces significant amount of soot at high pressure conditions.

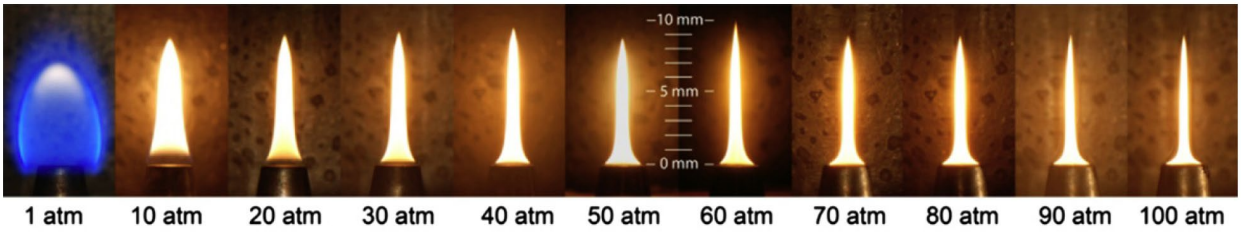

Figure 56. Pictures of laminar methane-air co-flow diffusion flames from atmospheric pressure to 100 atm. Methane flow rate is constant at 0.55 mg/s [4]

As a summary for the evaluation of kinetic models, flame experiments at sCO_2 power cycle relevant conditions are urgently needed.

E. FUNDING AND COSTING PROFILE

Figure 57 shows the earned value chart through June. The team has made good progress. The chart shows the progress (earned value) is ahead of the spend rate (good progress being made) and the actual spend is lagging behind the planned spend rate because of billing/invoicing time latency by the subcontractors and delays getting the subcontracts in place. The earned value shows that all tasks have been completed ahead of schedule.

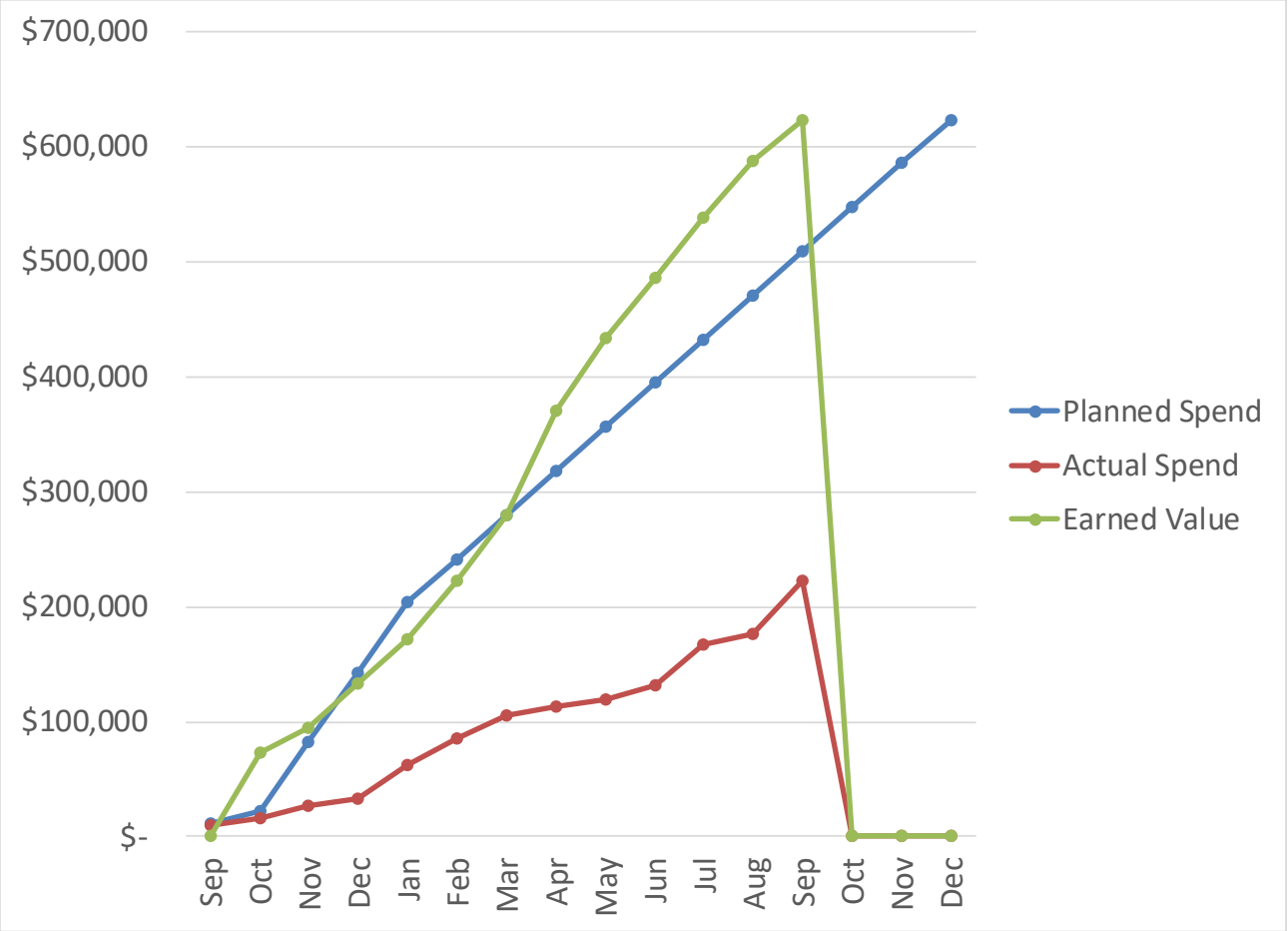

Figure 57. Earned Value Chart

F. SCHEDULE

The project will be executed in three phases that mirror the technology readiness level 3 to 6 development path including proof-of-concept, basic design, detailed design, engineering analysis, test rig development, and finally sub-scale prototype testing. Figure 58 shows a Gantt chart for the overall project with all major tasks and subtasks included showing the project is proceeding on schedule. So far, the team is holding close to the schedule. The 3D aero design and combustor design were delayed awaiting the results of the single vs. double flow optimization study previously described; this selection is now complete. The 3D aero design and preliminary heat transfer and stress analysis of stage one is complete.

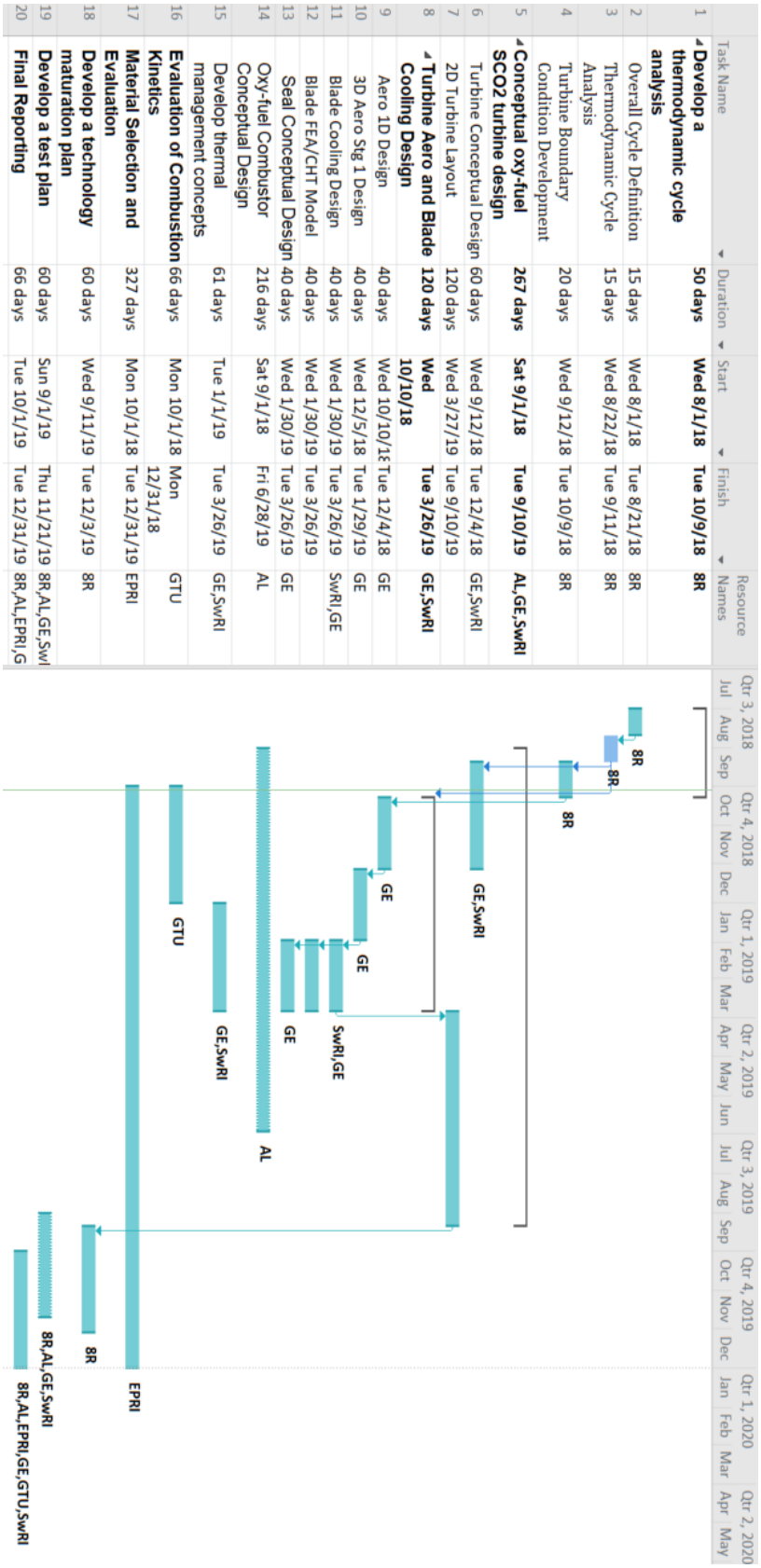

Figure 58. Project Schedule for Oxy-Fuel Turbine Conceptual Design

G. SUCCESS CRITERIA AT DECISION POINTS

- Achieve greater than 58% thermal efficiency in the cycle analysis: 10/3/18 – Complete.

Regarding the turbine design, the additional success criteria will be assessed at the decision point:

- Develop aerodynamic design for first stage nozzle and turbine blade with efficiency greater than 85%: 9/30/19.
- Develop cooled nozzle and turbine blade design with metal temperature in high-stress areas less than 700°C: 9/30/19.
- Develop a conceptual design for the oxy-fuel combustor to achieve a firing temperature of 1,200°C: 9/30/19.

H. REFERENCES

[1] Town, Jason, et al. “State-of-the-Art Cooling Technology for a Turbine Rotor Blade.” Journal of Turbomachinery 140.7 (2018): 071007.

[2] B. Koroglu, O. M. Pryor, J. Lopez, L. Nash, and S. S. Vasu, “Shock tube ignition delay times and methane time-histories measurements during excess CO2 diluted oxy-methane combustion,” Combust. Flame, vol. 164, pp. 152–163, 2016.

[3] M. Karimi, B. Ochs, Z. Liu, D. Ranjan, and W. Sun, “Measurement of methane autoignition delays in carbon dioxide and argon diluents at high pressure conditions,” Combust. Flame, vol. 204, pp. 304–319, 2019.

[4] Z. Q. Gregory P. Smith, David M. Golden, Michael Frenklach, Nigel W. Moriarty, Boris Eiteneer, Mikhail Goldenberg, C. Thomas Bowman, Ronald K. Hanson, Soonho Song, William C. Gardiner, Jr., Vitali V. Lissianski, “GRI-3.0 Mechanism.” 2008.

[5] A. E. Karatas and Ö. L. Gülder, “Soot formation in high pressure laminar diffusion flames,” *Prog. Energy Combust. Sci.*, vol. 38, pp. 818–845, 2012.

[6] DE-FE0024007, “Development of Low-Leakage Seals for Utility-Scale SCO_2 Turbines”, 2016-2019.

[7] DE-FE0031586, “Transformational Reduction Using Sealing Technology in LCOE for Coal-based Power Plants – Phase I”, 2018-2019.

[8] Deepak Trivedi, Rahul A. Bidkar, Christopher E. Wolfe and Jason Mortzheim, “Supercritical CO_2 tests for Hydrostatic film Stiffness in Film-Riding Seals,” Proceedings of ASME Turbo Expo 2019: Turbomachinery Technical Conference and Exposition, GT2019-90975, June 17 – 21, 2019, Phoenix, AZ, USA.

[9] Bunker, Ron S. "Turbine Cooling Design Analysis." *Gas Turbine Handbook* (2005).

[10] Suchánek, Libor, and Ivana Zetková. "Evaluation of the surface small holes drilled by unconventional methods." *Procedia Engineering* 100 (2015): 1582-1590.

[11] Adams, Thomas, Christopher Grant, and Heather Watson. "A simple algorithm to relate measured surface roughness to equivalent sand-grain roughness." *International Journal of Mechanical Engineering and Mechatronics* 1.2 (2012): 66-71.

[12] R. Purgert et al., “Materials for Advanced Ultrasupercritical Steam Turbines.” DE-FE0000234 Final Technical Report. Dec. 2015.

[13] N. Muktinutalapati, “Materials for Gas Turbines – An Overview.” 2011. Available online: https://www.intechopen.com/books/advances-in-gas-turbine-technology/materials-for-gas-turbines-an-overview

[14] J. Wahl, K. Harris, “Superalloys in Industrial Gas Turbines – An Overview.” 9th World Conference on Investment Casting, 1996. San Francisco, CA.

[15] H. Harada, “High Temperature Materials for Gast Turbines: The Present and Future.” Proceedings of the International Gas Turbine Congress, 2003. Tokyo, Japan.

[16] R. Viswanathan, “Gas Turbine Blade Superalloy Material Property Handbook.” EPRI, Palo Alto, CA. 2001. 1004652.

[17] J. Dong, “Relationship of Long-term Creep Behavior with Microstructural Evolution in a Nickel-Base Superalloy Udimet 500.” Intl. Conf. on Creep and Fatigue at Elevated Temperatures. 2001.

[18] D.W. Seaver, A.M. Beltran. “Nickel Base Alloy GTD-222, a New Gas Turbine Nozzle Alloy.” ASME, New York, NY. 1991. 91-GT-73.

[19] W.S. Walston et al., “RENE N6: Third Generation Single Crystal Superalloy.” Superalloys 1996, TMS.
[20] D. Gandy, “Gas Turbine Blade Superalloy Material Property Handbook.” EPRI, Palo Alto, CA. 2003. 1008477.
[21] S. Miyashita et al., “Development and Evaluation of Large-Scale Rotor Forging for Over 700C-Class A-USC Steam Turbine.” 7th International Conference on Advances in Materials Tech. for Fossil Power Plants. ASME International. 2013.
[22] C. Berger et al. “Creep Rupture Behaviour of Nickel Base Alloys for 700C - Steam Turbines.” Superalloys 2001.
[23] B. Scarlin, T. Kern, M. Staubli. “European Efforts in Materials For 650°C USC Power Plants - Cost 522.” 4th International Advances in Materials for Fossil Power Plants. ASME International. 2004.
[24] S. Kang et al., “Manufacturing and Mechanical & Metallurgical properties of 9 ~ 12% Cr Rotor Forgings for advanced Steam Turbine.” Super High Strength Steels – Rome. Associazione Italiana di Metallurgica, 2005.
[25] J. Suk et al. “Cyclic Fatigue Characteristics of 10% Cr Blade Steels for Advanced Steam Turbines.” Super High Strength Steels – Rome. Associazione Italiana di Metallurgica, 2005
[26] A. Gotti, P. Lombardi, S. Neri, A. Di Gianfrancesco, “Mechanical Performance in the Creep and Cyclic Regimes of an Industrial 9% Cr Forged Material” ECCC 2017.
[27] Jan Dzugan, Zbysek Novy, Pavel Konopik, Pavel Podany, Eva Folková, “Creep Properties of HAZ in Heterogeneous Welded Rotor.” 7th International Conference on Advances in Materials Tech. for Fossil Power Plants. ASME International. 2013.
[28] A. Di Gianfrancesco, L. Cipolla, M. Paura, S. Tiberi Vipraio, D. Venditti, S. Neri, M. Calderini, “The Rule of Boron in Long Term Stability of a CrMoCoB (FB2) Steel for Rotor Application.” 6th International Conference on Advances in Materials Tech for Fossil Power Plants ASME International. 2010.
[29] A. Di Gianfrancesco, S. Budano, P. Lombardi, M. Paura, S. Neri, M. Calderini, N. Longari, “Experience in Manufacturing of High Chromium Forged Rotor Steels.” 7th International Conference on Advances in Materials Tech. for Fossil Power Plants. ASME International. 2013.
[30] T.-U. Kern, K.H. Mayer, B. Donth, G. Zeiler, A. DiGianfrancesco, “The European Efforts In Development of New High Temperature Rotor Materials - COST 536.” Liege Conference on Materials, 2010.
[31] S. Baumgartner, M. Schuler, R. Schnitzer, N. Enzinger, “Influence of Nickel on the Mechanical Properties of a Creep resistant CB2 Flux Cored Wire Weld Metal.” Liege Conference on Materials, 2014.
[32] M. Mikami, K. Sawada, S. Kobayashi, T. Hara, K. Kimura, “Effect of Tempering Condition on Creep Strength and Microstructure in High Cr Steel Rotor Forgings for Steam Turbines.” Liege Conference on Materials, 2014.
[33] N. Blaes, B. Donth, A. Diwo, D Bokelmann, “Rotor Forgings For Steam Turbines with High Efficiency.” 7th International Conference on Advances in Materials Tech. for Fossil Power Plants. ASME International. 2013.

[34] Günter Zeiler, Wilfred Meyer, Krystyna Spiradek, Jaroslaw Wosik, “Experience in Manufacturing and Long-Term mechanical & Microstructural Testing on 9-12% Chromium Steel Forgings for Power Generation Plants.” 4th International Conference on Advances in Materials Tech. for Fossil Power Plants. ASME International. 2004.
[35] M. Taylor, D.V. Thornton, R.W. Vanstone, “Experience in the Manufacture of Steam Turbine Components in Advanced 9-12% Chromium Steels.” Liege Conference on Materials, 1998.
[36] T.-U. Kern, B. Scarlin, R.W. Vanstone, K.H. Mayer, “High Temperature Forged Components for Advanced Steam Power Plants.” Liege Conference on Materials, 1998.
[37] Reinhard Knodler, Stefan Straub, “Influence of Surface Treatment on the Oxidation Kinetics of Advanced Steels in Flowing Steam at 650°C.” Liege Conference on Materials, 2006.
[38] M. Staubli, R. Hanus, T. Weber, K.-H. Mayer, T.-U. Kern, “The European Efforts in Development of New High Temperature Casting Materials - COST 536.” Liege Conference on Materials, 2006.
[39] E. Baune, H. Cerjak, St. Caminada, C. Jochum, P. Mayr, J. Pasternak, “Weldability and Properties of New Creep Resistant Materials for use in Ultra Supercritical Coal Fired Power Plants.” Liege Conference on Materials, 2006.
[40] F. Kager, N. Bock, K. Spiradek-Hahn, S. Hofinger, M. Brabetz, G. Zeiler, “Superior Long-Term Creep Behavior and Microstructural Evolution of 9%Cr Steels with Boron.” Liege Conference on Materials, 2006.
[41] Christina Berger, Michael Schwienheer, Alfred Scholz, “Creep and Creep Fatigue Properties of Turbine Steels for Application Temperatures up to 625°C.” Liege Conference on Materials, 2006.
[42] M. Staubli, K-H. Mayer, W. Giselbrecht, J. Stief, A. DiGianfrancesco, T-U. Kern, “Development of Creep Resistant Cast Steels within the European Collaboration in Advanced Steam Turbine Materials for Ultra Efficient Low Emission Steam Power Plant / COST 501-522.” Liege Conference on Materials, 2002.
[43] K.H. Mayer, R. Blum, P. Hillenbrand, T.-U. Kern, M. Staubli, “Development Steps of New Steels for Advanced Steam Power Plants.” Liege Conference on Materials, 2002.
[44] M. Schwienheer, H. Haase, A. Scholz, C. Berger. “Long Term Creep and Creep Fatigue Properties of the Martensitic Steels of type (G)X12CrMoWVNbN10-1-1.” Liege Conference on Materials, 2002.
[45] Reinhard Knodler, Brendon Scarlin, “Oxidation of Advanced Ferritic/Martensitic Steels and of Coatings in Flowing Steam at 650°C.” Liege Conference on Materials, 2002.
[46] J. Hawk, P. Jablonski, G. Holcomb, J. Licavoli, and M. Gao, “NETL Advanced 9%Cr Steel: Update and Current Development Status.” NETL Cross Cutting Meeting, April 2019.
[47] S. Baumgartner, A. Holy, R. Schnitzer, “Properties of a Creep Resistant 9Cr-1.5Mo-1Co Cast Steel Joint Welded with a Matching Flux-Cored Wire.” Zavarene Konstrukcije, 2014.
[48] R. Oruganti, M. Karafge, S. Swaminathan, “A Comprehensive Creep Model for Advanced 9-10% Cr Ferritic Steels.” Procedia Engineering 55, 2013.

[49] D. Purdy, “Appendix to Metallurgical Guidebook for Steam Turbine Rotors and Discs, Volume 2: High Temperature Steels from COST Programs.” EPRI, Palo Alto, CA. 3002014469. 2019.
[50] A. Bridges, J. Foulds, “Creep Rupture Assessment Handbook” EPRI, Palo Alto, CA. 3002016956. 2019.